Carbon nanotubes: Innovative heterogeneous gas phase catalysts

Dissertation

zur Erlangung des akademischen Grades

Doctor rerum naturalium (Dr. rer. nat.)

vorgelegt dem Rat der Chemisch-Geowissenschaftlichen Fakultät

der Friedrich-Schiller-Universität Jena

von

M. Ing. Chem. Qui Nguyen Van

geboren am 01. April 1974 in Saigon Stadt, Vietnam

Gutacher

1. Prof. Dr. Bernd Ondruschka
2. Prof. Dr. Rainer Beckert

Tag der öffentlichen Verteidigung: 26.10.2011

Table of contents

Kurzzusammenfassung

Da die Kohlenstoffablagerung auf dem Eisenoxidkatalysator im Verlauf der oxidierenden Dehydrierung von Ethylbenzen (ODEB) zum Styren als die katalytisch wirksame Substanz angesehen werden, wurden verschiedene kohlenstoffhaltige Materialien auf ihre Eignung als Katalysator hin geprüft. Weil Carbon nanotubes überlegene elektrische, mechanische und thermische Eigenschaften besitzen, wurden sie als ein viel versprechendes Material für diese Reaktion angesehen worden. Es wurde bestätigt, dass sauerstoffhaltige funktionelle Gruppen auf der Katalysatoroberfläche, besonders Carbonyl/Chinon- und Hydroxylgruppen die katalytische Wirksamkeit erhöhen. Folglich liegt der Fokus dieser Arbeit in der Modifizierung der Oberfläche von Carbon nanotubes mit sauerstoffhaltigen funktionellen Gruppen durch Oxidation mittels verschiedener Oxidationsmittel wie Hydroxylradikale und Ozon in der Gasphase und den Einfluss dieser Gruppen auf den Verlauf der ODEB zu Styren.

Die Einflüsse der oxidierenden Behandlungen auf die strukturellen, elektronischen und chemischen Eigenschaften der Oberfläche von MWCNTs sowie vergleichenden Untersuchungen der Katalysatoren vor und nach der ODEB wurden mit einer Reihe von analytischen Methoden, wie TGA, BET-Oberfläche, Raman-Spektroskopie, TEM, FTIR und XPS untersucht.

Es wurde gefunden, dass „as-received" MWCNTs niedrigere Umsätze und niedrigere Selektivitäten bei der ODEB aufweisen. Die oxidierenden Behandlungen haben mehr Sauerstoff enthaltene funktionelle Gruppen auf as-received MWCNT-Oberflächen erzeugt. Infolgedessen wurden die katalytischen Leistungen von oxidierten MWCNTs erheblich verbessert. Die optimalen Reaktionszustände wurden bei 450 °C und einem molaren Verhältnis zwischen EB und Sauerstoff von 1:2 gefunden. Ethylbenzenumsatz und Styrenselektivität können 80% beziehungsweise 92% auf C2-CNTs bei Langzeituntersuchungen erreichen. Dies ist das beste Resultat im ODEB, dass uns bekannt ist.

Die katalytische Leistung wurde im Wesentlichen durch den angewendeten Anregungsmodus für die Reaktion beeinflusst. So wurde eine bei vergleichenden Untersuchung unter herkömmlicher Heizung und Mikrowellenheizung auf die Katalysatorleistung herausgefunden, dass der Umsatzunterschied zwischen herkömmlicher Heizung und Mikrowellenheizung unwesentlich, die Styrenselektivität unter herkömmlicher Heizung aber viel höher als die unter Mikrowellenheizung war.

Die Untersuchung der gebrauchten Katalysatoren unter herkömmlicher und Mikrowellenheizung zeigte, dass bei konventioneller Heizung eine Zunahme und bei Mikrowellenheizung eine Abnahme beobachtbar war. Die Boehm-Titration wurde eingesetzt, um carboxylhaltige Gruppen auf den MWCNTs zu neutralisieren und um die Einflüsse der carboxylhaltigen Gruppen in der ODEB zu erforschen. Die Styrenausbeute von Carboxylgruppen-freien MWCNTs war um 16% geringer als die von Carboxylgruppen-haltigen MWCNTs. Die Untersuchung beider Katalysatoren nach der Reaktion zeigte, dass sich auf Carboxylgruppen-freien MWCNTs während der Reaktion kein aktiver Kohlenstoff ablagert. Dieses zeigt, dass carboxylhaltige Oberflächengruppen die katalytische Leistung indirekt verbessern.

Chapter 1

Background of carbon nanotubes

1.1. History of carbon nanotubes

1.1.1. Carbon allotropes

Carbon in the solid phase has several allotropic forms because it is able to exist in three hybridization states sp^3, sp^2 and sp^1 (Figure 1.1).
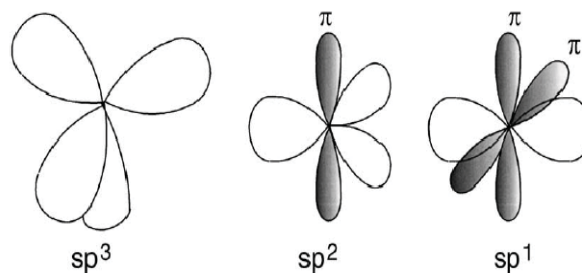
Figure 1.1. sp^3, sp^2 and sp^1 hybridized bonding of carbon [1].

Depending on their structures, carbon allotropes can be divided into two categories: amorphous and crystalline.

Amorphous carbon is a non-crystalline phase of carbon without long range order and containing carbon atoms in different hybridization states [2]. Depending on preparation techniques [3], phases with various macroscopic properties can be produced. Notably, the atomic density and the ratio of sp^2/sp^3 hybridization can vary significantly from sample to sample. The three relatively well known amorphous carbons are charcoal, lampblack (soot) and activated carbon.

Carbons in crystalline phase include diamond, graphite, buckminsterfullerenes, carbon nanotubes and graphene (Figure 1.2).
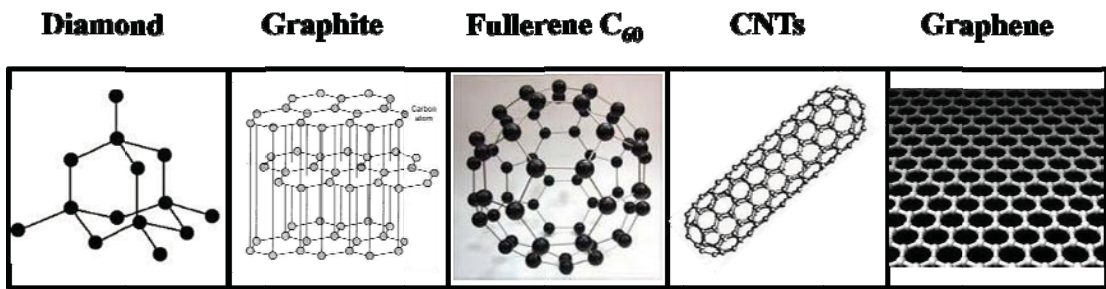
Figure 1.2. Various crystalline structures of carbon.

Diamond has a crystalline structure where each sp^3-hybridized carbon atom is bonded to four others in a tetrahedral arrangement. Diamond is renowned as a material with superlative physical qualities, most of which originate from the strong covalent bonding between its atoms. In particular, diamond has the highest hardness and thermal conductivity of any bulk material. The sp^3-hybridized bonds account for its electrically insulating property and optical transparency.

Graphite consists of layered planar sheets of sp^2-hybridized carbon atoms bonded together in a hexagonal network. The different geometry of the chemical bonds makes graphite soft, slippery, opaque and electrically conductive. In contrast to diamond, each carbon atom in the graphite sheet is bonded to only three other atoms; electron can move freely from a nonhybridized p-orbital to another, forming an endless delocalized π-bond network that gives rise to the electrical conductivity.

Buckminsterfullerenes or fullerenes are the third allotrope of carbon and consist of a family of spheroidal or cylindrical molecules wherein all the carbon atoms are sp^2-hybridized. The tubular form of the fullerenes, named nanotubes, will be the subject of this work, and a detailed description of their history, properties and potential applications in the catalytic processes is given in the next following sections.

Graphene is the latest allotrope of carbon discovered by A. Geim and K. Novoselov from the University of Manchester in 2004. The Nobel Prize in Physics for 2010 was awarded to them [3]. Graphene is a one-atom-thick planar sheet of sp^2-bonded carbon atoms that are densely packed in a honeycomb crystal lattice. Graphene is extracted

from graphite, which is how it gets its name. In fact, graphene provides the structural basis of all other graphitic materials, from graphite itself to fullerenes and carbon nanotubes. Perfect graphene is in hexagonal form, although imperfections can cause heptagonal or pentagonal structures. Graphene has attracted considerable interest in the past several years due to its significant potential for both the fundamental studies and technological applications [4].

1.1.2. Formation of carbon nanotubes

The fullerene C_{60} was discovered in 1985 by R. Curl, H. Kroto and R. Smalley from Rice University [5]. For this discovery they were awarded with the 1996 Nobel Prize in chemistry. Fullerene C_{60} with 60 carbon atoms bonded together arranged in a network of five pentagons and six hexagons that looks like a soccer ball.

The carbon atoms are sp^2-hybridized, but in contrast to graphite, they are not arranged in a plane. The geometry of C_{60} strains the bonds of the sp^2-hybridized carbon atoms, creating new properties for fullerenes. Graphite is a semimetal, whereas fullerene is a semiconductor. The fullerenes are not a single material, but a family of molecules. C_{60}, C_{70}, C_{76}, C_{78} and C_{84} have become well-known [6]. The discovery of fullerenes generated considerable interest in the scientific community and in the general public. It appears that the spherical fullerenes such as C_{60} are not the only type of large curve carbon molecules.

In 1991, S. Iijima first discovered nanotube-like graphitic structures in the carbon deposit formed on the cathode during the process of generating fullerenes soot in a arc discharge. These nanotubes comprise concentrically rolled graphene sheets with diameters ranging of 4-30 nm and about 1 μm length (Figure 1.3) [7]. They were called multi-walled carbon nanotubes (MWCNTs). Two years later, single walled carbon nanotubes (SWCNTs) were discovered also [8, 9].
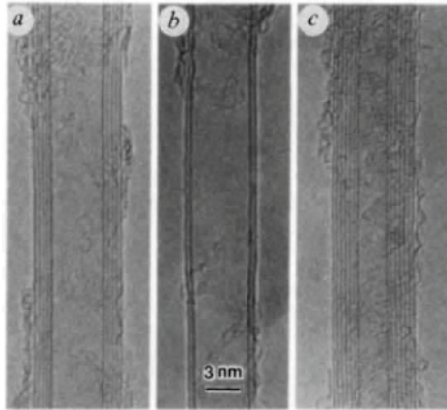
Figure 1.3. TEM micrographs of CNTs: five-sheet tube, diameter 6.7 nm (a), two-sheet tube, diameter 5.5 nm (b), and seven-sheet tube, diameter 6.5 nm (c) [7].

1.2. Properties of carbon nanotubes

1.2.1. Structural properties

Ideally, SWCNTs consist of one perfect graphene sheet rolled up into a cylinder and closed by two caps (semi-fullerenes). The way in which graphene sheet can be rolled to form a nanotube cylinder is represented by the helicity vector C_h (Figure 1.4A).
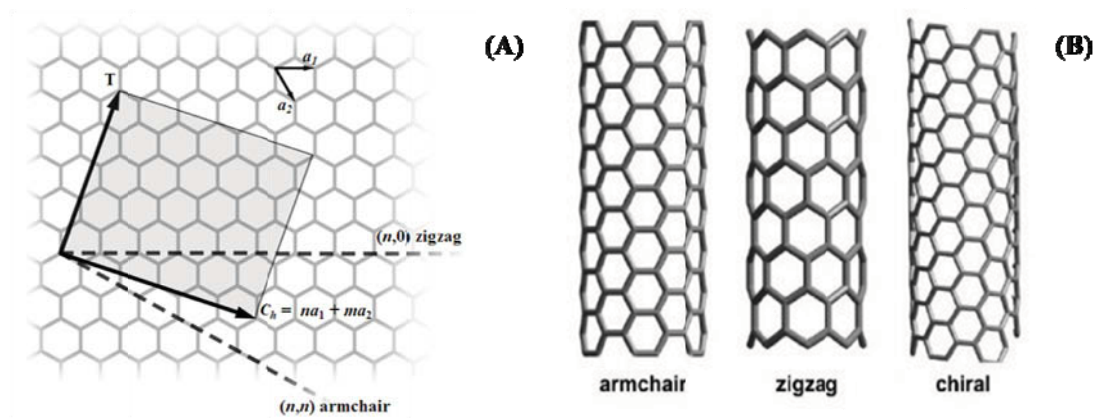
Figure 1.4. Graphene sheet with helicity vector (A), and three types of SWCNTs (B).

The helicity vector is modulated by a pair of indices *n* and *m* as a following description:

$$C_h = na_1 + ma_2$$

where a_1 and a_2 are the unit vectors of graphene in real space.

12

The indicest *n* and *m* denote the number of unit vectors along two directions in the honeycomb crystal lattice of graphene (Figure 1.4B). If *m = 0*, the nanotubes are called "zigzag". If *n = m*, the nanotubes are called "armchair". Otherwise, they are called "chiral". The diameter can vary between 0.4 and 2.5 nm, and the length ranges from a few microns to several milimeters. Due to high surface energy of these one-dimensional carbon macromolecules, SWCNTs are commonly arranged in bundles.

MWCNTs can be considered as concentric SWCNTs with increasing diameter and coaxially deposited. The number of walls can vary from two (double-walled nanotubes) to several tens, so that the external diameter can reach 100 nm. The concentric walls are regularly spaced by 0.34 nm, similar to the distance between layers in graphite material.

1.2.2. Electronic properties

Extensive studies of electronic properties of CNTs were reported in the literature [10]. SWCNTs behave as a pure quantum wire (1D-quantum) where the electrons are confined along the tube axis. Electronic properties are mainly involved by two factors: the tube diameter and the helicity. In particular, armchair SWCNTs display metal-like conductivity, and zigzag ones display semiconductors behavior. The curvature of the grapheme sheet induces strong modification of the electronic properties and in comparison with graphite a modification of the π-electron cloud is shown. The rolling-up of the graphene sheet to form the tube causes a rehybridization of carbon orbital (non-planar sp^2 configuration), thus leading to a modification of the π density in the graphene sheet [11]. It is also noteworthy that the theoretically predicted electronic properties are often drastically modified by the presence of defects such as pentagons, heptagons, vacancies or impurities [12].

Studies on MWCNTs have shown [13] that their electronic properties behave like an ultimate carbon fiber: at high temperature the electrical conductivity can be described by the semi-classical models already used for graphite, whilst at low temperature they reveal 2D-quantum transport features. A reliable prediction of their electronic properties is even more difficult than in the case of SWCNTs due to the higher complexity of their

structure, and experimental measurements on MWCNTs resistivity have not given reliable values due to different CNTs purities and measurement conditions.

1.2.3. Mechanical and thermal properties

CNTs are unique materials because they are the strongest and stiffest materials discovered in terms of tensile strength and elastic modulus. In particular, the Young's modulus and the tensile strength of MWCNTs are 1260 and 150 GPa, respectively, which would be ten times higher than those observed for steel while weighting six times less [14, 15]. In addition, it has been shown that CNTs are flexible and can be bent at 90° several times without undergoing structural changes. Experiment values showed that the structure suffer the modification at very high temperatures and pressures (5.5 GPa, 800 °C) [16]. Concerning flexural modulus, MWCNTs exhibit higher values than SWCNTs, with flexibility decreasing when the number of wall increases [17]. The superior characteristics are attributed to the covalent sp^2-bonds formed between the individual carbon atoms [18].

The conductivity and thermal stability of CNTs are important features that should be taken into consideration when CNTs are used as catalysts or catalyst supports. The most common and simple ways to study the resistance of a carbonaceous material towards temperature is a thermogravimetric analysis (TGA). Generally, CNTs are more stable to oxidation than activated carbon. However, the presence of surface defects and residual metals on or inside the nanotubes that can catalyze carbon oxidation may lower their withstanding temperatures. The maximum gasification temperature of MWCNTs (containing of 3% metal) is located around 650 °C. TGA of the MWCNTs (7.5% metal) has a value at around 550 °C [19]. The experimental studies of the thermal stability of CNTs have shown that SWCNTs could be obtained the highest burning temperatures than MWCNTs due to the big bundles and well-defined crystallinity [20]. In summary, the thermal stability of nanotubes varies with several parameters, the content of residual metals, the bundles diameter, the number of walls and the crystallinity.

Since the thermal control of nanocatalysts has become an increasingly important issue as the size of system diminishes, especially in exothermic reactions, the thermal conductivity of CNTs should play a critical role in controlling the performance of the catalyst. The measured thermal conductivities of graphite along the basal plane range of 940 - 2000 W K^{-1} m^{-1}. CNTs present a value of ca. 3000 W K^{-1} m^{-1} [21]. In general, the measured experimental values about the physical properties of CNTs are lower than theoretical predictions due to the presence of structural defects. Most of the studies on CNTs thermal conductivity agree that values are very high, comparable to those of diamond and to in-plane graphite sheet and that the thermal conductivity is significant improved for CNTs-polymer composite [22].

1.2.4. *Adsorption properties*

From the view point of structural properties, CNTs have inner hollow cavities which can be filled by certain substances. This leads to interesting possible applications, such as gas storages, gas sensors and gas separations [23]. Yang et al. [24] identified that pores in MWCNTs can be mainly divided into the hollow cavities of smaller diameter (narrowly distributed, mainly 3.0 - 4.0 nm) and the aggregated pores (widely distributed, 20 - 40 nm) formed by interaction of isolated MWCNTs. The aggregated pores contribute to 78.5% of the total adsorption capacity, much more important for adsorption issues than their inner cavities. Gas adsorption into SWCNTs bundles can occur inside the tubes, in the interstitial triangular channels among the tubes, on the outer surface of the bundle or in a groove formed at the contact between adjacent tubes on the outside of the bundles (Figure 1.5). It was found that the inside of the SWCNTs has stronger affinity for N_2 adsorption than the interstitial channel of bundles [25]. For MWCNTs, the adsorption gases can occur in the aggregated pores, inside the tube or on the external walls. In the latter case, the presence of defects, as in complete graphene layers, has to be taken into consideration. Although adsorption between the walls has been proposed in the case of hydrogen adsorption in herringbone type graphite nanofibers [26], it is unlike to occur in the case of MWCNTs due to the steric effects and should not prevail for small molecules due to long diffusion paths [27]. It has been

found that, for butane, MWCNTs with smaller outside diameters adsorbed more butane, consistently with other finding that the strain incurved graphitic surface affect sorption. Most of butane adsorbed on the external surface of the MWCNTs and only a small fraction of the gas condensed in the pores of tubes [28].
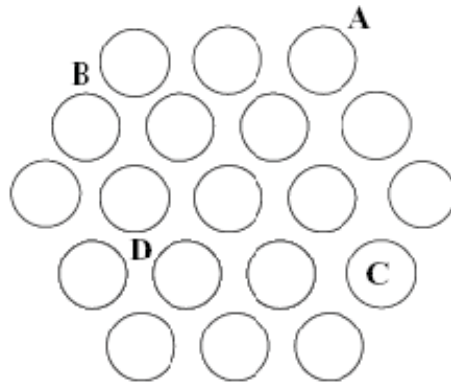
Figure 1.5. Different adsorption sites in SWCNTs bundles: surface (A); groove (B); pores (C); and interstitial (D) [27].

Several studies have been reported that the adsorption enthalpy of small gas molecules, such as H_2, CH_4, Xe and Ne, on SWCNTs is lower than that on graphite, but the binding energy between adsorbents and SWCNTs are higher up to 75% [29-31]. The observed change of the binding energy can be attributed to an increase of the effective coordination in binding sites as the groove sites [32, 33].

Most experiments have shown that the specific surface area of SWCNTs is often larger than that of MWCNTs. Typically, the total surface area of as-grown SWCNTs ranges between 400 and 900 $m^2\,g^{-1}$ (specific pore volume, 0.15 - 0.3 $cm^3\,g^{-1}$), whereas for as-produced MWCNTs values ranging of 150 - 300 $m^2\,g^{-1}$ are often reported. The chemical activation of CNTs such as treatment with KOH or NaOH can efficiently raise the surface area, as high as 1050 $m^2\,g^{-1}$, and pores size of the nanotubes due to opening and cutting CNTs [34, 35]. It is noteworthy that the opening/closing of the central canal affects the adsorptive properties of nanotubes noticeably.

In summary, it appears that CNTs present specific adsorption properties as compared to graphite or activated carbon, mainly due to their peculiar morphology, existing defects, opening/closing of the tubes, chemical purification or the presence of catalyst particles as impurities can affect the adsorption properties.

1.2.5. Carbon nanotubes synthesis

Nowadays CNTs can be produced in large scale by arc discharge method (ADC) [7-9], pulsed laser ablation technique [36], and chemical vapor deposition method (CVD) [37, 38]. The ADC method is based on the electric discharge between two graphite electrodes at high current power under an inert gas atmosphere. During the process, the carbon of anode sublimates by high temperature (3000 - 4000 °C) and is then deposited on the cathode. It is possible to grow MW- and SWCNTs, but SWCNTs could only be formed with a metal-impregnated graphite cathode. The laser ablation was first developed by Smalley [36] to grow SWCNTs. In this process, the composite target of graphite and metal catalysts is vaporized by laser irradiation under flowing inert gas atmosphere at high temperature (~ 1200 °C). The product with high purity is collected via condensation on a cold finger downstream from the target. However, the yield and cost of production are hindering for the commercial scale. The CVD method is the best effective method and widely used to produce CNTs on ton scale due to its facility and economy. Briefly, a carbon source such as benzene, acetylene, or ethanol, is decomposed on the surface of nanoparticle catalysts (Co, Ni or Fe), then carbon atoms diffuse and precipitate at the edges of the particle to form CNTs. The diameters of tubes are generally related to the size of nanoparticles. The catalyst particles can stay at the tips or at the base of nanotubes depending on the interaction between catalyst and support (Figure 1.6) [39].
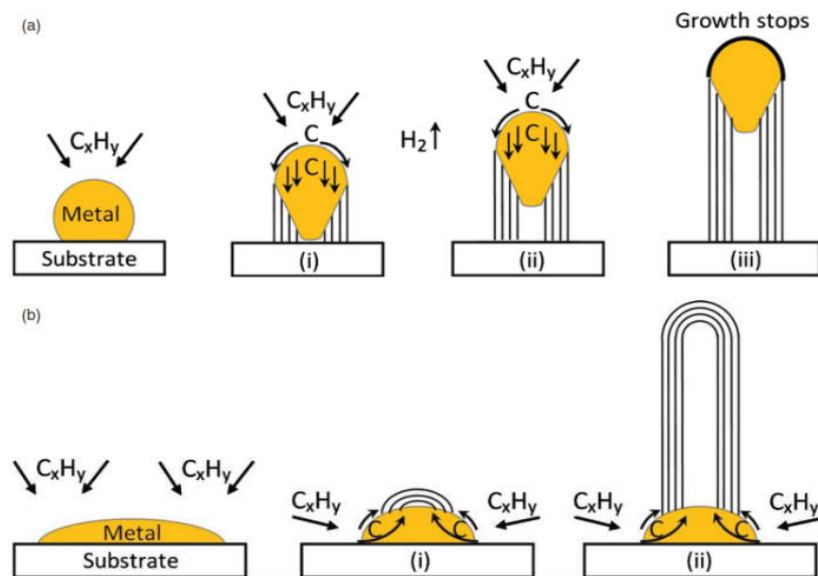
Figure 1.6. Growth mechanisms for CNTs: tip-growth (a) and base-growth (b) model [39].

1.3. Functionalized Carbon nanotubes in catalysis

CNTs possess unique electronic, chemical, and mechanical properties that make them leading materials for a wide variety of potential applications. In principle, CNTs are perfect graphitic sheets rolled into nanocylinders. The outer wall of pristine CNTs is remarkable chemically inert. In reality, as-produced CNTs contain a low number of functional groups and surface defects [40], such as vacancies, dangling bonds at open ends, Stone-Waals defects and sp^3-hybridized defects (Figure 1.7). The functional groups on CNTs could be considered as active sites catalyst [41], or anchoring sites in the deposition of precious metal supported catalyst [42]. The broad spectrum of CNTs has permitted the development of reliable methods for chemical functionalization, and today chemical reactions on CNTs receive an increasing attention.
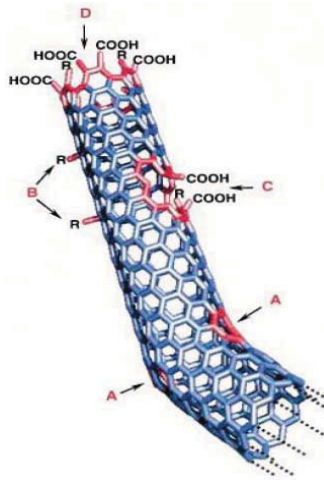
Figure 1.7. Scheme of typical defects in SWCNTs: pentagon-heptagon defects (A), sp^3-hybridized defects (B), 'hole' defects (C), end tube defects (D) [40].

One of the most common functionalization of CNTs techniques is the oxidative treatment by liquid phase or gas phase oxidizing agents. It was shown that gas phase oxidation of nanotubes mainly increased the concentration of hydroxyl and carbonyl surface groups, while treatments in the liquid phase increased especially the concentration of carboxylic acids [43]. Various oxygen-containing surface functional groups formed after oxidation treatments are represented in Figure 1.8.
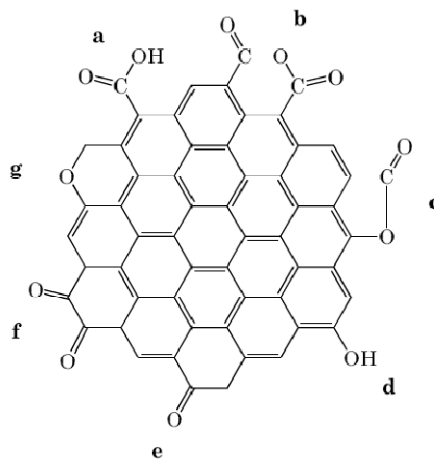
Figure 1.8. Schematic representation of oxygen-containing groups present on the CNTs: carboxylic group (a), anhydride group (b), lactone group (c), phenol (d), carbonyl group (e), o-quinoid group (f), and ether group (g).

19

The nature and concentration of surface functional groups might be modified by suitable thermal or chemical post-treatments. Oxidation in the gas or liquid phase could be used to increase the number of oxygenated surface groups, while heating under inert atmosphere might be used to remove some of these functions selectively [43]. The introduction of oxygen-containing groups on the surface of CNTs enhances their solubility in aqueous or organic solvents and reduces the van der Waals interactions between different CNTs, promoting the separation of nanotube bundles into individual tubes.

1.3.1. *Liquid phase functionalization*

Acid treatment was generally used to oxidize CNTs surface. It enhanced the acidic properties, removed the mineral elements and improved the hydrophilic properties of surface.

The HNO_3 or H_2SO_4/HNO_3 are the most widely methods of chemical surface modification of CNTs. Mostly carboxylic and anhydride groups are introduced at defect sites on the outer and possibly inner walls of CNTs [44-46]. A careful and slow oxidation in diluted HNO_3 is needed to create surface oxygenated groups, and to minimize bulk damage of the material [47]. When the oxidation of CNTs was carried out by refluxing the nanotubes in concentrated HNO_3, a high density of oxygen-containing groups can be obtained [48]. Prolonged reflux induces the opening of MWCNT tips, damages the walls and slightly increases the specific surface area. Marques et al. [49] have developed a methodology to tailor the introduction of oxygenated functionalities using HNO_3 hydrothermal oxidation procedure. Kim et al. [50] have chemically treated carbon nanotubes using a mixture of H_2SO_4/HNO_3. The effects of acid treatment methods on the diameter dependent length separation of SWCNTs were investigated. They have found that smaller diameter nanotubes were preferentially shortened by the acid treatment process and migrated further from the original sample during the gel electrophoresis. This technique can provide a preparative, scalable method for separating nanotubes by length and diameter. Chiang et al. [51] also have investigated the influence of treatment duration on MWCNTs functionalized by

H_2SO_4/HNO_3 oxidation. They found that the oxygen content increased with increasing treatment time. The samples oxidized for two days had the most abundant carboxylic surface groups. The oxidation mechanism of MWNTs in mild mixture of H_2SO_4/HNO_3 was proposed, which was a successive and interative process, including the initial attack on active sites, and next the hexagon electrophilic attack generating new defects and introducing more oxygenated groups, and then the tubes becoming thinner and shorter. Besides the classical acid treatment, other oxidative agents have been used to prepare functionalized CNTs. Peng et al. [52] studied the oxidation of MWCNTs with hydrogen peroxide. The physical charaterization results demonstrated that several functional groups, such as carboxylic (COOH), carbonyl (C=O) and hydroxyl groups (OH) were formed on the surface of the treated MWCNTs. However, hydroxyl groups were preferentially formed and reached a maximum atomic concentration of about 46% in four days of oxidation. The graphitization degree decreased in the first day of oxidation. However, it readily increased in the continued oxidation days. Compared with acid treated MWCNTs, basic oxidant (NH_4OH/H_2O_2) generated lower oxygenated surface groups and less addition of defects on the graphitic surface [53].

1.3.2. Gas phase functionalization

The advantages of gas phase oxidation of CNTs than the liquid phase method is simple and eliminate hazardous chemical waste. Li et al. [54] studied the air oxidation of CNTs in the range of 480 – 750 °C. The reaction allows the attachment of a wide variety of functional species onto the nanotubes surface, enhances the specific surface area and improves the intrinsic morphologies of CNTs. Low temperature oxygen plasma is a relatively simple method for tailoring the surface chemical composition of CNTs [55, 56]. By using an oxygen radio frequency plasma treatment at 13.56 MHz to functionalize MWCNTs, Felten et al. [56] reported that for too high oxygen plasma power, chemical etching occur at the surface of CNTs, thus destroying its structure. On the other hand, for optimal values of the plasma parameters both the concentration and type of the functional groups are in close connection with the plasma conditions. These results were compared to interaction energies predicted by *ab initio* calculation for

different functional groups, showing that functionalization by oxygen plasma produces mainly functional groups with lower interaction energy (Figure 1.9). The interaction energies were theoretically calculated for the functional groups identified with XPS, resulting in the following sequence: CNT-OH (116 kcal mol^{-1}) > CNT-COOH (80 kcal mol^{-1}) > CNT=O (70 kcal mol^{-1}) > CNT=C=O (- 36 kcal mol^{-1}).
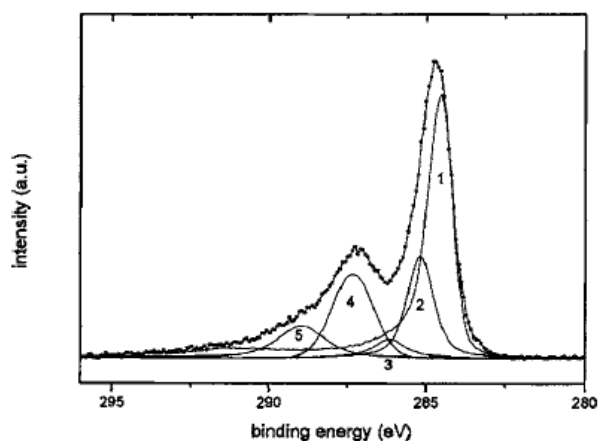

Figure 1.9. XPS C1s spectrum of oxygen plasma treated CNTs. The curve fitting suggests the existence of five species: graphite signal (1), sp^3 carbon (2), hydroxyl group (3), carbonyl group (4), and carboxyl group (5) [56].

Ozone as a strong oxidizing agent was widely applied in organic degradation. It could also oxidize the CNTs surface to introduce oxygen-containing groups. The ozone dose and oxidation time affected the resultant nature and concentration of these groups [57-59]. Mawhinney et al. [57] studied the oxidation of SWCNT with ozone gas (3% ozone in oxygen). IR spectra of ozonated samples revealed that the ozone reaction with nanotubes produced two distinct surface-bound functional groups, esters and quinones, as well as gas phase CO_2 and CO. The formation rate of these groups diminishes at higher ozone exposures when the number of active sites on the SWCNTs reduces. Li et al. [59] used diluted aqueous ozone with or without ultrasound to functionalize SWCNTs. The results of XPS showed that the surface oxygen to carbon atom ratio increased by more than 600-times after 72 h of treatment. Compared to acid treated MWCNs, ozone treated CNTs forms a lower number of surface defects but the dispersion level of both samples are similar [60].

1.3.3. Other functionalization methods

Since hydroxyl radical is an extremely reactive radical, it is able to oxidize fully saturated organic compounds and many unsaturated molecules [61]. Li et al. [62] studied the effect of hydroxyl radicals generated by Fenton's reaction on the structure of MWCNTs. The results have shown that hydroxyl radicals can attack on defect sites and unsaturated bonds of C=C in the MWCNTs. FTIR spectra identified the introduction of various oxygen-containing groups onto the nanotubes surfaces after the reaction.

Imasaka et al. [63] successfully dispersed MWCNTs and SWCNTs in water by a pulsed streamer discharge generated in a suspension of nanotubes in water. The functional hydroxyl groups bound to the CNTs surface seem to be responsible for the solubilization effect. The advantage of this method is that there is no need of any chemical agents to assist the dispersion of CNTs in water.

Xu et al. [64] studied γ-ray irradiation of MWCNTs in air and in epoxy chloropropane (ECP). The results indicated that γ-ray irradiation in two different media improved the amount of oxygen-containing functional groups on nanotubes surface, and the irradiation in ECP was more efficient.

1.4. Role of oxygen-containing surface groups in catalysis

1.4.1. Carbon as support

The oxygen-containing groups were introduced on the surface of oxidized CNTs that provide nucleation sites for subsequent deposition of metal species supported CNTs [65]. One of the most studied catalytic reactions is the hydrogenation in both liquid and gas phase. Yegres et al. [66] prepared a Rh-complex anchored on the original activated carbon, oxidized supports and MWCNTs for hydrogenation of cyclohexene. The oxidized carbons with hydroxyl groups on the surface which exploited for the effective immobilization of the Rh-complex were reported very active in the reaction. A 5% w/w platinum catalyst deposited on CNTs (100 m^2 g^{-1}) was found to be significant more active than a 5% Pt/AC and 5% Pt/graphite for the hydrogenation of *trans*-stilbene and *trans*-1-phenylpropene [67]. Solhy et al. [68] compared the loading of Pt on HNO_3

oxidized MWCNTs, mechanically treated MWCNTs and high temperature activated MWCNTs with the performances of the catalytic systems in the selective hydrogenation of cinnamaldehyde to cinnamyl alcohol. They found that the oxidative nitric acid treatment creates primarily carboxylic groups that Pt-clusters bound to MWCNTs surface via bonding with ionic form of carboxylate –COOPt. The air oxidation introduces moderate amount of oxygenated groups, mainly phenol and carbonyl or quinone groups. The best catalyst activity is achieved on the acid treated MWCNTs. The selective hydrogenation of acetylene to ethylene was reported on NiB/CNTs catalyst [69]. The activation of CNTs with NH_3 (particle size 9 nm) provides better dispersions than does treatment with HNO_3 (particle size 16 nm), resulting in acceleration of the hydrogenation rate and an increase in the selectivity to ethylene.

CNTs have been employed as supports for Fischer-Tropsch synthesis (FTS). Trepanier et al. [70] investigated the influence of acid treatment conditions (30% HNO_3 at 25 and 100 °C for 14 h) on CNTs supported cobalt catalyst in FTS. The acid treatment at 25 and 100 °C, respectively, (i) increased the BET surface area by 18% and 25%, (ii) decreased the cobalt particle size and increased the cobalt dispersion, (iii) increased the FTS activity and % CO conversion by 36 and 114%. The product selectivity showed distinct shift to lower molecular hydrocarbons [71]. A closely similar results obtained on iron supported on raw and treated MWCNTs in a FTS. Higher surface area (up to 31%) and smaller iron particles size (lower 20%) has been found on treated MWCNTs. As a result, the catalyst activity for FTS increases significantly, the CH_4 selectivity decreases and the selectivity to C_{5+} increases.

Activated carbon (AC)-supported ruthenium based materials are effective catalysts for ammonia synthesis [72, 73]. However, the main risk of Ru/AC catalysts has been pointed out whether the catalysts could not be sufficiently resistant to the methanation of the carbon supports [74]. Hence, CNTs has been considered as an alternative to AC due to their high stability. Investigation of ammonia synthesis on Ru/K/MWCNTs catalyst, Chen et al. [75] reported that the presence of oxygenated surface groups on MWCNTs improves the dispersion and interaction between Ru and MWCNTs significantly. A

removal of functional groups in helium gas at high temperature leads to reduce of the dispersion and interaction of Ru and K with MWCNTs. Consequently, the ammonia synthesis activity on the treated catalyst is lower than that of the catalyst without helium treatment.

Recently, the catalytic decomposition of ammonia to generate high purity hydrogen free of CO_x for fuel cell applications have been received much attention [76]. Carbon-based Ru catalysts have been tested successfully as catalysts for NH_3 synthesis, thus, they could be considered to catalyze the decomposition of NH_3, because the synthesis and the decomposition are reversible reactions. Yin et al. [77] compared the activity of the series of Ru catalysts supported on AC, MgO, Al_2O_3, TiO_2 and CNTs for NH_3 decomposition. They found that among the catalysts tested, Ru/CNTs is the best catalyst for the decomposition reaction. The high activity of the Ru/CNTs can be related to the high dispersion of Ru particles, high graphitization and high purity of the CNTs. The modification of Ru/CNTs with KOH leads to a remarkable increase in activity and to a decrease in apparent activation energy of the decomposition reaction. The effective promoters in the catalytic activities for this reaction were established in the order: Ru/K/CNTs > Ru/Na/CNTs > Ru/Li/CNTs > Ru/Ce/CNTs > Ru/Ba/CNTs > Ru/La/CNTs > Ru/Ca/CNTs > Ru/CNTs [78].

In addition, CNTs have been considered as catalyst supports in a variety of reactions, such as Rh/MWCNTs for NO decomposition [79], Co/MWCNTs for dehydrogenation of cyclohexanol [80, 81], Co-Mo/MWCNTs for hydrodesulfurization [82], Pt/MWCNTs cathode for fuel cell electrocatalysis [83].

1.4.2   Carbon as catalyst

Besides being used as catalyst supports, CNTs have been considered as non-metal catalysts for methane decomposition [84, 85], hydroxylation of aromatic hydrocarbons [86], oxidation of *p*-toluidine [87], conversion of aniline to azobenzene [88], oxidative dehydrogenation of 1-butene to butadiene [89] and oxidative dehydrogenation of ethylbenzene to styrene (ODEB) [90-93]. Kang et al. [86] carried out the hydroxylation

of aromatic hydrocarbons on oxidized MWCNTs, graphite and amorphous carbon as catalysts. The results indicated that MWCNTs were highly-active, highly-selective, and well-reproducible heterogeneous catalysts. The curved sp^2-hybridized carbon surface of MWCNTs played an important role in these selective catalytic reactions. Interestingly, functional groups, primarily carboxylic groups, created by open-ended MWCNTs with HNO_3 are not the key factor for the reaction.

Carbon-catalyzed decomposition of methane is an environmentally attractive low emission approach for the hydrogen production for fuel cell applications [84]. Carbon-based catalysts offer several advantages toward metal catalysts, including no need for the regeneration of the catalyst by burning off carbon from the catalyst surface, no contamination of hydrogen with carbon oxides and possibility of production of both hydrogen and carbon with minimum CO_2 emission. Muradov et al. [85] tested the decomposition of methane on a wide range of carbon materials. It was demonstrated that the catalytic activity of carbon materials for methane decomposition is mostly determined by their structural and surface properties. The surface concentration of high-energy sites, which are presumed to be catalytic active sites, is the most important factor governing the activity of carbon. The catalytic activity of deactivated carbon can be generated via surface gasification reactions using steam and/or carbon dioxide.

The direct dehydrogenation of ethylbenzene to styrene (DHEB) is one of the ten most important industrial processes. Low conversion of EB and high energy consumption are the real challenges of this process. The ODEB has been attracted as a promising alternative to avoid the thermodynamic limitations and waste energy [94]. It was assumed that quinoid/carbonyl groups presented on the carbon surface are involved in the mechanism of the reaction [95]. Thus, carbon materials are available to be promising candidates for the ODEB. The matters of the ODEB are presented extensively in the next chapter.

1.5. References

[1] J. Robertson, Mater. Sci. Eng. Res. 37 (2002) 1289.

[2] P.H. Gaskell, A. Saeed, P. Chieux, D.R. McKenzie, Phys. Rev. Lett. 67 (1991) 1286.

[3] J. Robertson, Prog. Solid State Chem. 21 (1991) 199.

[4] L. Liao, X. Duan, Mater. Sci. Eng. Res. 70 (2010) 354.

[5] H.W. Kroto, J.R. Heath, S.C. O'Brien, R.F. Curl, R.E. Smalley, Nature 318 (1985) 162.

[6] H. Yang, C.M. Beavers, Z. Wang, A. Jiang, Z. Liu, H. Jin, B.Q. Mercado, M.M. Olmstead, A.L. Balch, Angew. Chem. Int. Ed. 48 (2009) 1.

[7] S. Iijima, Nature 354 (1991) 56.

[8] S. Iijima, T. Ichihashi, Nature 363 (1993) 603.

[9] D.S. Bethune, C.H. Kiang, M.S. de Vries, G. Gorman, R. Savoy, J. Vaquez, R. Beyers, Nature 363 (1993) 605.

[10] J.E. Fischer, A.T. Johnson, Curr. Opin. Solid State Mater. Sci. 4 (1999) 28.

[11] T. Dumitrica, C.M. Landis, B.I. Yakobson, Chem. Phys. Lett. 360 (2002) 182.

[12] J.C. Charlier, Acc. Chem. Res. 35 (2002) 1063.

[13] J.P. Issi, J.C. Charlier, The Science and Technology of Carbon Nanotubes, Elsevier (1999), p. 107.

[14] D.H. Robertson, D.W. Brenner, J.W. Mintmire, Phys. Rev. B 45 (1992) 12592.

[15] E.W. Wong, P.E. Sheehan, C.M. Lieber, Science 277 (1997) 1971.

[16]   M. Corrias, P. Serp, P. Kalck, G. Dechambre, J.L. Lacout, C. Castiglioni, Y. Kihn, Carbon 41 (2003) 2361.

[17]   M.F. Yu, O. Lourie, M.J. Dyer, K. Moloni, T.F. Keley, R.S. Ruoff, Science 287 (2000) 637.

[18]   A. Krishnan, E. Dujardin, T.W. Ebbsen, P.N. Yianilos, M.M.J. Treacy, Phys. Rev. B 58 (1998) 14013.

[19]   D. Born, R. Andrews, D. Jaques, J. Anthony, B. Chen, M.S. Meyer, J.P. Selegue, Nano Lett. 2 (2002) 615.

[20]   H.Z. Geng, D.S. Lee, K.K. Kim, S.J. Kim, J.J. Bae, Y.H. Lee, J. Korean Phys. Soc. 53 (2008) 979.

[21]   P. Kim, L. Shi, A. Majumda, P. L. Maceuen, Phys. Rev. Lett. 87 (2001) 215502.

[22]   P. Serp, J.L. Figueiredo, Ed., Carbon material for catalysis, John Wiley & Sons Inc., Hoboken, New Jersey, 2009, p. 331.

[23]   M. Monthioux, P. Serp, E. Flahaut, C. Laurent, A. Peigney, M. Razafinimanana, W. Basca, J.M. Broto, in B. Bhushan, Ed., Springer Handbook of Nanotechnology, 2nd rev, Springer-Verlag, Heidelberg, Germany, 2007, p. 43-112.

[24]   Q.H. Yang, P.X. Hou, S. Bai, M.Z. Wang, H.M. Cheng, Chem. Phys. Lett. 345 (2001) 18.

[25]   A. Fujiwara, K. Ishii, H. Suematsu, H. Kataura, Y. Maniwa, S. Suzuki, Y. Achiba, Chem. Phys. Lett. 336 (2001) 205.

[26]   A. Chambers, C. Park, R.T.K. Baker, N.L. Rodriguez, J. Phys. Chem. 102 (1998) 4253.

[27]   P. Serp, M. Corrias, P. Kalck, Appl. Catal. A 253 (2003) 337.

[28] J. Hilding, E.A. Grulke, S.B. Sinnott, D. Qian, R. Andrews, M. Jagtoyen, Langmuir 17 (2001) 7540.

[29] S. Talapatra, A.Z. Zambano, S.E. Weber, A.D. Migone, Phys. Rev. Lett. 85 (2000) 138.

[30] S. Inoue, N. Ichikuni, T. Suzuki, T. Uematsu, K. Kaneko, J. Phys. Chem. B 102 (1998) 4689.

[31] E. Diaz, S. Ordonez, A. Vega, J. Colloid Interface Sci. 305 (2007) 7.

[32] H. Ulbricht, G. Moos, T. Hertel, Phys. Rev. B 66 (2002) 075404.

[33] H. Ulbricht, G. Kriebel, G. Moos, T. Hertel, Chem. Phys. Lett. 360 (2002) 252.

[34] E.R. Pinero, P. Azais, T. Cacciaguerra, D.C. Amoros, A.L. Solano, F. Beguin, Carbon 43 (2005) 786.

[35] D. Lucio, D. Laurent, G. Roger, S. Yasushi, Y. Noriko, Carbon Sci. Technol. 3 (2009) 120.

[36] T. Guo, P. Nikolaev, A. Thess, D.T. Colbert, R.E. Smalley, Chem. Phys. Lett. 243 (1995) 49.

[37] M. Endo, K. Takeuchi, S. Igarashi, K. Kobori, S. Shiraishi, H.W. Kroto, J. Phys. Chem. Solids, 54 (1993) 1841.

[38] P. Nikolaev, M.J. Bronokowski, R.K. Bradley, Chem. Phys. Lett. 313 (1999) 91.

[39] M. Kumar, Y. Ando, J. Nanosci. Nanotechnol. 10 (2010) 3739.

[40] A. Hirsch, Angew. Chem. Int. Ed. 41 (2002) 1853.

[41] D. Yu, E. Nagelli, F. Du, L. Dai, J. Phys. Chem. Lett. 1 (2010) 2165.

[42] J.Z. Luo, L.Z. Gao, Y.L. Leung, C.T. Au, Catal. Lett. 66 (2000) 91.

[43]   J.L. Figueiredo, M.F.R. Pereira, M.M.A. Freitas, J.J.M. Orfao, Carbon 37 (1999) 1379.

[44]   T.G. Ros, A.G. van Dillen, J.W. Geus, D.C. Koningsberger, Chem. Eur. J. 5 (2002) 1151.

[45]   A. Kusnetzova, I. Popova, J.T. Yates, M.J. Bronikowski, C.D. Huffamnn, J. Liu, R.E. Smalley, H.H. Hwu, J.G. Chen, J. Am. Chem. Soc. 123 (2001) 10699.

[46]   T. Kyotani, S. Nakazaki, W.H. Xu, A. Tomita, Carbon 39 (2001) 771.

[47]   G. Ovejero, J.L. Sotelo, M.D. Romero, A. Rodriguez, M.A. Ocana, G. Rodriguez, J. Garcia, Ind. Eng. Chem. Res. 45 (2006) 2206.

[48]   Z. Liu, X. Lin, J.Y. Lee, W. Zhang, M. Han, L.M. Gan, Langmuir 18 (2002) 4054.

[49]   R.R.N. Marques, B.F. Machado, J.L. Faria, A.M.T. Silva, Carbon 48 (2010) 1515.

[50]   Y. Kim, D. Lee, Y. Oh, J. Choi, S. Baik, Synth. Metals 156 (2006) 999.

[51]   Y.C. Chiang, W.H. Lin, Y.C. Chang, Appl. Surf. Sci. 257 (2011) 2401.

[52]   Y. Peng, H. Liu, Ind. Eng. Chem. Res. 45 (2006) 6483.

[53]   V. Datsyuk, M. Kalyva, K. Papagelis, J. Parthenios, D. Tasis, A. Siokou, I. Kallitsis, C. Galiotis, Carbon 46 (2008) 833.

[54]   C. Li, D. Wang, T. Liang, X. Wang, J. Wu, X. Hu, J. Liang, Powder Technol. 142 (2004) 175.

[55]   Y.J. Kim, H. Ma, Q. Yu, Nanotech. 21 (2010) 295703.

[56]   A. Felten, C. Bittencourt, J.J. Pireaux, G.V. Lier, J.C. Charlier, J. Appl. Phys. 98 (2005) 074308.

[57] D.B. Mawhinney, V. Naumenko, A. Kuznetsova, J.T. Yates, J. Liu, R.E. Smalley, J. Am. Chem. Soc. 122 (2000) 2383.

[58] W. Sun, U. Khaled, H. Tomita, Z. Li, K. Imasaka, J. Suehiro, Jap. J. Appl. Phys. 49 (2010) 055002.

[59] M. Li, M. Boggs, T.P. Beebe, C.P. Huang, Carbon 46 (2008) 466.

[60] A.B. Sulong, C.H. Azhari, R. Zulkifli, M.R. Othman, J. Park, Eur. J. Sci. Res. 33 (2009) 295.

[61] L.M. Dorfman, G.E. Adams, National Bureau of Standards issued June 1973.

[62] W. Li, Y. Bai, Y. Zhang, M. Sun, R. Cheng, X. Xu, Y. Chen, Y. Mo, Synth. Metals 155 (2005) 509.

[63] K. Imasaka, J. Suehiro, Y. Kanatake, Y. Kato, M. Hara, Nanotechnol. 17 (2006) 3421.

[64] Z. Xu, C. Min, L. Chen, L. Liu, G. Chen, N. Wu, J. Appl. Phys. 109 (2011) 054303.

[65] X. Bao, Chem. Commun. (2008) 6271.

[66] L.L. Yegres, I.S. Basanez, C.S.M.D. Lecea, P. Serp, M.C.R. Martinez, Carbon 44 (2006) 587.

[67] T. Onoe, S. Iwamoto, M. Inoue, Catal. Commun. 8 (2007) 701.

[68] A. Solhy, B.F. Machado, J. Beausoleil, Y. Kihn, F. Goncalves, M.F.R. Pereira, J.J.M. Orfao, J.L. Figuereido, J.L. Faria, P. Serp, Carbon 46 (2008) 1194.

[69] C.Y. Hu, F.Y. Li, L. Hua, R.B. Zhang, J. Serb. Chem. Soc. 71 (2006) 1153.

[70] M. Trepanier, A. Tavasoli, A.K. Dalai, N. Abatzoglou, Fuel Process. Technol. 90 (2009) 367.

[71] R.M.M. Abbaslou, A. Tavasoli, A.K. Dalai, Appl. Catal. A 355 (2009) 33.

[72]   Z. Kowalczyk, J. Sentek, S. Jodzis, E. Mizera, J. Goralki, T. Paryjczak, R. Diduzsko, Catal. Lett. 45 (1997) 65.

[73]   L. Forni, D. Molinari, I. Rossetti, N. Pernicone, Appl. Catal. A 185 (1999) 269.

[74]   Z. Kowalczyk, S. Jodzis, W. Ragoz, J. Zienlinski, J. Pielaszek, Appl. Catal. A 173 (1998) 153.

[75]   H.B. Chen, J.D. Lin, Y. Cai, X.Y. Wang, J.Yi, J.Wang, G. Wei, Y.Z. Lin, D.W. Liao, Appl. Surf. Sci. 180 (2001) 328.

[76]   F.R.G. Garcia, J.A. Rodriguez, I.R. Ramos, A.G. Ruiz, Carbon 48 (2010) 267.

[77]   S.F. Yin, B.Q. Xu, W.X. Zhu, C.F. Ng, X.P. Zhou, C.T. Au, Catal. Today 93-95 (2004) 27.

[78]   S.J. Wang, S.F. Yin, L. Li, B.Q. Xu, C.F. Ng, C.T. Au, Appl. Catal. B 52 (2004) 287.

[79]   J.Z. Luo, L.Z. Gao, Y.L. Leung, C.T. Au, Catal. Lett. 66 (2000) 91.

[80]   Z.J. Liu, Z. Xu, Z.Y. Yuan, D. Lu, W. Chen, W. Zhou, Catal. Lett. 72 (2001) 203.

[81]   Z.J. Liu, Z.Y. Yuan, W. Zhou, L.M. Peng, Z. Xu, Phys. Chem. Chem. Phys. 3 (2001) 2518.

[82]   K. Dong, X. Ma, H. Zhang, G. Lin, J. Nat. Gas. Chem. 15 (2006) 28.

[83]   W. Li, C. Liang, J. Qiu, W. Zhu, H. Han, Z. Wei, G. Sun, Q. Xin, Carbon 40 (2002) 787.

[84]   N. Muradov, Catal. Commun. 2 (2001) 89.

[85]   N. Muradov, F. Smith, A.T. Raissi, Catal. Today 102-103 (2005) 225.

[86]   Z. Kang, E. Wang, B. Mao, Z. Su, L. Gao, L. Niu, H. Shan, L. Xu, Appl. Catal. A 299 (2006) 212.

[87]   M. Croston, J. Langston, R. Sangoi, K.S.V. Santhanam, P. Ajayan, Int. J. Nanosci. 1 (2002) 277.

[88]   M. Croston, J. Langston, G. Takacs, T.C. Morrill, M. Miri, K.S.V. Santhanam, P. Ajayan, Int. J. Nanosci. 1 (2002) 285.

[89]   X. Liu, D.S. Su, R. Schlögl, Carbon 46 (2008) 544.

[90]   N. Maksimova, G. Mestl, R. Schlögl, Stud. Surf. Sci. Catal. 133 (2001) 383.

[91]   M.F.R. Pereira, J.L. Figuereido, J.J.M. Orfao, P. Serp, P. Kalck, Y. Kihn, Carbon 42 (2004) 2807.

[92]   D.S. Su, N. Maksimova, J.J. Delgado, N. Keller, G. Mestl, M.J. Ledoux, R. Schlögl, Catal. Today 102-103 (2005) 110.

[93]   B. Nigrovski, P. Scholz, T. Krech, N.V. Qui, K. Pollok, T. Keller, B. Ondruschka, Catal. Commun. 10 (2009) 1473.

[94]   F. Cavani, F. Trifiro, Appl. Catal. A 133 (1995) 219.

[95]   G. Emig, H.J. Hofmann, J. Catal. 84 (1983) 15.

Chapter 2

Styrene synthesis from dehydrogenation of ethylbenzene and alternative processes

2.1. Styrene properties and applications in polymers

Chemical name = Styrene

CAS number = 100-42-5

Molecular formula = C_8H_8

Molar mass = 104.2 gmol^{-1}

Melting point = - 31 °C

Boiling point = 145 °C

Density = 0.91 g cm^{-3}
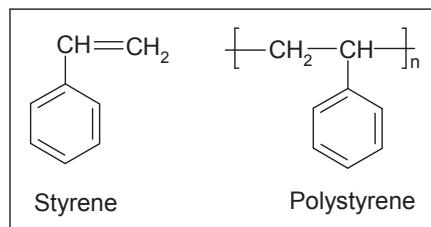
Styrene is clear, colorless, flammable liquid with a sweet odor. It is used as monomer in polystyrene production when heated or using free radical polymerization. Polystyrene is used as a co-polymer with a number of other materials. Examples of co-polymers are acrylonitrile-butadiene-styrene, styrene-acrylonitrile and styrene-butadiene rubber. Polystyrene is used in paints, coatings, adhesives and resins.

The first commercial polystyrene plant was opened in 1931 by BASF in Germany. Dow started producing polystyrene in 1938. World demand for styrene monomer in 2006 was approximately 25 million tons [1].

2.2. Industrial styrene production

Styrene is produced predominately from ethylbenzene (EB). EB is made by the catalytic alkylation of benzene with ethylene, using either aluminium chloride or zeolite catalysts [2]. The EB is then converted to styrene by either dehydrogenation or indirect oxidation with propylene to produce propylene oxide and styrene as co-product. Worldwide, more than 90% styrene is made by the vapour phase catalytic dehydrogenation of ethylbenzene (DHEB) at high temperature using Fe-K based mixed oxide catalysts [3]. The main reaction produces styrene and hydrogen.
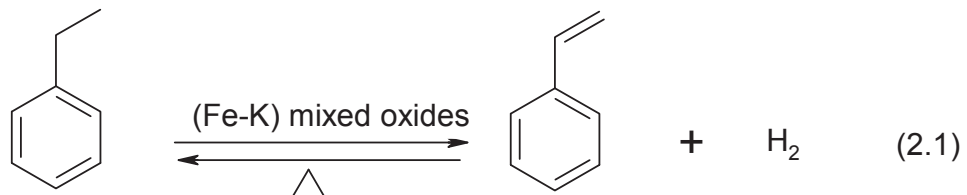
$$\Delta H (620 \ °C) = 124.83 \ \text{kJ mol}^{-1}$$

The main by-products are benzene and toluene:

$$C_6H_5C_2H_5 \quad \rightarrow \quad C_6H_6 \ + \ C_2H_4 \qquad (2.2)$$

$$C_6H_5C_2H_5 \ + \ H_2 \quad \rightarrow \quad C_6H_5CH_3 \ + \ CH_4 \qquad (2.3)$$

The reaction is endothermic and equilibrium-limited. At 627 °C the equilibrium constant and degree of completeness of DHEB are 0.378 and 52.4%, respectively [4]. The reaction is running in an adiabatic reactor between 580 and 610 °C. Since the reaction is endothermic with increase in reaction temperature, the conversion increases also. When temperatures rise above 610 °C, the thermal cracking of EB and styrene becomes significantly.
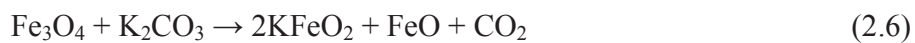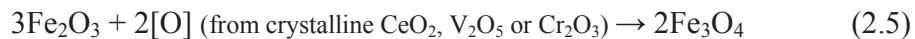
A family of catalysts based on Fe_2O_3-K_2O has been employed for the process. It has been claimed that potassium loading increases conversion and selectivity to styrene, and stabilizes the catalyst. It has also been found that potassium stabilizes the active phase Fe^{3+} in the form of $KFeO_2$, $K_2Fe_{22}O_{34}$ [5-9].

$$Fe_2O_3 + K_2CO_3 \rightarrow 2KFeO_2 + CO_2 \quad (2.4)$$

Kuhrs et al. [9] identified the sequence catalytic activity for the process as the following:

$$KFe_xO_y > Fe_2O_3 > Fe_3O_4$$

The addition of different promoters, such as Cr, Ce and V, in order to increase durability, discourages sintering and quenching the volatilization of potassium [5, 10]

$$3Fe_2O_3 + 2[O] \text{ (from crystalline } CeO_2, V_2O_5 \text{ or } Cr_2O_3) \rightarrow 2Fe_3O_4 \quad (2.5)$$

$$Fe_3O_4 + K_2CO_3 \rightarrow 2KFeO_2 + FeO + CO_2 \quad (2.6)$$

EB is typically diluted 1:15 in superheated steam to provide heat for the reaction, maximize conversion to styrene by reducing product partial pressures, and maintain catalyst activity by the gasification of carbonaceous surface [11]. Thus, the amount of energy spent for the process is very high. Under these conditions, the conversion per pass is about 55 - 65% at approximately 90% selectivity [12].

Styrene can also be dehydrogenated isothermally by EB. The main difference between the isothermal and adiabatic processes is in the way the endothermic reaction heat is supplied. In an adiabatic reactor, the endothermic heat of reaction is supplied by steam superheated to 800 - 950 °C that is mixed with EB feed prior to the reactor. As the reaction progresses, the temperature decreases. To keep a high conversion, usually two or three reactors are used in series with a reheating between the reactors to raise the temperature of the reaction mixtures. In the isothermal reactor, the reaction heat is provided by heat transfer from external source to internal reactor. In technical practice, to facilitate heat transfer a large number of expensive tubular reactors are required due to heat transfer rates are low. Over 75% of all styrene plants in operation are based on the adiabatic process. The process was discovered and developed by IG Farbe in 1931. Modified and improved technology was commercialised by, e.g., ABBLummus/UOP. Figure 2.1 shows the flow scheme of a typical adiabatic DHEB plant [13].
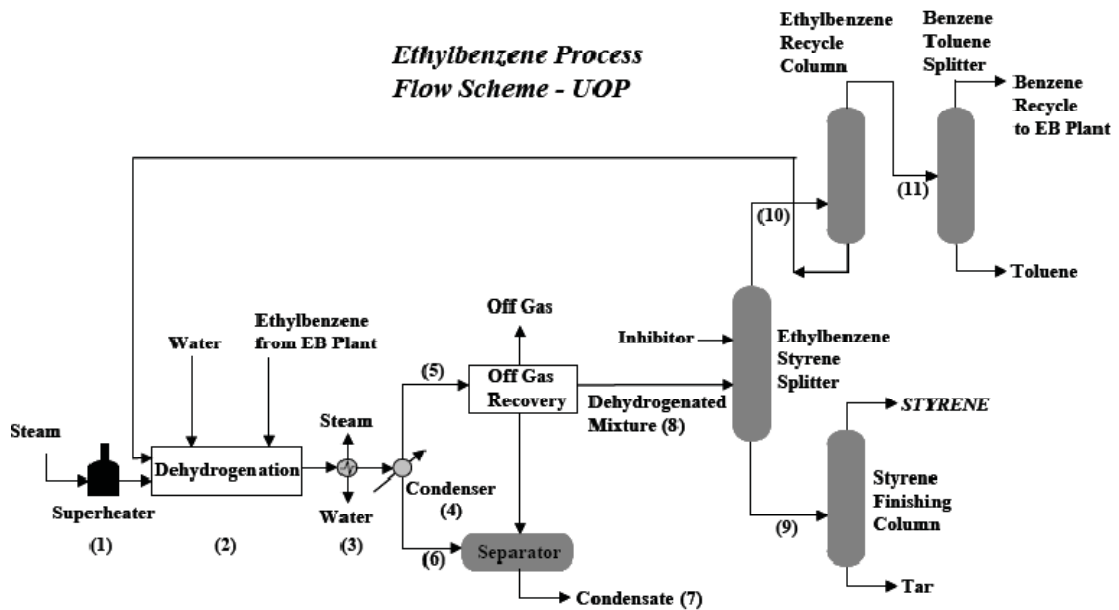
*Figure 2.1. Flow scheme of the adiabatic DHEB plant [13].*

The separation of styrene from products is really difficult because styrene and EB have a very close boiling point (EB boils at 138 °C and styrene at 145 °C), and styrene tends to polymerization at elevated temperatures. Therefore, low temperature vacuum distillation and inhibitors are employed necessarily in the separation stage of the process.

2.3. Alternative processes to DHEB

To overcome some intrinsic drawbacks of conventional DHEB as mentioned, such as low equilibrium conversion, high energy consumption, catalyst deactivation with time, a few alternative processes has been suggested. They include DHEB followed by oxidation of hydrogen, DHEB in membrane reactor, and oxidative dehydrogenation of ethylbenzene (ODEB).

2.3.1. DHEB followed by oxidation of hydrogen

The reaction 2.7 and 2.8 exemplify the reaction path for this process.

$$C_6H_5CH_2CH_3 \rightleftharpoons C_6H_5CH=CH_2 + H_2 \quad (2.7)$$

$$H_2 + 1/2O_2 \longrightarrow H_2O \quad (2.8)$$
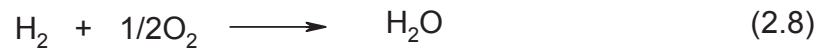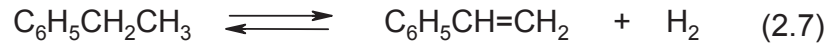
A gas mixture containing the oxygen is injected either in the effluent or in the feed of a DHEB reactor, in order to oxidize hydrogen as by-product catalytically. The oxidation of hydrogen not only reduces the cost of superheated steam but also shifts the dehydrogenation equilibrium towards higher conversion and selectivity [3].

Oxidation catalysts are required to be selective only to hydrogen, thus avoiding the oxidation of the reagent and of the products. Moreover, oxidation catalysts are able to resist the severe hydrothermal conditions, i.e., at high temperature (550 - 650 °C) and in the presence of steam. This is the reason why the application of this technology is claimed in the DHEB using iron oxide-based catalysts in the presence of steam and in the dehydrogenation of paraffin only with either spinel-type supports or supports based on alumina doped with rare earth, which are particularly stable in the presence of steam [14-18].

2.3.2. DHEB in membrane reactor

Using selectively permeable membrane to separate hydrogen from DHEB reaction, then, hydrogen reacts with an oxygen-containing gas on the other side of the membrane. As a result, the oxidative dehydrogenation can be carried out without mixing the hydrocarbon and oxygen-containing gas, thus, minimizing undesired oxygen insertion reactions and avoiding problems related to flammability of the mixtures and to run-away. Bitter [19] studied the separation of hydrogen from DHEB products on a systematic alumina membrane reactor. With a Fe/K/V/Li/Cr/O catalyst, at a temperature of 625 °C and a LHSV of 0.65 h^{-1}, a conversion of 65% and a selectivity of 94% could be obtained, while without membrane the conversion was only 50.7%. Moser et al. [20] tested the DHEB in alumina reactor. The conversion of EB could be increased from 10 to 23%, depending on the membrane configuration.
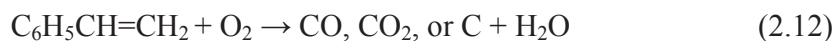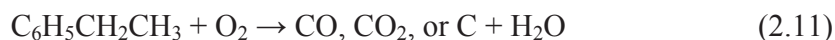
2.3.3. Oxidative dehydrogenation of ethylbenzene to styrene (ODEB)

The oxidative dehydrogenation of ethylbenzene to styrene (ODEB) is one of the most promising routes for styrene synthesis. The ODEB chemistry is presented as the following:
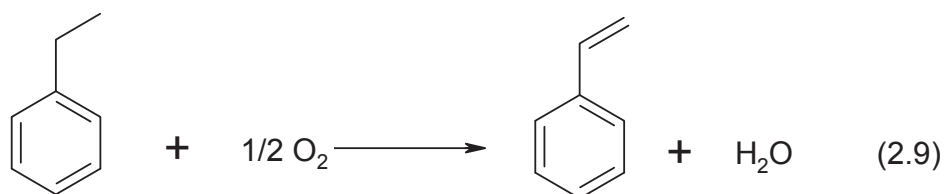
$$\Delta H^\circ_{298} = -124.2 \text{ kJ mol}^{-1}$$

Besides styrene as the desired product, the possible main side reactions occur in parallel and sequentially by cracking, partial or total oxidation reactions [21].

$$C_6H_5CH_2CH_3 \rightarrow C_6H_6 + C_2H_4 \tag{2.10}$$

$$C_6H_5CH_2CH_3 + O_2 \rightarrow CO, CO_2, \text{ or } C + H_2O \tag{2.11}$$

$$C_6H_5CH=CH_2 + O_2 \rightarrow CO, CO_2, \text{ or } C + H_2O \tag{2.12}$$

The main advantage of ODEB is the strong exothermic reaction, and shifts the equilibrium towards higher styrene yields [22]. However, the ODEB still faces two challenges: first, the selectivity of styrene may be low due to the parallel total oxidation of EB; and secondly, the operation is restricted by its flammability limits. The lower and higher limits of EB in air at 30 °C (those for styrene are similar) are 1.0 and 6.7%, respectively [4]. Until now, the ODEB is not operated commercially.

The utilization of carbon dioxide as an oxidant for the ODEB has also been tested for producing styrene as following reaction:

$$C_6H_5CH_2CH_3 + CO_2 \rightarrow C_6H_5CH=CH_2 + CO + H_2O \tag{2.13}$$

The realization of such process is a decrease in the amount of required energy, and an increase in styrene yield. The deactivation of oxides catalyst was restrained by the action of CO_2 [23].

2.4. ODEB over carbonaceous catalysts

Since the 1970s, there have been early studies on the ODEB over alumina and metal phosphate catalysts [24, 25]. The pioneering studies of Alkhazov et al. [24] provided firstly considerable evidence likely catalyzed coke in this reaction. It was known that the coke deposition does not occur on the more active transition metals or other variable valence ion oxides usually associated with oxidation catalysts, but less active materials, such as alumina, silica, phosphate and zeolite [26]. Observing the reaction on acidic oxides it has been shown that the activity of the initially clean surface is very low but it increases significantly over a few hours period of time, and then begins a slow decrease over many hours or days. The duration of the rise in activity is coincident with the accumulation of coke layers, which reaches a steady-state level of up to 5 - 15 wt.% [27-29]. Examining characterization of the active coke by X-ray photoelectron spectroscopy (XPS) and secondary ion mass spectroscopy (SIMS) it was identified that surface coke are islands of condensed aromatic rings with quinoid groups on the edges which are the oxidizing species and should be the active sites for the ODEB [30, 31]. A redox mechanism was proposed by Emig and Hofmann that the cleavage of the C-H bonds occurs on the quinone groups and regeneration of hydroxyl groups with oxygen followed via water removal (Figure 2.2) [28].
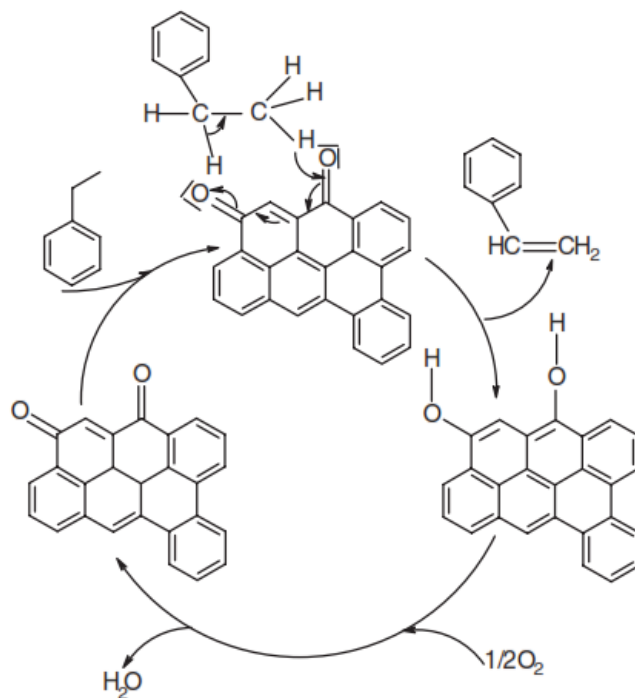
Figure 2.2. Schematic of the proposed mechanism for the ODEB [28].

Various carbonaceous adsorbents have been shown to be active and selective catalysts in the ODEB. Drago et al. [32] investigated the effect of various activated carbon and carbon molecular sieves, oxygen concentration in the feed stream, the contact time, and the addition of dopants and inhibitors to the reaction at 360 °C. The results indicated that comparable conversion and selectivity can be attained with these catalysts at significantly lower temperatures than those reported for metal oxide catalysts. A decrease in oxygen concentration results in a decrease in the conversion of EB and an increase in selectivity to styrene. In the case of 'Ambersorb 563' catalyst, 90% selectivity of styrene can be attained at 50% conversion of EB. Increasing contact time leads to an increase in conversion but a decrease in selectivity. The change in reactivity of Ambersorbs catalyst by doping KMnO$_4$ and NaOH is not significant. All the catalysts give a tendency of coke formation identified by increasing of the catalyst mass after the reaction. Coke deposit is possibly caused by the polymerization of styrene and its subsequent thermal decomposition. Carbon tetrabromide added in the feed stream acts as an inhibitor for coke formation. The graphite catalysts with surface area in the range

of 200 - 300 $m^2 g^{-1}$ for the ODEB give similar activity results. The activity of the activated carbon with the same area but different pores size is high in the beginning of the reaction. The carbon with smaller pores decreases in its activity with time on stream, while on the carbon with wider pores a slightly decrease at the beginning and stabilizing thereafter has been observed [33]. A systematic survey of the influence of carbon texture in the ODEB was carried out by Pereira et al. [34-37]. The following conclusions were reached:

- No direct proportionality was observed between the surface area and activity in the ODEB reaction (as shown in Figure 2.3).
- The pores of very small dimensions were quickly blocked, due to coke deposition during the process. Therefore, a wide pore structure is needed.
- Narrowing the pore sizes of the original activated carbons by coke deposition led to lower catalytic activity.
- The textural effects were found to be important up to an average pore width of 1.2 nm. For larger pores sizes the surface chemistry controls the catalyst performance.
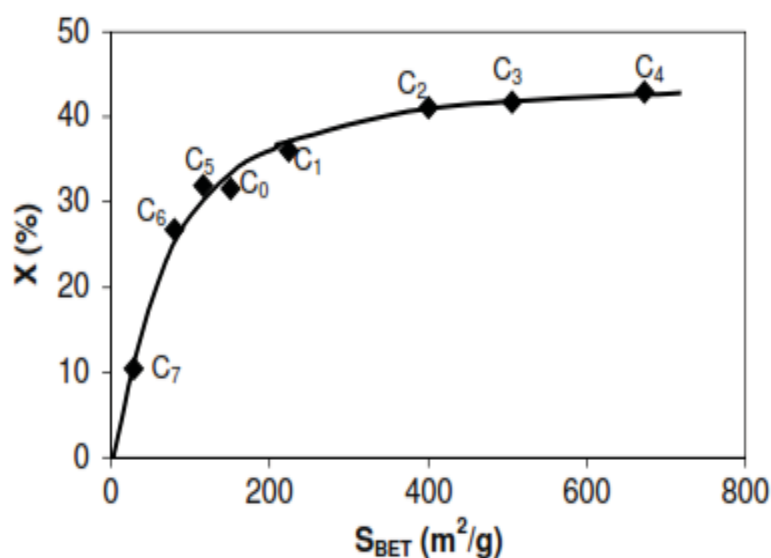

Figure 2.3. Conversion of EB versus surface areas of activated catalysts (measured after reaction) [34].

The role of surface chemistry on the activated carbon in the reaction was also intensively studied by Pereira et al. [35-37]. A number of activated carbons treated with a variety of oxidants, including oxygen, nitrous oxide, nitric acid and hydrogen peroxide were catalyzed the ODEB. The results indicated that the gas phase treatments lead to improve the catalyst performance in terms of conversion and styrene selectivity, and associated with an increase in the amount of carbonyl/quinoid groups on the surface catalysts after the reaction. It was observed that the catalytic activity increases with the degree of the oxidation conditions, while the styrene selectivity remains unchanged.

The thermal stability of the oxygenated surface functional groups depends on the reaction temperature. Carbonyl and quinoid groups can be removed at high as 1100 °C in nitrogen environment. Thermal treatment of the sample at 1100 °C in nitrogen flow leaded to a decrease in the catalyst activity due to an elimination of carbonyl surface groups [37].

The catalytic stability with time on stream on activated carbon revealed that the rate of carbon gasification becomes faster than the rate of coke deposition, leading to a decrease in catalyst weight (catalyst mass lost 26.9% after 72 h time on stream). Even if working under milder conditions for retarding this effect, the accumulation of oxygenated surface groups is not proportionate with increase in the catalyst activity because the majority of the new groups are not active for the ODEB [37]. Therefore, activated carbon is far from the realizable solution.

As compared with classical carbons like activated or carbon black, nanostructured carbons, such as CNFs, CNTs and onion-like nanocarbon, have been considered as good candidates for the reaction because their high crystallinity can hold a better thermal stability even under an oxidative atmosphere. Maksimova et al. [38] used different carbon materials, including carbon black, graphite and MWCNTs as the catalysts. They found that CNTs obtained the best catalysts of highest styrene selectivity at maximum conversion. Several evidence of sp^2-carbon deposits (Figure 2.4) during the induction period was regarded with the catalytic activity [39-41].
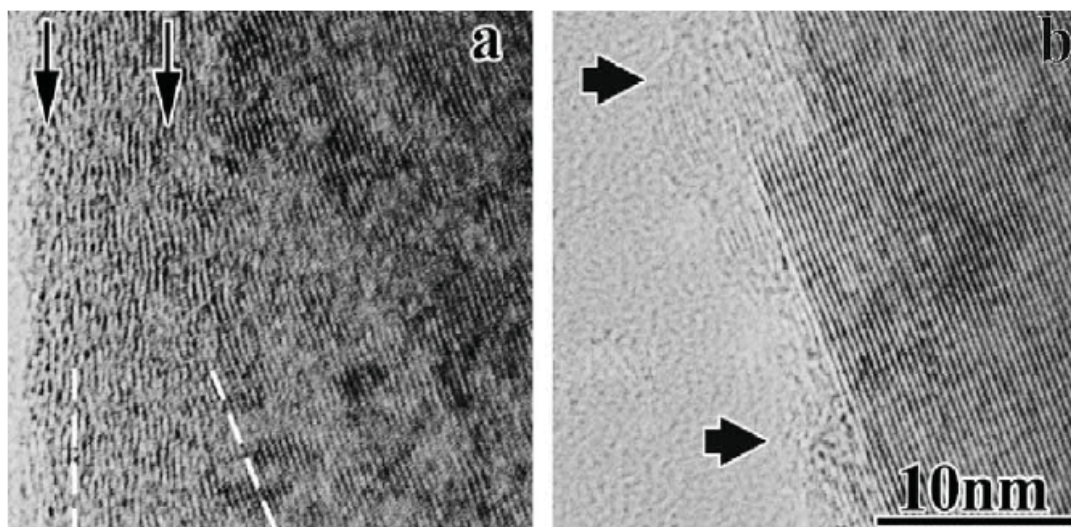
Figure 2.4. High-resolution TEM images of the CNT walls before the reaction (a), and after 20 h time on stream (b). The disappearance of the outer disordered carbon layers and the appearance of new sp^2-carbon layers after 20 h time on stream [37].

Characterizing CNFs before and after the ODEB by XPS, Mestl et al. [39] detected the presence of new peak in the XPS O1s of the tested catalyst, corresponding to the basic oxygenated surface groups, i.e. quinoidic groups. It was suggested that the function of these groups are responsible for the dehydrogenation reaction, and the oxidation with oxygen is then the next step for recovering active sites to their initial states.

2.5. References

[1]   R.L. Myers, The 100 Most Important Chemical Compounds, Greenwood Publishing Group, Inc., 2007, p. 266.

[2]   http://www.icis.com/v2/chemicals/9076473/styrene/process.html (06. 2011)

[3]   F. Cavani, F. Trifiro, Appl. Catal. A 133 (1995) 219.

[4]   N.I. Shuikin, I.I. Levitsky, Russ. Chem. Bull. 2 (1953) 365.

[5]   K. Shibata, T. Kiyoura, Bull. Chem. Soc. Jpn. 42 (1969) 871.

[6]   M. Muhler, R. Schlögl, A. Reller, G. Ertl, Catal. Lett. 2 (1989) 201.

[7]   T. Hirano, Appl. Catal. 26 (1986) 81.

[8]   M. Muhler, J. Schutze, M. Wessemann, T. Rayment, A. Dent, R. Schlögl, G. Ertl, J. Catal. 126 (1990) 339.

[9]   C. Kuhrs, Y. Arita, W. Weiss, W. Ranke, R. Schlögl, Top. Catal. 14 (2001) 111.

[10]   I. Serafin, A. Kotarba, M. Grzywa, Z. Sojka, H. Binczycka, P. Kustrowski, J. Catal. 239 (2006) 137.

[11]   J.N. Michaels, PhD Dissertation, Massachusettes Institute of Technology, Cambridge, Massachusetts, 1983.

[12]   W.W. Keading, Catal. Rev. 8 (1973) 307.

[13]   M. Rep, PhD Dissertation, University of Twente, Netherlands, 2002.

[14]   L.E. Drehman, D.W. Walker, US 3 437 703 (1969).

[15]   T. Imai, D.Y. Jan, US 4 788 371 (1988).

[16]   T. Imai, R.J. Schmidt, US 4 886 928 (1989).

[17]   J.J.F. Freide, M.J. Howard, T.A. Lomas, EU 332 289 (1989).

[18]   J.C. Bricker, T. Imai, D.E. Mackowiak, US 4 717 779 (1988).

[19]   J.G.A. Bitter, UK 2 201 159 (1986).

[20]   W.R. Moser, Y. Becker, A.G. Dixon, Y.H. Ma, in Proc. Fifth Annu. Meet. North Am. Membrane Soc. Lexington, Kentucky, 1992, 11E.

[21]   R. Craciun, N. Dulamita, Ind. Eng. Res. 38 (1999) 1357.

[22]   G.E. Vrieland, Appl. Catal. 77 (1991) 1.

[23]   N. Mimura, I. Takahara, M. Saito, T. Hattori, K. Ohkuma, M. Ando, Catal. Today 45 (1998) 61.

[24]   T.G. Alkhazov, A.E. Lisovskii, M.G. Safarov, A.M. Dadasheva, Kinet. Katal. 13 (1972) 509.

[25]   G.E. Vrieland, H.N. Nelson, US 3 733 327 (1973).

[26]   E.G. Shcheglova, T.G. Alkhazov, Kinet. Katal. 23 (1982) 1272.

[27]   T.G. Alkhazov, A.E. Lisovskii, Kinet. Katal. 17 (1976) 434.

[28]   G. Emig, H.J. Hofmann, J. Catal. 84 (1983) 15.

[29]   A. Schraut, G. Emig, H.J. Hofmann, J. Catal. 112 (1988) 221.

[30]   A. Schraut, G. Emig, H.G. Sockel, Appl. Catal. 29 (1987) 311.

[31]   L.E. Cadus, O.F. Gorriz, J.B. Rivarola, Ind. Eng. Chem. Res. 29 (1990) 1143.

[32]   R.S. Drago, K. Jurczyk, Appl. Catal. A 112 (1994) 117.

[33]   A.G. Ruiz, T.R. Ramos, Carbon 32 (1994) 23.

[34]   M.F.R. Pereira, J.J.M. Orfao, J.L. Figueiredo, Colloid Surf. A 241 (2004) 165.

[35]   M.F.R. Pereira, J.J.M. Orfao, J.L. Figueiredo, Appl. Catal. A 184 (1999) 153.

[36] M.F.R. Pereira, J.J.M. Orfao, J.L. Figueiredo, Appl. Catal. A 196 (2000) 43.

[37] M.F.R. Pereira, J.J.M. Orfao, J.L. Figueiredo, Appl. Catal. A 218 (2001) 307.

[38] N. Maksimova, G. Mestl, R. Schlögl, Stud. Surf. Sci. Catal. 133 (2001) 383.

[39] G. Mestl, N.I. Maksimova, N. Keller, V.V. Roddatis, R. Schlögl, Angew. Chem. Int. Ed. 40 (2001) 2066.

[40] D.S. Su, N. Maksimova, J.J. Delgado, N. Keller, G. Mestl, M.J. Ledoux, R. Schlögl, Catal. Today. 102-103 (2005) 110.

[41] B. Nigrovski, P. Scholz, T. Krech, N.V. Qui, K. Pollok, T. Keller, B. Ondruschka, Catal. Commun. 10 (2009) 1473.

Chapter 3

Experimental methods

3.1. Materials

MWCNTs "Baytubes$^{®}$" used in this study were purchased from Bayer Technology Services GmbH. As reported by manufacturer, MWCNTs with a high degree of purity (low concentration of free residual catalyst and absence of free amorphous carbon) were produced in a high-yield process based on catalytic chemical vapour deposition. The main properties of "Baytubes$^{®}$" MWCNTs are presented in Table 3.1.

Table 3.1. The properties of "Baytubes®" MWCNTs

Property	Value
C-purity	>95%
Number of walls	3-15
Outer mean diameter	13-16 nm
Inner mean diameter	4 nm
Length	1-10 μm
Apparent density	150-350 kgm^{-3}

Hydrogen peroxide was purchased from Solvay GmbH. Hydrochloride acid and styrene were purchased from Merck. Ethylbenzene (purity > 99%) was from VEB Jenapharm, Labor Chemie Apolda.

3.2. Characterization of samples

The **BET** specific surface area and the pore volume of several samples were determined from the adsorption isotherms of nitrogen at 77 K, using a Quantachrome Autosorb apparatus.

Transmission electron microscopy (**TEM**) images were obtained on a LEO 922 microscope at an accelerating voltage of 20 kV. The samples were dispersed in ethanol then grinded in a mortar and finally coated on Cu-Lacey-grids.

In chapter 4, the samples in the form of KBr disk were measured with Fourier transform infrared (**FTIR**) on a Bruker IFS 66 spectrometer. All spectra were smoothed (Savitsky-Golay-5 points function) and baseline corrected. In chapter 5 and 6, FTIR spectra of samples with KBr were recorded on a Spectrum 100 (Perkin-Elmer)

Raman spectra of samples were obtained on a JY-HR 800 at an excitation wavelength of 532 nm.

X-ray photoelectron spectroscopy (**XPS**) was measured on a Quantum 2000 instrument at room temperature with a focused monochromatic Al Kα source at 1486.6 eV for excitation.

Thermogravimetric analysis (**TGA**) was carried out from room temperature to 800 °C with heating rate 20 K min^{-1} on a Shimadzu TGA-60

3.3. ODEB catalytic test

The diagram of the ODEB catalytic testing system is shown in Figure 3.1. The catalytic tests under conventional heating were carried out in a tubular quartz reactor, inner diameter 20 mm, length 330 mm. Typically 1.0 g catalyst was held in the isothermal oven by quartz wool plugs. Mass flow controllers (Brooks 5890) were used to adjust the flow rates (Figure 3.1). A nitrogen flow was used for carrying EB vapor from the saturator which the temperature was fixed at 38 °C by a cryostat. EB vapor was then mixed with air and fed in the reactor. The concentration of EB in the stream was kept at 2.3 vol.%. The total flow rate was fixed at 55 ml min^{-1}. A Chromel/Alumel thermocouple was inserted into the catalyst bed for recording the reaction temperatures. All stainless steel transfer lines were kept at 110 °C by heating tape in order to prevent the condensation of ethylbenzene (EB) and styrene (ST).

The educts and products were analyzed by gas chromatograph (GC) on an Agilent 7890 A equipped with flame ionization detector (FID) and thermal conductivity detector

(TCD). Two columns HP-5 (50 m x 0.32 mm x 1.05 μm) and molsieve 5A PLOT (30 m x 0.32 mm x 30 μm) were used for the analysis of hydrocarbons and COx, respectively. For detailed information of GC parameters see Appendix A.
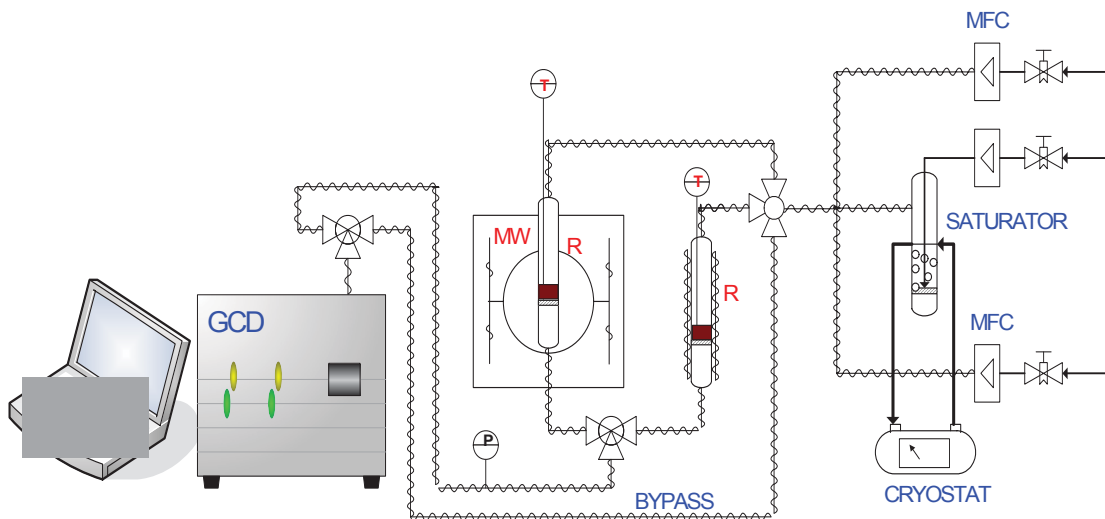

Figure 3.1. Schematic diagram of the ODEB catalytic testing system.

The reactions were considered in steady-state when at least three consecutive measurements showed constant composition (within 5% deviation).

The catalyst performance was evaluated in terms of the conversion of ethylbenzene (X_{EB}), selectivity of styrene (S_{ST}), and styrene yield (Y_{ST}) according to the following equations:

$$X_{EB} = \frac{EB_{reacted}}{EB_{fed}} \qquad (3.1)$$

$$S_{ST} = \frac{ST_{formed}}{EB_{reacted}} \qquad (3.2)$$

$$Y_{ST} = (X_{EB} \; x \; S_{ST}) \qquad (3.3)$$

The coke deposition (Δm) on catalysts after the ODEB reaction was calculated by:

$$\Delta m = \frac{mass\ of\ catalyst_{reacted} - mass\ of\ catalyst_{fresh}}{mass\ of\ catalyst_{fresh}} \qquad (3.4)$$

Chapter 4

Functionalization of MWCNTs by hydroxyl radicals

4.1. Introduction

As mentioned in chapter 2, styrene is an important monomer for polystyrene and its derivatives. It has been normally produced by the catalytic dehydrogenation of EB in the temperature range 550 - 650 °C on iron oxide catalysts and large amounts of steam.

A variety of nanostructured carbons, such as CNTs [1, 2], carbon nanofibers [3, 4], onion-like carbon [5] and nanodiamond [6] have been found to catalyze the ODEB to styrene efficiently. In comparison to the traditional metal oxide catalysts, certain nanocarbons demonstrate a comparable, or even better, catalytic performance and long-term stability for the reaction within the optimal temperature range of 300 - 450 °C. It was demonstrated that the presence of oxygen-containing surface functional groups on the nanocarbon catalysts were responsible for the catalytic reaction [7]. Functionalization of nanostructured carbon can provide numerous active sites, and hence increasing the catalytic activity.

CNTs are usually functionalized by harsh oxidative processes, such as refluxing in a mixture of H_2SO_4/HNO_3 to generate defects on the sidewalls and tube tips, those defects can serve as anchor groups for functionalization and/or can provide sites for the coordination chemistry [8]. However, such oxidation method usually reduces the crystallinity and corrosion resistance of CNTs due to the introduction of a large number of defects. Therefore, development of a better and more effective functionalization method that can not only introduce high density and homogeneous surface functional groups but also has little or no structural damage to CNTs remains a major challenge. Hydrogen peroxide in acidic solution, such as the 'piranha' solution of H_2SO_4/H_2O_2, is one of the most powerful oxidizers known, and has been used for chemical oxidation of

CNTs [9, 10]. Hydrogen peroxide in water is a relative mild oxidant. It is a significant oxidant in the advanced oxidation processes (AOP), such as Fenton reaction, which commonly have been used for the oxidation and destruction of various organic contaminants in pesticides [11] or in dye effluents [12]. In such reactions, H_2O_2 is an oxidizing agent, and can be utilized to produce highly reactive hydroxyl radicals that their participation in reaction enhances the effectiveness of the process. Indeed, hydroxyl radical is one of the strongest chemical oxidizing agents.

The redox potential is formally known as the oxidation potential. A higher positive potential means that the agent is a stronger oxidant. As shown in the Table 4.1 [13], the oxidation potential of hydroxyl radical is extremely high.

Table 4.1. Oxidation potential of some oxidizing agents

Type of oxidizing agent	Oxidation potential ($E°$), (V)
Fluorine	3.06
Hydroxyl radical	2.80
Oxygen (atomic)	2.42
Ozone gas	2.08
Hydrogen peroxide	1.78
Hypochlorite	1.49
Chlorine gas	1.36
Chlorine dioxide	1.27
Oxygen (molecular)	1.23

It was reported [14] that hydroxyl radical can be generated through the direct photolysis of H_2O_2 with light of wavelength 253.7 nm:

$$H_2O_2 \ + \ h\nu \ \rightarrow \ 2 \ HO^{\cdot} \qquad\qquad (4.1)$$

as well as through the Fenton reaction:

$$Fe^{2+} \ + \ H_2O_2 \ \rightarrow \ Fe^{3+} \ + \ HO^{\cdot} \ + \ OH^{-} \qquad (4.2)$$

Li et al. [15] were the first ones applying Fenton reaction to functionalize MWCNTs. The experimental results showed that the original graphene structure was disordered or destroyed by the newly generated oxygen-containing functional groups including -OH, -COOH and -C=O groups.

Nevertheless, insoluble iron-sludge (Fe^{3+}) that is derived from Fenton process could be deposited in nanotubes, and hence an additional purification step might be added to the process.

Here, we propose an efficient and easy method to functionalize MWCNTs with the presence of hydroxyl radicals formed by photodecomposition of H_2O_2 under ultraviolet light (UV). A series of functionalized MWCNTs were prepared with hydroxyl radicals. The textural and structural properties of the samples after functionalization as well as after the ODEB tests were characterized by a variety of techniques.

4.2. Functionalization of MWCNTs by hydroxyl radicals via UV irradiation of H_2O_2 (UV/H_2O_2)

The UV/H_2O_2 functionalization of MWCNTs was performed in a 1 L glass-vessel photoreactor (Figure 4.1).
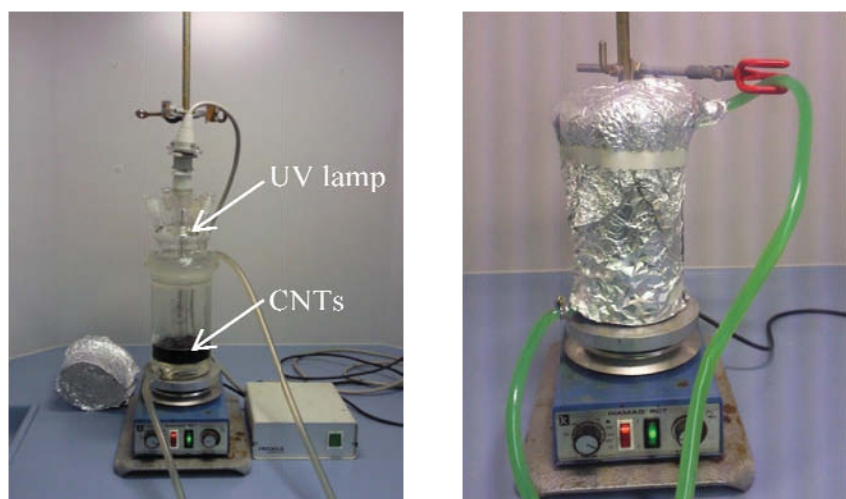
Figure 4.1. An experimental setup for UV/H_2O_2 functionalization of MWCNTs.

A Hanau low-pressure mercury vapor UV lamp emitting mainly at 254 nm with an input 15 W acted as photon supplying source. The UV lamp was inserted into a hollow quartz tube and located at the center of the reactor. The reactor was covered completely with aluminum foil in order to prevent some UV rays loss. Typically, 3 g as-received MWCNTs was placed into the reactor while UV light was turned on, then 500 ml of aqueous H_2O_2 solution at various concentrations were added slowly under vigorous stirring (250 rpm). The oxidative treatment of MWCNTs was carried out at 15 °C for 7.5 h. Next, the resulting mixture was filtered through a wide pore filter paper. The black solid was washed 3 times with de-ionized water and dried overnight in an oven at 120 °C. Finally, black powder was ground in a mortar and sieved at a fraction of 250 µm. In order to compare the influence of radicals on MWCNTs, a blank sample was also prepared similarly but without UV illumination.

Table 4.2. Codes of the prepared samples

Sample name	% H_2O_2 used for functionalization	UV
UV/H35	35	X
UV/H50	50	X
UV/H60	60	X
H35	35	N

(X: with UV irradiation; N: without UV illumination)

4.3. Results and discussion

4.3.1. Characterization

The presence of oxygen-containing surface groups on CNTs is detected by infrared spectroscopy. The IR spectra of as-received and functionalized materials are presented in Figure 4.2. The common features common of all samples are as follows: a wide peak at about 3434 cm^{-1} could be assigned to the O-H stretching mode of hydroxyl groups and absorbed water. Two sharp, narrow and intensive peaks at 2922 and 2855 cm^{-1} are a result of the aliphatic C-H stretching in CH_2 and CH_3, respectively [16]. A sharp intensity peak at 1630 cm^{-1} could be attributed to the adsorbed water [17]. Two small

peaks at 1583 and 1742 cm^{-1} originates from the aromatic ring vibration and C=O in carbonyl or carboxylic groups, respectively [17]. The broad peak at 1059 cm^{-1} could be indicated to the C-O stretching in acids, alcohols, phenols, esters and ethers [16, 18].

This result indicates that oxygenated functional groups existed previously on as-received MWCNTs as a result of the CVD process [19]. The intensities of C-O and C=O peaks on UV/H35 are higher than those on H35, indicating that the presence of hydroxyl radicals in the oxidative process improved the formation of oxygenated surface groups on the MWCNTs.
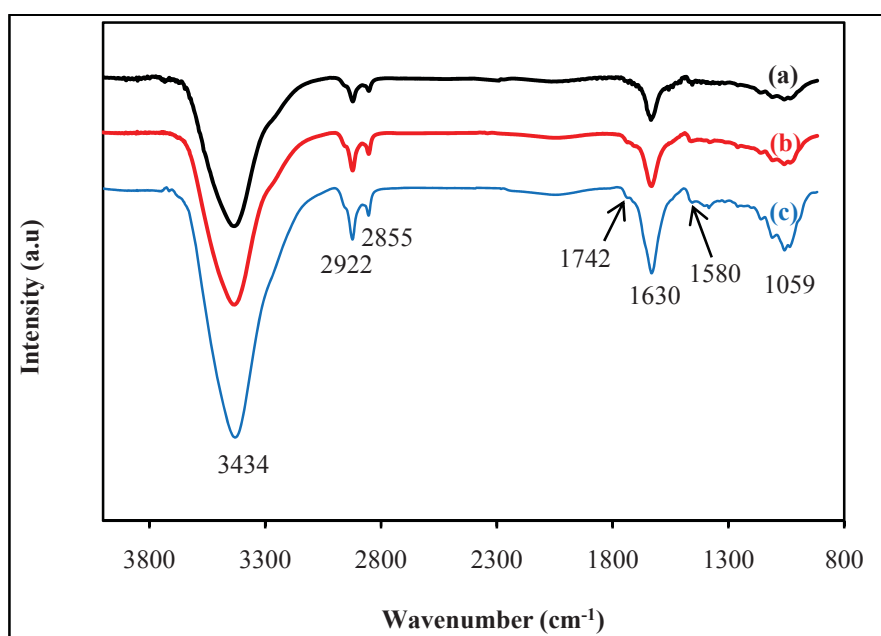
Figure 4.2. FTIR spectra of as-received (a), H35 (b), and UV/H35 (c) in KBr.

Raman spectroscopy is commonly used as a tool for reflecting the order of CNTs structure. The Raman spectra of as-received, H35 and UV/H35 samples are shown in Figure 4.3.
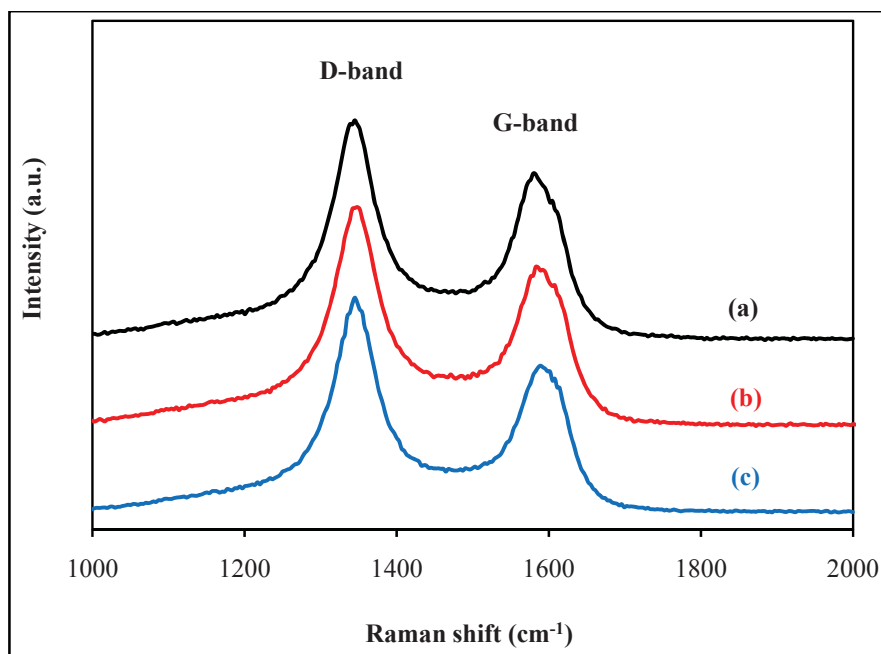
Figure 4.3. Raman spectra of as-received CNTs (a), H35 (b), and UV/H35 (c).

Each of them consists of two characteristic bands, namely the D-band at $\sim$ 1348 cm^{-1} and the G-band at $\sim$ 1583cm^{-1}. The D-band is usually attributed to the disorder or sp^3-hybridized carbon and the G-band corresponds to the graphite in-plane vibration [15]. It can be seen that there is no change in frequencies of D- and G-band in H35 sample. However, the center position of G-band in UV/H35 sample is moved from 1583 to 1592 cm^{-1}. This change could be related to a significant change of chemical surface of the sample. The relative intensity ratio of D- and G-band (I_D/I_G) could be used to evaluate this change [20, 21]. The I_D/I_G ratio (Table 4.3) of the oxidized MWCNTs are higher than that of as-received CNTs, implying that more oxygenated functional groups could be attached on the surface of the nanotubes. In addition, a higher relative intensity I_D/I_G ratio of UV/H35 than that of H35 was observed, indicating that the presence of hydroxyl radicals in the UV/H$_2$O$_2$ oxidative treatment might strength the formation of oxygenated surface groups in the oxidative treatment, well agreement with the FTIR results.

Table 4.3. D- and G-band frequencies, relative intensity ratio I_D/I_G of as-received CNTs, H35 and UV/H35.

Sample	vD (cm^{-1})	vG (cm^{-1})	I_D/I_G
as-received CNTs	1348	1583	1.29
H35	1348	1583	1.34
UV/H35	1348	1592	1.42

The TEM pictures of as-received MWCNTs and UV/H35 are illustrated in Figure 4.4. It is seen that as-received MWCNTs are closed at the tubes ends. They also contained metallic particles and amorphous carbon impurities. These impurities were removed effectively after the UV/H_2O_2 treatment.
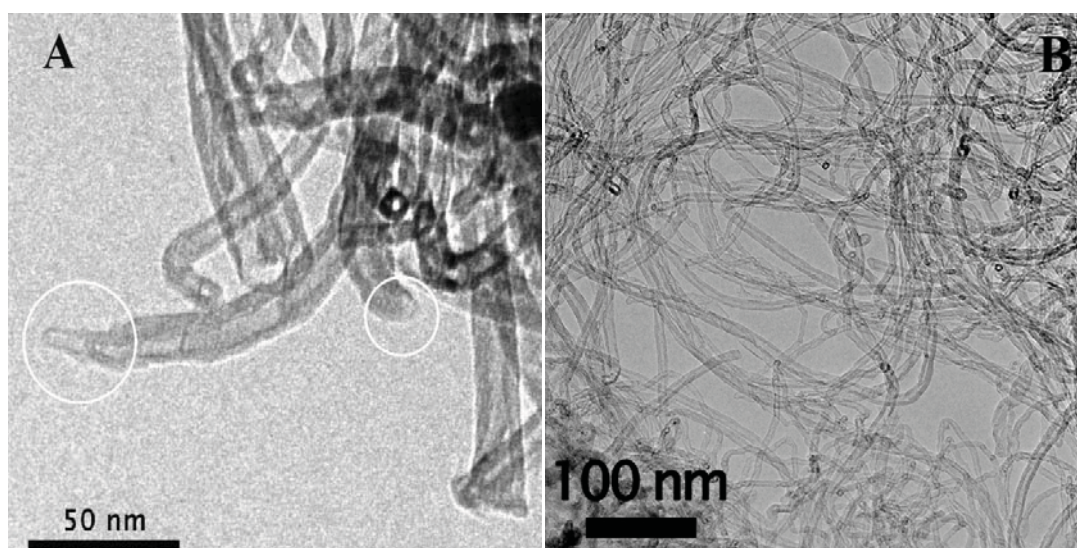
Figure 4.4. TEM pictures of as-received CNTs (A) and UV/H35 (B).
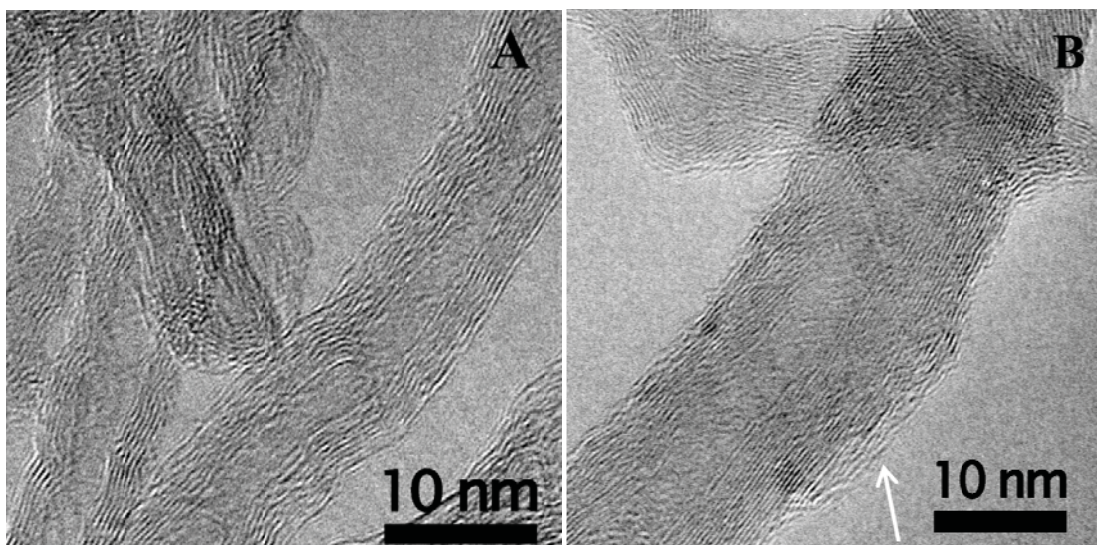
Figure 4.5. High resolution TEM pictures of UV/H35 before (A) and after (B) 24 h time on stream.

High resolution TEM pictures of UV/H35 before and after 24 h time on stream ODEB are illustrated in Figure 4.5. After the catalytic reaction, the wall structure of UV/H35 has been altered (Figure 4.5B): the external surface of tubes are covered incompletely by new several layers of carbon deposit (as arrows shown): one side of tube is thicker due to adding of new carbon layers but the other side remains unchanged. The new layers on the outer shell look like graphitic carbon with short-range ordering. Additionally, the ends of the new layers seem to be partially oxidation [1, 4]. It was proposed that these partially oxidized prism faces presumably play an important role in the catalytic reaction. In addition, our previous study showed new sp^2-carbon deposit layers have been observed on the oxidized CNTs under microwave heating [2].

XPS is typically used to analyze the chemical surface of materials. It can provide useful information about functional groups and defects of the nanotubes [21, 22]. The XPS C1s spectra could be deconvoluted into five points, including C=C (284.6), C-OH (285.6), C=O (287.1), COOH (288.9) and π-π^* stacking at (290.9 eV) [22]. Figure 4.6 displays the XPS C1s deconvolution of the different oxidized MWCNTs.
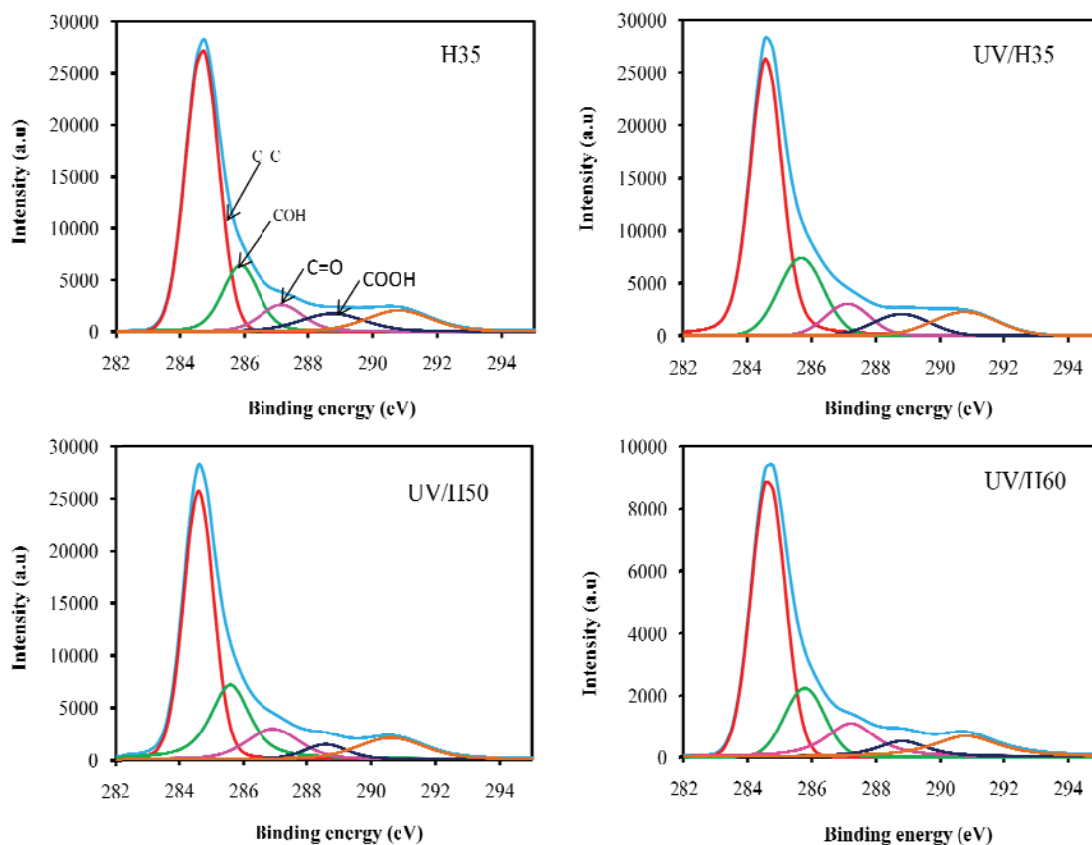
Figure 4.6. XPS C1s deconvolution of H35, UV/H35, UV/H50 and UV/H60.

Figure 4.7 compares the XPS C1 deconvolution of H35 and UV/H35 catalysts after the ODEB reaction.
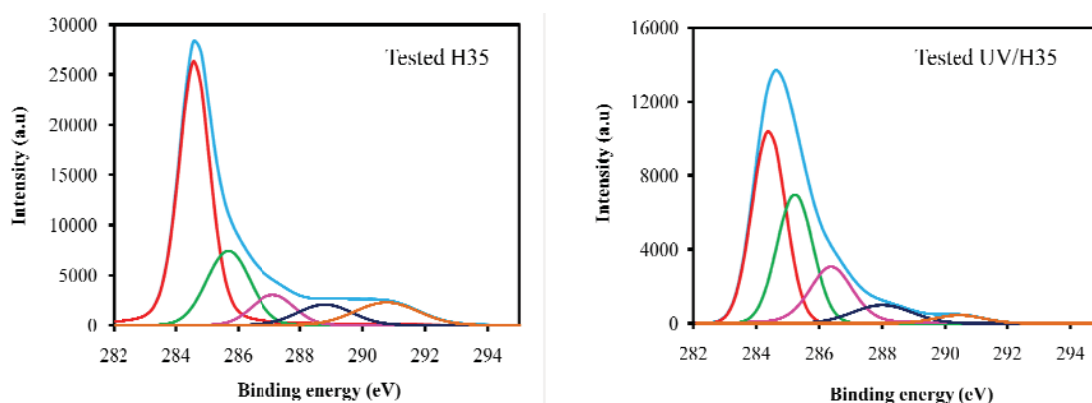
Figure 4.7. XPS C1s deconvolution of H35 and UV/H35 after the ODEB.

Table 4.4 summarizes the fractions of oxygenated surface functional groups on different MWCNTs. As shown in Table 4.4, oxygenated surface functional groups have existed previously on the surface of as-received CNTs. After the oxidative treatment, more oxygenated functional groups were introduced onto the treated MWCNTs. This fact is consistent with the results of XPS C1s and FTIR analyses above (Figure 4.2). It is seen that the oxidation of nanotubes can be assisted with the presence of hydroxyl radicals in the process. Indeed, at the same concentration of hydrogen peroxide solution (35 wt.% H_2O_2), more oxygenated functional groups (hydroxyl and carbonyl groups) are generated on the surface of MWCNTs with UV illumination rather than without UV illumination.

Table 4.4. XPS C1s fractions of functional groups on different MWCNTs

Sample	C=C (%)	C-OH (%)	C=O (%)	COOH (%)
as-received CNTs	63.9	20.7	8.1	4.9
H35	57.6	16.7	8.1	8.1
UV/H35	52.0	18.8	15.2	3.1
UV/H50	55.4	14.0	13.3	6.7
UV/H60	53.7	13.2	6.2	5.9
Tested H35	56.7	19.7	7.9	6.9
Tested UV/H35	42.3	30.4	17.5	7.1

When H_2O_2 in the in the UV/H_2O_2 process was used at concentrations greater than 35 wt.%, it is seen that the fraction of C=O and C-OH on UV/H50 and UV/H60 decreased continuously as compared with UV/H35, indicating that the available amount of hydroxyl radicals for the oxidation possibly can be reduced due to the scavenging of these radicals in the process, as expressed by the following equations [23, 24]:

$$HO^{\cdot} + H_2O_2 \rightarrow H_2O + HO_2^{\cdot} \qquad (4.3)$$

$$HO_2^{\cdot} + HO^{\cdot} \rightarrow H_2O + O_2 \qquad (4.4)$$

$$HO^{\bullet} + HO^{\bullet} \rightarrow H_2O_2 \qquad\qquad (4.5)$$

The scavenging can reduce the number of hydroxyl radicals for the process, leading to a decline in the oxidation of nanotubes

TGA results of as-received and oxidized MWCNTs are presented in Figure 4.8. The samples weights as a function of temperature could be divided into three levels, corresponding to three regions of temperature. Below 150 °C, all samples diminish a minor weight (< 1%) corresponding to an evaporation of the adsorbed water. Between 150 and 500 °C, the observed samples weights are relatively high, and could be attributed to the decarboxylation of carboxylic groups and the elimination of hydroxyl groups attached to the sidewalls of MWCNTs [19]. The drastic loss occurring above 500 °C for as-received and above 550 °C for oxidized MWCNTs could be related to the degradation of disordered or amorphous carbon. The weights of oxidized MWCNTs are not as strong as in the as-received ones. This result indicates that amorphous carbon in the oxidized MWCNTs eliminated substantially by the oxidative treatment, agreement with previous investigations [19, 25].
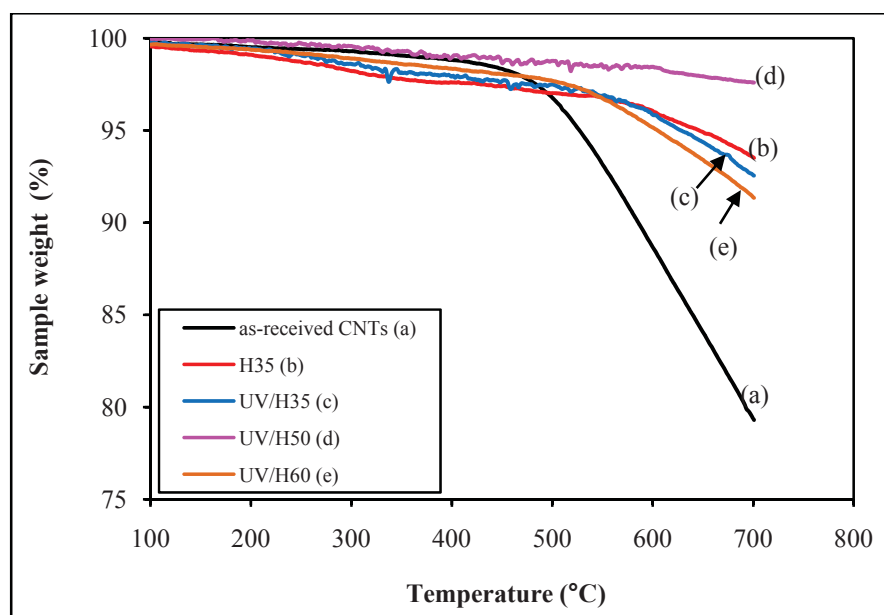
Figure 4.8. TGA curves of as-received and oxidized CNTs under nitrogen flow rate of 30 ml min^{-1}and heating rate of 20 K min^{-1}.

4.3.2. ODEB catalytic tests

Table 4.5 shows the results of ethylbenzene conversion (X_{EB}), styrene selectivity (S_{ST}) and styrene yield (Y_{ST}) as a function of the reaction temperatures of various catalysts. For H35 and UV/H35, EB conversion increases rapidly while ST selectivity decreases slightly in the temperature range from 350 to 400 °C. At different reaction temperatures, the EB conversion of H35 and UV/H35 are similar, but styrene selectivity of UV/H35 is always higher than that of H35. In particular, ST selectivity has been found to be 88 and 94% at 350 °C, 86 and 92% at 375 °C, 83 and 91% at 400 °C of H35 and UV/H35, respectively. Therefore, it can be concluded that MWCNTs oxidized with radicals reached a higher selectivity than the samples treated without radicals. For UV/H50 and UV/H60 catalysts, EB conversion and ST selectivity increase simultaneously with the rise of reaction temperature from 350 to 375 °C. The increase of EB conversion and the decrease of ST selectivity have been observed at 400 °C. It is seen that an increase in hydrogen peroxide concentration of the oxidative treatment from 35 to 50 and 60 wt.% did not lead to an improve of ST yield for the catalysts as expected. At 400 °C, ST yield obtained 42% for UV/H35, 38% for UV/H50 and 35% for UV/H60 (Table 4.5). At 400°C, the ST yield of UV/H35 achieved two times higher than that of as-received CNTs.

Table 4.5. EB conversion (X_{EB}), ST selectivity (S_{ST}) and ST yield (Y_{ST}) versus the reaction temperatures. Test conditions: 1.0 g catalyst, $EB/O_2/N_2 = 2.3:2.3:95.4$ (vol.%), total flow 55 ml min^{-1}.

Samples	350 °C			375 °C			400 °C		
	X_{EB}	S_{ST}	Y_{ST}	X_{EB}	S_{ST}	Y_{ST}	X_{EB}	S_{ST}	Y_{ST}
as-received CNTs	27	65	18	35	64	22	34	61	21
H35	20	88	18	32	86	28	47	83	39
UV/H35	20	94	19	32	92	29	46	91	42
UV/H50	19	81	15	28	89	25	47	80	38
UV/H60	24	82	20	33	87	29	43	81	35

In order to investigate the stability of the catalysts, long-term catalytic tests were carried out at 400 °C for 24 h time on stream (Figure 4.9).All catalysts displayed a stable performance for a long-term catalytic test. The conversion of UV/H35 exhibits a slight decrease at the beginning of the reaction then it tends to increase slightly with time on stream. The ST selectivity of UV/H35 still maintains the highest value (~ 91%) after 24 h time on stream.
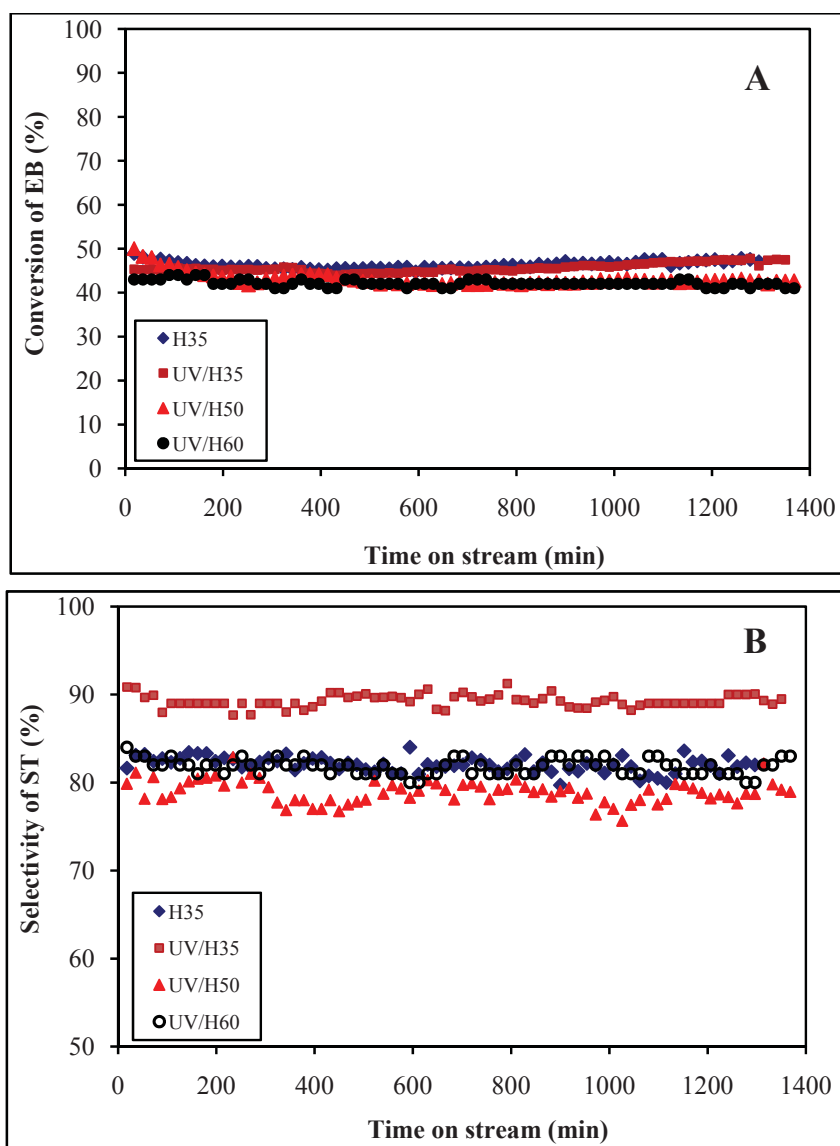
Figure 4.9. EB conversion (A) and ST selectivity (B) of different oxidized MWCNT as a function of time on stream at 400 °C. Test conditions:1.0 g catalyst, EB/O_2/N_2 = 2.3:2.3:95.4 (vol.%) total flow 55 ml min^{-1}

The chemical surface of catalysts has been altered after the ODEB test. As compared the XPS C1s fractions of fresh UV/H35 and tested UV/H35 (Table 4.4), it is seen that the C=C fraction is diminished and the content of oxygenated functional groups enlarged for tested UV/H35. This indicates more oxygenated groups formed on the catalyst after the ODEB. In particular, an increase in hydroxyl and carbonyl groups has been observed on tested UV/H35 catalyst. It has been ascribed that these groups can be the active sites for the reaction. For H35, an increase in hydroxyl groups has been found but the fraction of carbonyl groups seems to be unchanged after the reaction. It is concluded that MWCNTs oxidized with radicals result in a higher catalytic performance than samples treated without radicals.

4.4. Conclusions

The oxidative treatment of MWCNTs with H_2O_2 and with UV/H_2O_2 is applied successfully to introduce a variety of oxygenated functional group to the surfaces of nanotubes. The characteristic of the oxidized CNTs indicated that the presence of hydroxyl radicals via UV illumination of H_2O_2 increased the content of oxygenated surface functional groups on the MWCNTs as compared with the treating without radicals. That is confirmed by Raman and XPS results. Using hydrogen peroxide solutions with concentrations higher than 35 wt.% for the radical oxidation of MWCNTs did not enhance the surface oxygen content as expected. The effectiveness of the oxidation could be declined by the scavenging of radicals instead. As a result, the catalytic performance of UV/H35 catalyst is better than that of UV/H50 or UV/H60. At 400 °C and molar ratio EB/O_2 of 1:1, ethylbenzene conversion and styrene selectivity of UV/H35 catalyst achieved 47 and 91%, respectively, for several hours time on stream. The styrene yield of UV/H35 is two times higher than that of as-received MWCNTs. New layers of graphitic carbon deposited on the outer side of MWCNTs have been observed on UV/H35 catalyst after the ODEB. A significant increase in the fraction of

hydroxyl and carbonyl groups has also been observed on the UV/H35 after the reaction. These functional surface groups seem to be the active phases for the reaction.

4.5. References

[1]   D.S. Su, N. Maksimova, J.J. Delgado, N. Keller, G. Mestl, M.J. Ledoux, R. Schlögl, Catal. Today 102-103 (2005) 110.

[2]   B. Nigrovski, P. Scholz, K. Krech, N.V. Qui, K. Pollok, T. Keller, B. Ondruschka, Catal. Commun. 10 (2009) 1473.

[3]   T.J. Zhao, W.Z. Sun, X.Y. Gu, M. Ronning, D. Chen, Y.C. Dai, W.K. Yuan, A. Holmen, Appl. Catal. A 323 (2007) 135.

[4]   G. Mestl, N. Maksimova, N. Keller, V. Roddatis, R. Schlögl, Angew. Chem. Int. Ed. 40 (2001) 2066.

[5]   N. Keller, N.I. Maksimova, V.V. Roddatis, M. Schur, G. Mestl, Y.V. Butenko, V.L. Kuznetsov, R. Schlögl, Angew. Chem. Int. Ed. 41 (2002) 1885.

[6]   D.S. Su, N. Maksimova, G. Mestl, V. Kuznetsov, V. Keller, R. Schlögl, N. Keller, Carbon 45 (2007) 2145.

[7]   M.F.R. Pereira, J. J. M. Orfao, J. L. Figueiredo, Appl. Catal. A 218 (2001) 307.

[8]   L. Li, Y. Xing, J. Phys. Chem. C 111 (2007) 2803.

[9]   A. Rasheed, J.Y. Howe, M.D. Dadmun, P.F. Britt, Carbon 45 (2007) 1072.

[10]   A. Kuznetsova, I. Popova, J.T.J. Yates, M.J. Bronikowski, C.B. Huffman, J. Liu, R.E. Smalley, H.H. Hwu, J.G. Chen, J. Am. Chem. Soc. 123 (2001) 10699.

[11]   W.Z. Tang, C.P. Huang, Environ. Technol. 17 (1996) 1371.

[12]   M.S. Lucas, J.A. Peres, Dyes Pigm. 71 (2006) 236.

[13]   A. Al-Kdasi, A. Idris, K. Saed, C.T. Guan, Global Nest Int. J. 6 (2004) 226.

[14]   N.A. Milas, P.F. Kurz, W.P. Anslow, J. Amer. Chem. Soc. 59 (1937) 343.

[15]   W. Li, Y. Bai, Y. Zhang, M. Sun, R. Cheng, X. Xu, Y. Chen, Y. Mo, Synth. Metals 155 (2005) 509.

[16]   M.M. Rao, A. Ramesh, G.P.C. Rao, K. Seshaiah, J. Hazard. Mater. B 129 (2006) 123.

[17]   M.S.P. Shaffer, X. Fan, A.H. Windle, Carbon 36 (1998) 1603.

[18]   A.M. Puziy, O.I. Poddubnaya, A.M. Alonso, F. S. Garcia, J.M.D. Tason, Carbon 41 (2003) 1181.

[19]   F. Aviles, J.V.C. Rodriguez, L.M. Tah, A.M. Pat, R.V. Coronado, Carbon 47 (2009) 2970.

[20]   K. Imasaka, J. Suehiro, Y. Kanatabe, Y. Kato, Nanotechnol. 17 (2006) 3421.

[21]   X. Zhang, L. Lei, B. Xia, Y. Zhang, J. Fu, Electrochim. Acta 54 (2009) 2810.

[22]   P. Serp, J.L. Figueiredo, Ed., Carbon material for catalysis, John Wiley & Sons Inc., Hoboken, New Jersey, 2009, p. 67.

[23]   C.L. Hsueh, Y.H. Huang, C.C. Chen, J. Mol. Catal. A 245 (2006) 78.

[24]   G.S. Wang, S.T. Hsieh, C.S. Hong, Wat. Res. 34 (2000) 3882.

[25]   V. Datsyuk, M. Kalyva, K. Papagelis, J. Parthenios, D. Tasis, A. Siokou, I. Kallitsis, C. Galiotis, Carbon 46 (2008) 833.

Chapter 5

Effects of ozone treatment and microwave heating on the surface properties and the catalytic behavior of MWCNTs in the ODEB

5.1. Introduction

Since the presence of carbon deposits on metal oxide catalysts give an increase in the catalytic activity of the ODEB to styrene, a variety of carbonaceous materials have been tested and found to catalyze the reaction efficiently (Figure 5.1).
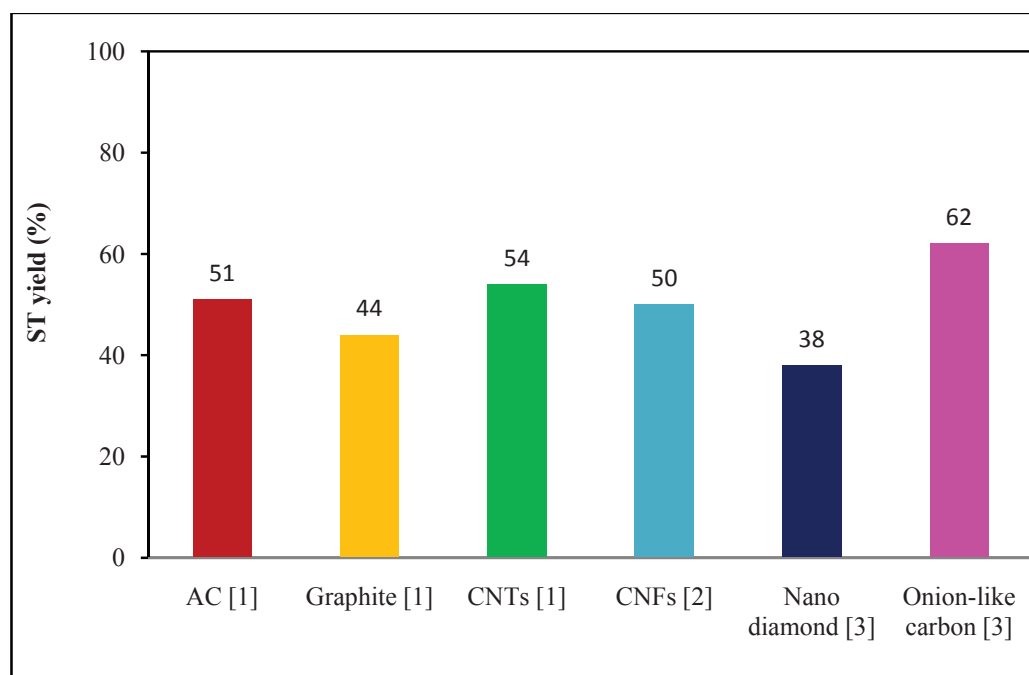
Figure 5.1. Comparison of ST yield over various carbon catalysts in the ODEB.

It is speculated that C=O bonds of oxygen-containing groups (carbonyl, quinone) on the carbon catalysts are the active sites in the reaction [4, 5]. The proposed mechanism consists of a redox reaction between the pair of carbonyl/hydroxyl and styrene/ethylbenzene [5-7].

There have been some efforts to improve the performance of the carbon catalysts by enhancing more oxygenated surface groups through the oxidative functionalization methods [8, 9]. The number of oxygenated surface groups is strongly dependent on the preparation ways, leading to a large difference in the styrene yield [8]. Typically, oxidation in liquid phase, mostly using hot concentrated HNO_3 or HNO_3/H_2SO_4, introduces largely carboxylic groups, while gas phase treatment, such as exposure to air or ozone, generate more carbonyl than carboxylic groups [10].

In previous chapter, we have examined the oxidation of MWCNTs using hydroxyl radicals, and these oxidized samples are used as the catalysts for the ODEB. The results showed that the ST yield can achieve 42% at 400 °C on UV/H35 catalyst, two times higher than that of as-received samples. As compared with the ST yield of the previously tested sp^2-carbon catalysts it is realized that the ST yield of UV/H35 catalyst is lower (Figure 5.1).

It could be possible to improve the catalytic performance of MWCNTs by controlling the chemical surface of the oxidized samples via oxidative treatments. For the UV/H_2O_2 oxidative process the number of hydroxyl radicals seems to be one of the factors to impact the number of oxygenated surface groups of the oxidized MWCNTs. The control of the number of hydroxyl radicals in the process is really not facile because of the very short life of hydroxyl radicals. Although ozone is less active than hydroxyl radical (Table 4.1 in chapter 4) but the half-life of ozone in air is much longer than that of radical [11], thus, the choice of ozone for the oxidative treatment of CNTs can be more feasible than radical.

Ozonization process has been found to occur selectively on the π-conjugated fullerenes C_{60}, producing the intermediate like fullerene ozonide ($C_{60}O_3$) followed by the formation of $C_{60}O$ which reacts to produce $C_{60}O_2$ [12-15]. This mechanism is similar to Criegee's mechanism between ozone and as described in Figure 5.2 [16].
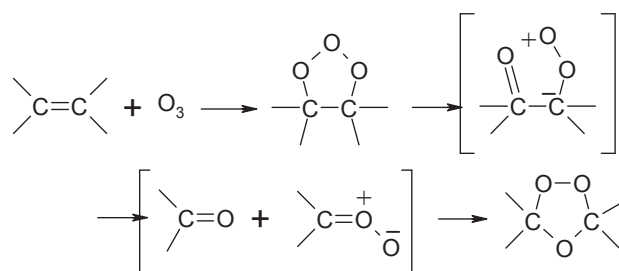
Figure 5.2. Criegee's mechanism of ozone with olefins [16].

Mawhinney et al. [17, 18] studied the oxidation of SWCNT with ozone gas (3% ozone in oxygen). IR spectra showed that the reaction produces two distinct surface-bound functional groups, esters and quinones. Treatment of MWCNTs with ozone has been reported to be effectively on their surface without morphological defects accompanying [19, 20].

It has become common knowledge that ozone is generated in one of two generally accepted ways - by passing an oxygen-containing gas through either a high energy electrical field or through a source of ultraviolet radiation [21, 22]. The first method is known as corona discharge, the other one as ultraviolet irradiation. In ultraviolet produced ozone, air (usually ambient) is passed over an ultraviolet lamp (mostly 185 nm lamp), which can split oxygen molecules into oxygen atoms (O). These atoms attach to other oxygen molecules, forming ozone. In corona discharge method, dried oxygen or air gas is passed through a high energy electrical field (Figure 5.3). The electrical current causes the "split" in the oxygen molecules as described in the section on ultraviolet ozone generation. Since 85% to 95% of the electrical energy supplied to a corona discharge ozone generator produces heat, some method for heat removal is required.
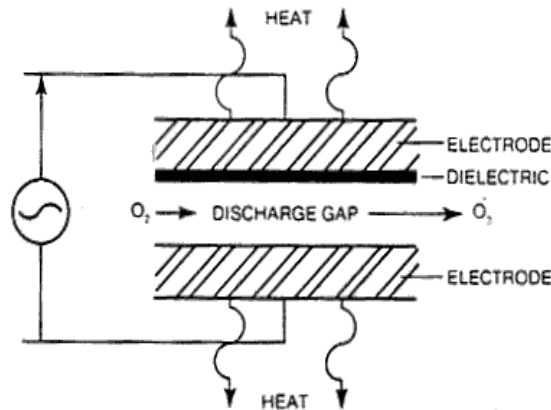
Figure 5.3. Schematic operation of a corona discharge-type ozone generator [22].

Microwave heating chemical reactions have become popular technique because it offers a number of advantages as compared with conventional heating, such as: (i) contactless heating; (ii) energy transfer instead of heat transfer; (iii) rapid heating; (iv) selective material heating; volumetric heating; (vi) quick start-up and stopping; (vii) heating from the interior of the material body; and (viii) higher level of safety and automation [23].

It is known that microwave is a form of electromagnetic energy with wavelength between 0.001 and 1 m, corresponding to frequencies between 300 to 0.3 GHz [24]. Within this range, there are four frequencies assigned to industrial applications: 0.915, 2.450, 5.800 and 22.125 GHz [25]. Most industrial microwave systems utilize 2.450 GHz as their operating frequency.

Materials that absorb microwave radiation are called dielectric materials or microwave absorbers [26]. The ability of a material to be heated in the presence of microwave field is defined by its dielectric loss tangent:

$$\tan \delta = \varepsilon'' / \varepsilon' \qquad (5.1)$$

where ε' is the electric constant (or real permittivity), and ε'' is the dielectric loss factor (or imaginary permittivity).

The dielectric constant (ε´) determines how much of the incident energy is reflected and how much is absorbed, while the dielectric loss factor (ε´´) measures the dissipation of electric energy in form of heat within the material [27].

It is well known that CNTs are excellent microwave absorbents [28]. It has been exploited the advantages of interaction between microwave irradiation and CNTs for the chemical functionalization and purification [29-31] of CNTs. The experiment results of the ODEB on metal oxides supported MWCNTs under microwave irradiation showed a significant improvement in the catalysts performance and consumed energy as compared with conventional heating [9, 32].

In this chapter we perform the remove of amorphous carbon by the thermal oxidation and the elimination of residual catalyst in as-received MWCNT by treatment in hydrochloric acid. Next, the purified MWCNTs are ozonated by ozone in air generated from an ozone-corona discharge generator. The changes on the textural properties and surface chemistry of nanotubes after the modification processes as well as after the ODEB testing are examined by using a variety of analytic techniques. The catalytic behavior of the samples in the ODEB is conducted to evaluate the influence of the treatment. A comparison of the catalytic performance conducted with dielectric heating and conventional heating is examined.

5.2. Experimental

5.2.1. Purification of as-received MWCNTs

The as-received MWCNTs were purified to remove graphitic particles, amorphous carbon and catalyst impurities prior to the deposition. For eliminating amorphous carbon, MWCNTs were treated in air at 400 °C for 1h. To remove the metal oxide catalyst residues, MWCNTs subsequently were dispersed and refluxed in 6M HCl solution at 90 °C for 2 h. Then rinsed with distilled water until the pH of the solution returns to neutral. Finally, the samples were dried at 120 °C over night.

5.2.2. Ozonation of purified MWCNTs

2 g of purified MWCNTs were placed into the tubular glass reactor. Ozone was produced by passing a dry, clean air through a corona discharge-type ozone generator (Fischer Ozon 500). The mixture of ozone in air then was introduced continuously into the reactor chamber at room temperature for 24 h. The gas flow rate was kept at $60 \, l \, h^{-1}$. At the outlet of the reactor the concentration of ozone was measured in situ using an ozone monitor (Fischer Monitor EG-2001). After treatment, samples were dried at 75 °C for 1h then 150 °C for 3 h. The samples were weighted and stored till using. Samples treated in the ozone flows with (730 ± 50), (2900 ± 50) and (13000 ± 50 ppm) were designated as C1-CNTs, C2-CNTs and C3-CNTs, respectively. After the treatment, the weight losses of C1- and C2-CNTs samples are negligible (< 1%). Unfortunately, C3-CNTs sample have been lost up to 96% by deep oxidation to carbon oxides, thus, it is not investigated in this study.

5.2.3. ODEB catalytic tests

The ODEB catalytic tests under conventional heating were described in chapter 3. The reaction under microwave irradiation was performed at the same reaction conditions as in the conventional test in order to obtain comparable results. The quartz tube fixed-bed reactor (20 mm i.d., 610 mm length) was inserted into the multimode microwave oven (MLS-Ethos 1600). Microwave energy input was controlled by switched-mode power supplies from 10 to 1000 W for each magnetron. Because a metallic thermocouple (K-type) is sensitive to microwave irradiation, thus, the temperature of catalyst bed was measured by a rapid insertion of the thermocouple onto a catalyst at the moment that microwave power was shortly interrupted, as described in detail by Will et al. [33].

5.3. Results and discussion

5.3.1. Characterization of the MWCNTs after the purification and ozonation

5.3.1.1. Thermal stability

The most common and simple way to study the resistance of the carbonaceous material towards temperature is thermogravimetric analysis [20]. Figure 5.4 shows the results of TGA in oxygen flow of as-received, p-, C1- and C2-CNTs. The as-received CNTs were

oxidized completely at 580 °C and remained 2.4% residual metal, while the p-CNTs were oxidized totally at 720 °C and no residues have been observed after burning. The maximum gasification temperatures of C1- and C2-CNTs are similar at 700 °C. It has to be noticed that the thermal stability of CNTs depends on the concentration of surface groups, the extent of defects and the presence of residual metal particles. Metal particles in nanotubes can be the catalysts for the carbon oxidation.
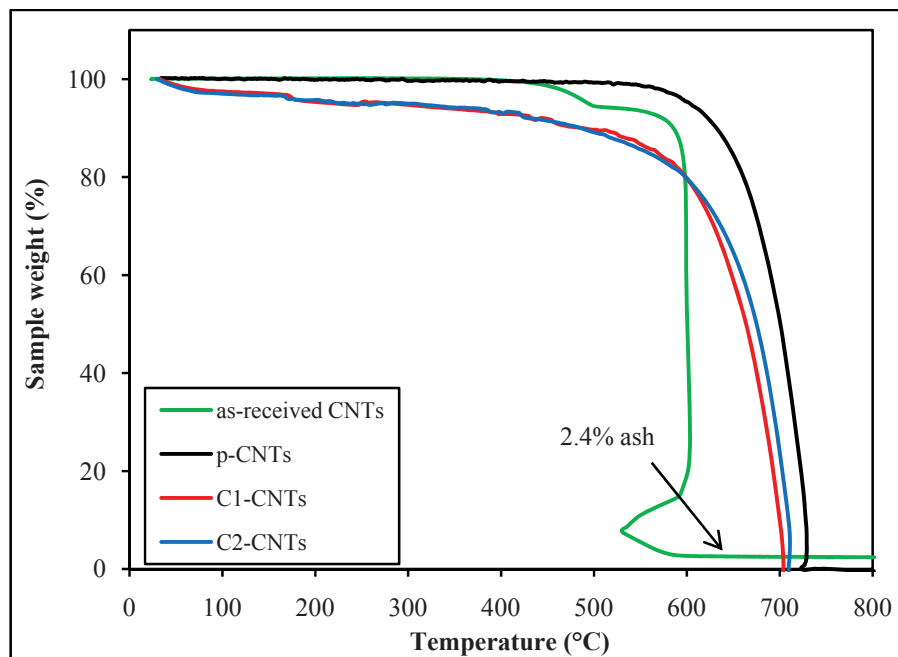
Figure 5.4. TGA curves of as-received and purified MWCNTs under oxygen flow of 30 ml min^{-1}and heating rate of 20 K min^{-1}.

5.3.1.2. Textural properties

The textural properties of as-received, p-, C1- and C2-CNTs investigated by means of nitrogen physisorption and TEM images are listed in Table 5.1.

Table 5.1. Textural properties of different MWCNTs before the ODEB

Sample	Specific total surface area (BET)($m^2\,g^{-1}$)	Specific total pore volume ($cm^3\,g^{-1}$)	Average pore diameter (nm)
as-received CNTs	293	2.829	3.868
p-CNTs	311	2.220	2.856
C1-CNTs	344	2.128	2.478
C2-CNTs	397	2.491	2.513

It is seen that a significant increase in the total surface area of MWCNTs after purification and ozonation takes place. The specific surface area of as-received CNTs increased from 293 to 311$m^2\,g^{-1}$ after the purification step. The ozone treatment of purified CNTs increased continuously the BET surface to 344 and 397 $m^2\,g^{-1}$ on C1- and C2-CNTs, respectively.

In most cases, purification and oxidation of nanotubes often result in an increase in the surface area because of removing of amorphous carbon and fragmentation of tubes.

In this study, the surface area increased but the pore size decreased. The increase in the surface area could be attributed to the fragmentation, opened end caps, intrinsic defect sites, and aggregated pore structure of nanotubes, as shown in Figure 5.5. Fragmentation of the long tubes into shorter species strongly increased the surface area also [18].

The total pore volume and average pore diameter of p-, C1- and C2-CNTs are lower than that of as-received ones. This phenomenon could be explained by the dense packing of tubes. Accordingly, the pore volume is the space between the entangled tubes [2], and hence a very high fragmentation of tubes may result in a decrease of pore volume, as illustrated in Figure 5.5C.

Exposure of MWCNTs in higher ozone concentration flows might be lead to the formation of new pores on the surface of tubes, as in the case of C2-CNTs (Figure 5.5E), relating to the raise of volume and diameter of the pores. Moreover, the BET surface areas of C2-CNTs is higher than that of C1-CNTs, thus, it is conclude that the surface area of ozonated CNTs is proportional with the ozone concentration in flow treatment.
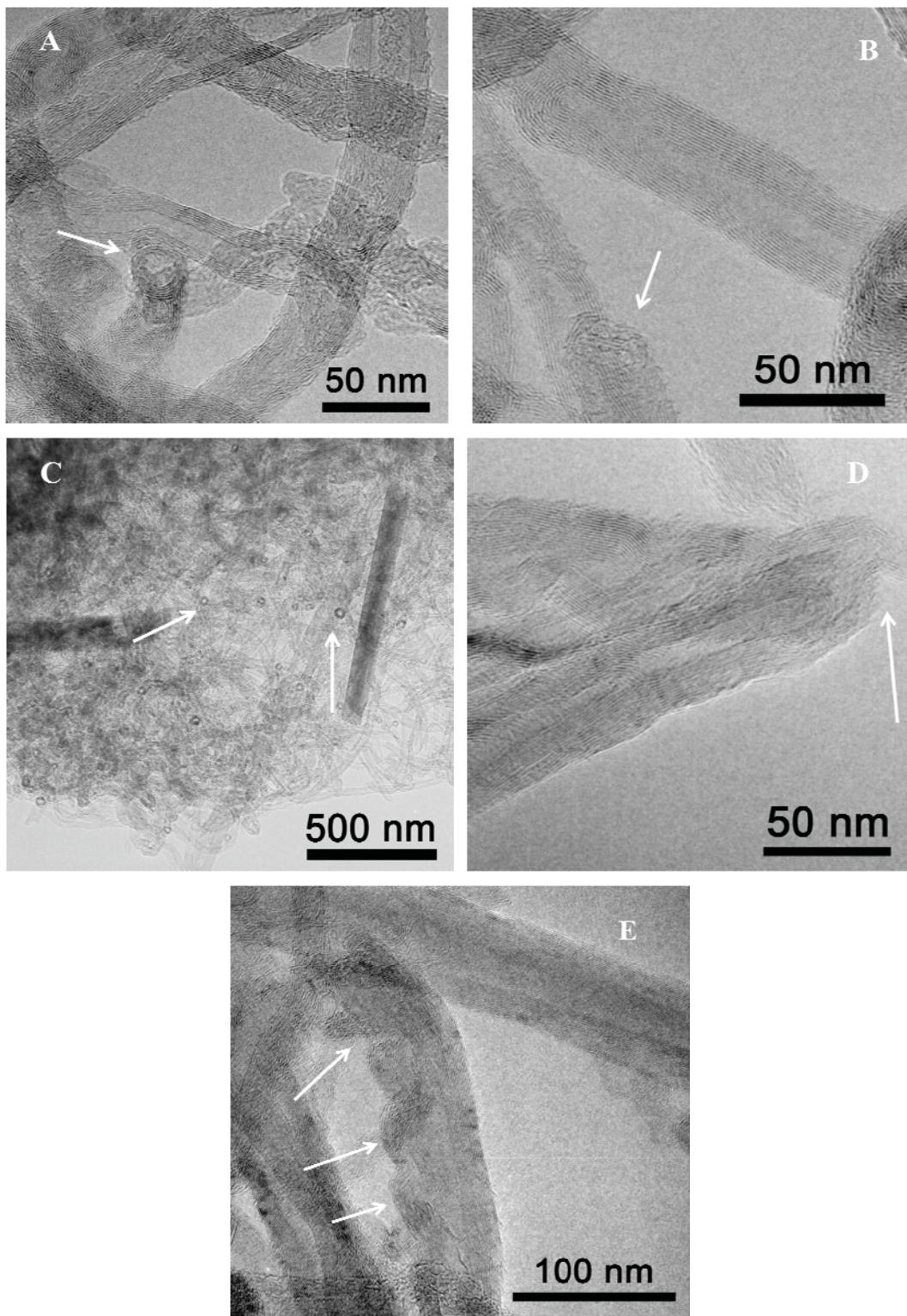
Figure 5.5. TEM images of p-CNTs (A and B), C1-CNTs (C and D) and C2-CNTs (E) before the ODEB.

5.3.1.3. Chemical surface characterization

The IR spectra of as-received, p-, C1-, C2-CNTs before the ODEB are shown in Figure 5.6.
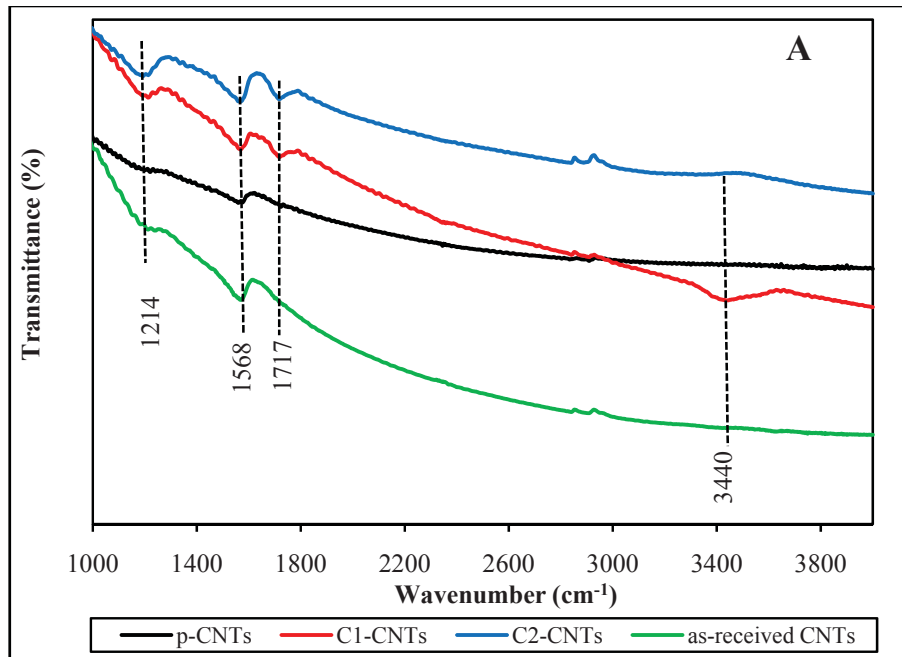
Figure 5.6. FT-IR spectra of as-received, p-, C1- and C2-CNTs before the ODEB.

It is seen that all samples show the peak at 1568 cm^{-1} which is commonly assigned to the C=C asymmetric stretching vibration in graphene sheet [34, 35]. The peak at 1217 cm^{-1} may be assigned to C-O-C of ether and epoxy groups [36]. On the C1- and C2-CNTs, a sharp peak at 1717 cm^{-1} could be attributed to ν(C=O) of carboxyl and carbonyl groups as a result of the ozonation process.

Raman spectroscopy is a powerful technique to evaluate the order of carbon material structure. Raman spectra at excitation of 532 nm of as-received, the purified and ozonated CNTs are presented in Figure 5.7. In the region of 500 - 2000 cm^{-1}, the spectra of samples distinguish two distinct bands. The G mode or (TM-Tangential Mode) corresponds to the stretching mode in the graphite plane. This mode is located around 1580 cm^{-1}. The D mode (D for 'disorder') is related to the defects and disorders in the hexagonal graphitic layers. This mode is located around 1340 cm^{-1}. In the region of

2000 - 3200 cm^{-1} there are two peaks at about 2690 and 2921 cm^{-1}. The peak at 2690 cm^{-1} is the overtone of D band, and the peak at 2921 cm^{-1} is attributed to the combination of the D and G bands [37, 38].
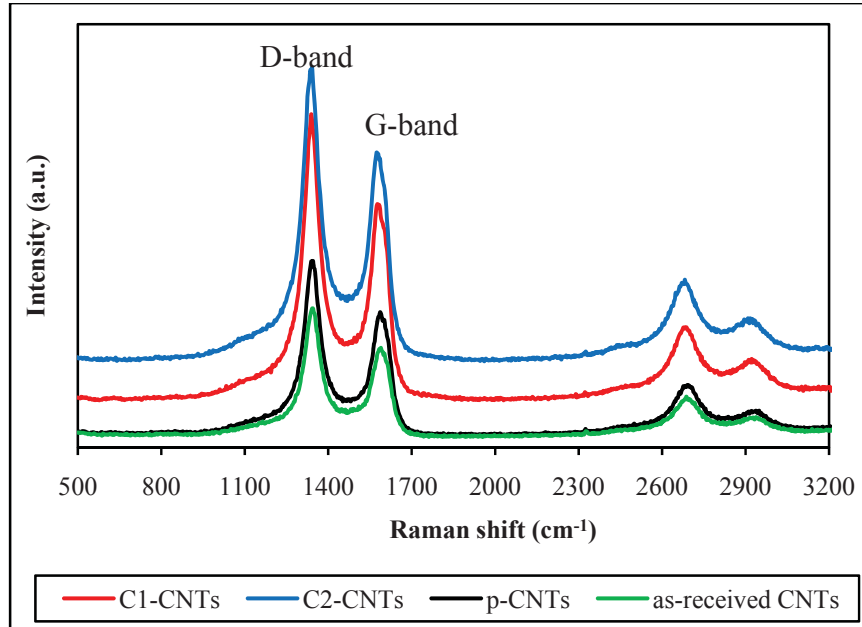
Figure 5.7. Raman spectra of p-, C1- and C2-CNTs before the ODEB.

The appearance of the strong D-band of all the samples can be interpreted as being due to: (1) the turbostratic structure of carbon sheets in tube, namely the finite size (nanometer order) of the crystalline domains, and (2) the high density of the aligned tubes [38]. The intensities of D- (I_D) and G band (I_G) can be calculated using the integrated intensities of the line profiles of the D and G band. The frequencies and the relative intensity ratio I_D/I_G of as-received, p-, C1- and C2-CNTs are given in Table 5.2.

Table 5.2. Frequencies of D- and G-band, I_D/I_G of different MWCNTs before the ODEB.

Sample	νD (cm^{-1})	νG (cm^{-1})	I_D/I_G
as-received CNTs	1343.1	1587.8	1.62
p-CNTs	1342.1	1589.3	1.78
C1-CNTs	1340.5	1582.5	1.89
C2-CNTs	1337.7	1581.3	2.02

In Table 5.2, the relative intensity ratio I_D/I_G of p-CNTs is higher than that of as-received CNTs, corresponding the defects on the surface of p-CNTs are higher than them on the as-received ones. The purification in this study can be considered as mild oxidation process. The relative intensity ratio I_D/I_G of C2-CNTs shows a higher value than that of C1-CNTs, relating to the number of defects on C2-CNTs is more than that on C1-CNTs. This phenomenon indicates that extent of disruption of the nanotubes increased with increasing ozone concentration in flow.

Although Raman spectroscopy detected the disruption of oxidized CNTs it does not provide information about the nature of the functional groups, resulting from the oxidation, attached to the surface of nanotubes. To understand this issue, X-ray photoelectron spectroscopy (XPS) was employed. Figure 5.8 presents the XPS survey spectra of as-received, p-, C1- and C2-CNTs before ODEB.
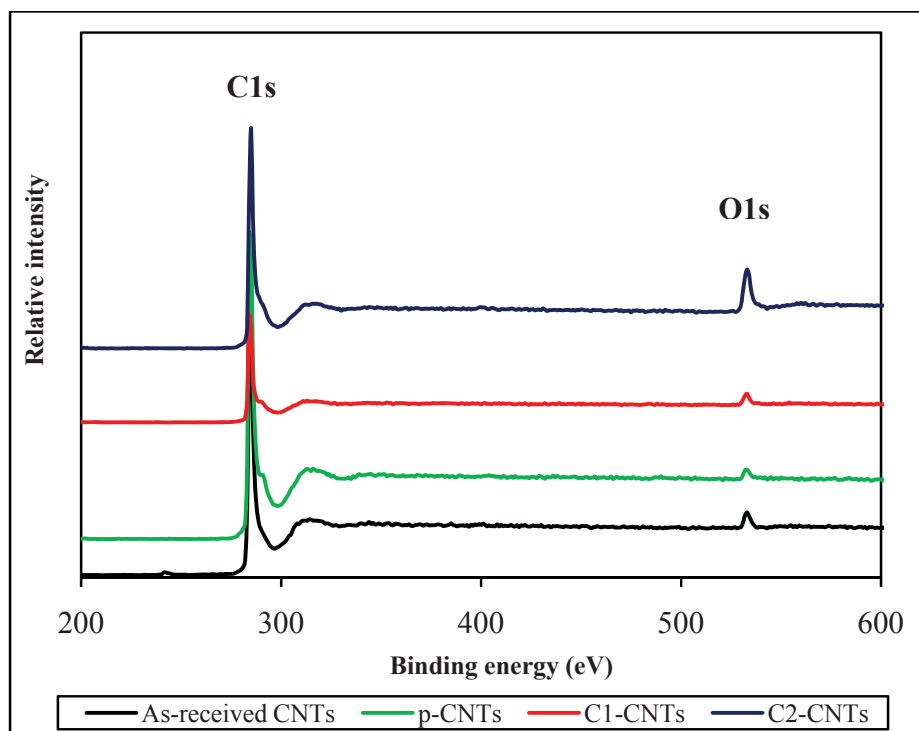
Figure 5.8. XPS survey spectra of different MWCNTs before the ODEB.

As seen from XPS survey spectra of all the samples exhibit two distinct peak carbon (C1s) and peak oxygen (O1s) at a binding energy of 284 and 532 eV, respectively. The

high-resolution C1s spectra could be deconvoluted into five individual peaks, namely the following: C=C (284.6), C-OH (285.6), C=O (287.1), COOH (288.9) and π-π^{*} stacking (290.9 eV) (Figure 5.9).
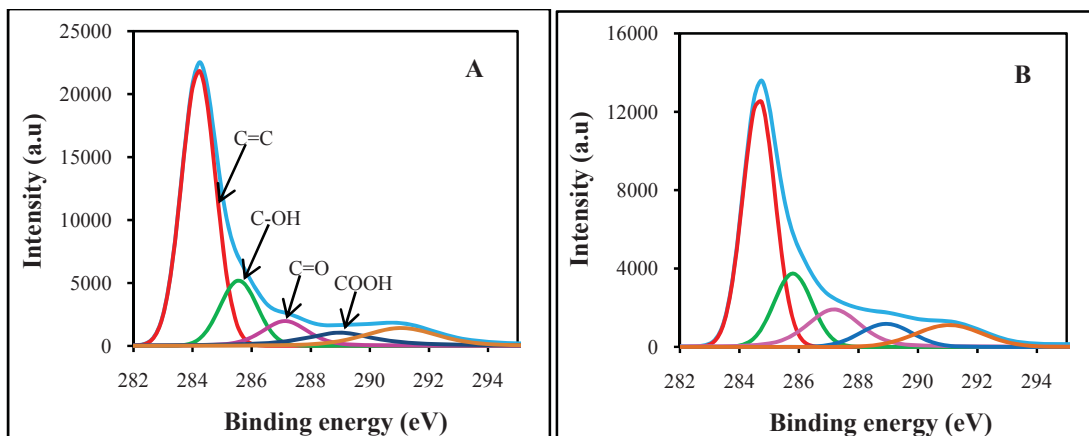
Figure 5.9. Deconvolution of XPS C1s spectra of p-CNTs (A) and C1-CNTs (B) before ODEB.

The fraction of the specific functional groups and surface oxygen content detected by XPS of different samples are shown in Table 5.3. It is indicated that a significant increase in surface oxygen content on the MWCNTs after treatment with ozone takes place. The surface oxygen content increased 1.4% of p-CNTs to 9.4 at.% of C2-CNTs, corresponding a 7–fold increase in surface oxygen on the nanotubes caused by the ozonation. In addition, a higher concentration of ozone flow introduces more surface oxygen content, as compared C1-CNTs (5.3 at.%) and C2-CNTs (9.4 at.%). The fraction of total oxygenated functional groups increased and fraction of C=C carbon in graphitic surface structures decreased due to the purification and ozonation. It should be noted that the remove of amorphous carbon in as-received MWCNTs by thermal oxidation may be considered as an oxidative treatment due to having amorphous carbon oxidation step at higher temperatures.

In Table 5.3, it is indicated that hydroxyl and carboxylic groups increased with increasing the extent of oxidation, but a direct proportional between the concentration of ozone in flow and the fraction of carbonyl groups on the nanotubes has been found.

Table 5.3. Fractions of the XPS C1s functional groups and surface oxygen content of different MWCNTs before the ODEB.

Sample	C=C (%)	C-OH (%)	C=O (%)	COOH (%)	O (at.%)
p-CNTs	59.9	16.3	7.5	6.1	1.4
C1-CNTs	56.5	15.4	9.2	8.8	5.3
C2-CNTs	54.5	17.2	7.5	9.3	9.4

5.3.2. Catalytic reactivity under conventional heating

5.3.2.1. Effect of the EB/O$_2$ molar ratio and reaction temperature on the catalytic performance

The dependence of EB conversion and ST selectivity on EB/O$_2$ molar ratio and the reaction temperatures on C1-CNTs and C2-CNTs catalysts are summarized in Table 5.4. Generally, both catalysts exhibit a rapid increase in conversion of EB with increasing of the reaction temperature and the amount of oxygen in the reactant feed.

Table 5.4. Effects of EB/O$_2$ molar ratio and reaction temperature on the EB conversion and ST selectivity of C1- and C2-CNTs catalysts under conventional heating.

Temperature (°C)	EB/O$_2$ molar ratio	Sample	Product (%)	
			X_{EB}	S_{ST}
350			26	99
400	1:1		54	96
450			69	94
350			29	95
400	1:2	C1-CNTs	63	92
450			86	88
350			33	94
400	1:3		68	85
450			90	78

350			28	97
400	1:1		54	94
450			69	93
350		C2-CNTs	30	93
400	1:2		68	90
450			88	85
350			35	91
400	1:3		68	81
450			89	76

As shown in Table 5.4, over both C1- and C2-CNTs catalysts, the conversion of EB increased monotonously and the ST selectivity decreased slightly with increasing of the reaction temperatures in the range of 350 - 450 °C and EB/O_2 molar ratio of 1:1. But the conversion of EB and ST selectivity decreased rapidly with increasing reaction temperature as EB/O_2 molar ratio of 1:2 and 1:3. This phenomenon indicates that high temperatures accelerated the dehydrogenation and the total oxidation of EB and ST to carbon dioxides, resulting in remarkably decreasing of styrene selectivity. The traces of benzene and toluene, relating to cracking of EB, have been found at 450 °C. It should be noted that the conversion of EB still raises slightly but the selectivity to ST decreases remarkably with increasing reaction temperature at EB/O_2 molar ratio of 1:3, and this result is not in agreement with the previous observations [2], that at higher ratio of oxygen to EB (more than 2), an increase of the EB conversion has not observed.

It is realized that at the same reaction conditions (EB/O_2 molar ratio of 1:1, 400 °C), the catalytic activity and selectivity of C1- and C2-CNTs are higher than them of UV/H35 (Table 5.4 and 4.5). In particular, the EB conversion and ST selectivity of UV/H35 are 46% and 91%, respectively, whereas 54% conversion and 96% selectivity of C1-CNTs; and 54% conversion and 94% selectivity of C2-CNTs, thus, it can be concluded that in this study the catalytic performance of the MWCNTs treated with ozone is better than that of the MWCNTs oxidized with hydroxyl radicals.

5.3.2.2. Catalytic performance with time on stream

In order to examine the influence of working time on the activity and structure of catalysts, long-term catalytic tests with different samples are performed at 450 ^{o}C. Figure 5.10 shows the EB conversion and ST selectivity as a function of time over C1-CNTs at EB/O$_2$ molar ratio of 1:1, 450 ^{o}C.
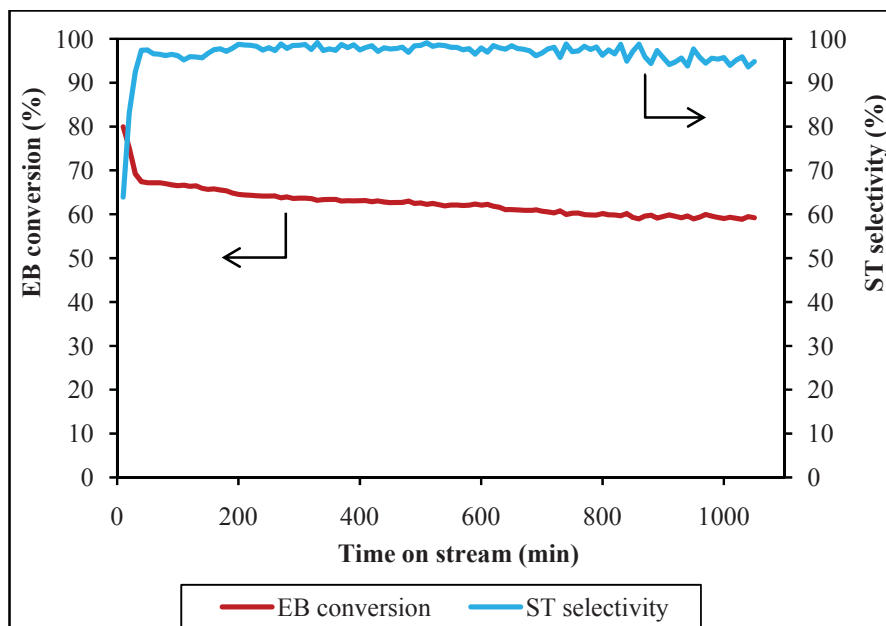
Figure 5.10. EB conversion and ST selectivity of C1-CNTs with time on stream under conventional heating. Test conditions: 1 g catalyst; EB/O$_2$/N$_2$=2.3:2.3:95.4 (vol.%); total flow of 55 ml min^{-1}; 450 ^{o}C.

At the induction period over C1-CNTs test at EB/O$_2$ molar ratio of 1:1, 450°C, the ST selectivity increased strongly from 63 to 98% while the EB conversion decreased rapidly from 80 to 68%. At steady-state the ST obtained 95% and conversion of 59% over C1-CNTs catalysts.

Figure 5.11 displays the EB conversion and ST selectivity as a function of reaction time over as-received, p-, C1- and C2-CNTs at EB/O$_2$ molar ratio of 1:2, 450 ^{o}C.
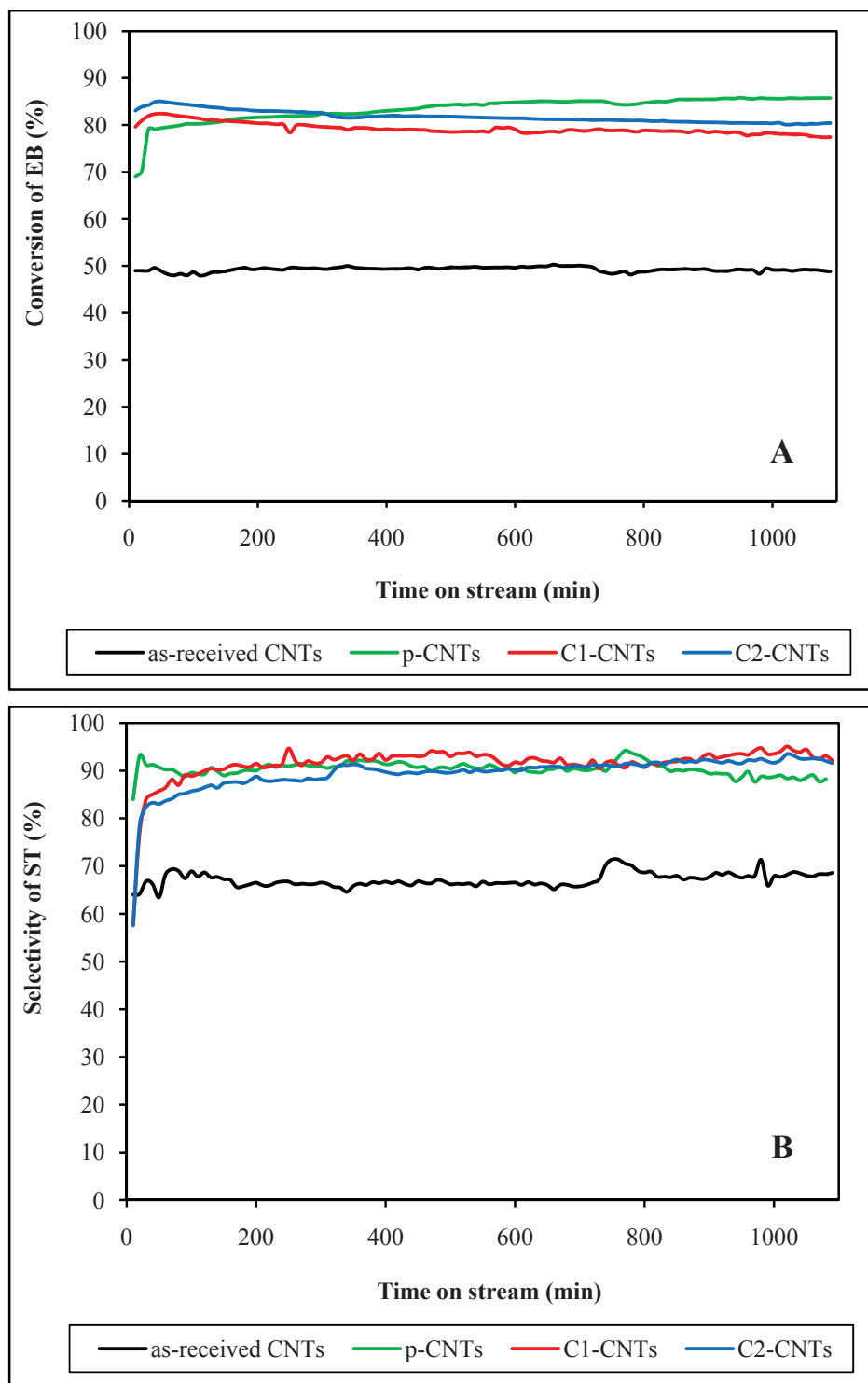
Figure 5.11. EB conversion (A) and ST selectivity (B) of different MWCNTs with time on stream under conventional heating. Test conditions: 1 g catalyst; $EB/O_2/N_2$=2.3:4.6:93.1 (vol.%); total flow of 55 ml min^{-1}; 450 ^{o}C.

As-received CNTs exhibit a relatively stable activity and styrene selectivity with 49% conversion and 68% ST selectivity from the beginning to the end of the test. No activation period has been observed on this sample.

For p-, C1- and C2-CNTs, the catalytic behavior shows an activation period of about half an hour. The conversion of EB on p-CNTs then tends upwards, and obtained a high stability of 86% at steady-state. In contrast, the selectivity to ST on p-CNTs decreases slightly with time on stream and obtained 88% at steady-state.

After induction period, the EB conversion of C1- and C2-CNTs tends to diminish slightly, and kept stable conversion of 77% and 80% over C1- and C2-CNTs, respectively. At steady-state, the ST selectivity of C1- and C2-CNTs are similar around 92%. The catalytic behavior of C1- and C2-CNTs reached a slight difference, thus, a higher of ozone concentration in treating flow improved slightly the conversion of catalyst.

In that EB/O_2 molar ratio raises from 1:1 to 1:2, the EB conversion of C1-CNTs catalyst increased significantly from 59% to 77%, respectively, while the selectivity changes a small value (92% to 95%). Therefore, it is concluded that the EB/O_2 of 1:2 is the best ratio in this study.

Moreover, the EB conversion of C2-CNTs was higher than that of C1-CNTs at the EB/O_2 molar ratio of 1:2, 450 ^{o}C therefore it can be concluded that C2-CNTs catalyst is the best one among the prepared samples.

The main properties of different MWCNTs after several hours time on stream under conventional heating are summarized in Table 5.5.

Table 5.5. Properties of different MWCNTs after the ODEB tests under conventional heating.

Sample	BET (m^2g^{-1})	Total pore volume (cm^3g^{-1})	Average pore diameter (nm)	Δm (%)
as-received CNTs	-	-	-	2.0
p-CNTs	225	1.650	2.929	18.0
C1-CNTs	259	1.679	2.597	21.0
C2-CNTs	204	1.203	2.356	20.0

After several hours time on stream under conventional heating, the textural properties of p-, C1- and C2-CNTs catalyst have been altered significantly. As compared the respective characteristic in Table 5.1 and 5.5, it is demonstrated that the BET surface area of all the tested samples are diminished dramatically after the catalytic reaction. In particular, the surface area of p-, C1- and C2-CNTs lost 86, 85 and 193 m^2 g^{-1}, respectively. The total pore volume of the samples was also reduced. The pore diameters increased slightly (less than 5%)

It has been observed that during the initial stage (activation period) ethylbenzene and most of styrene product could be polymerized and then convert to coke deposited on the pores of carbon catalysts, which was confirmed by a reduction in BET surface area as well as in pore size and by an increase in weight of catalyst [4, 39, 40].

As observation the TEM images of C1-CNTs after several hours time on stream (Figure 5.12) demonstrates that a distorted carbonaceous structure, not totally graphitic carbon, covered the outside of the tubes partially.
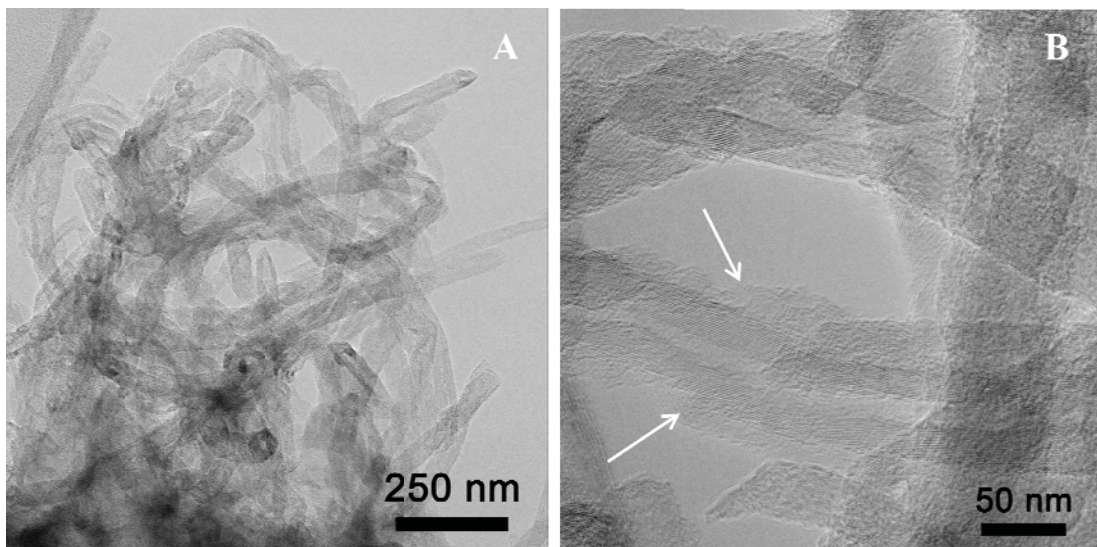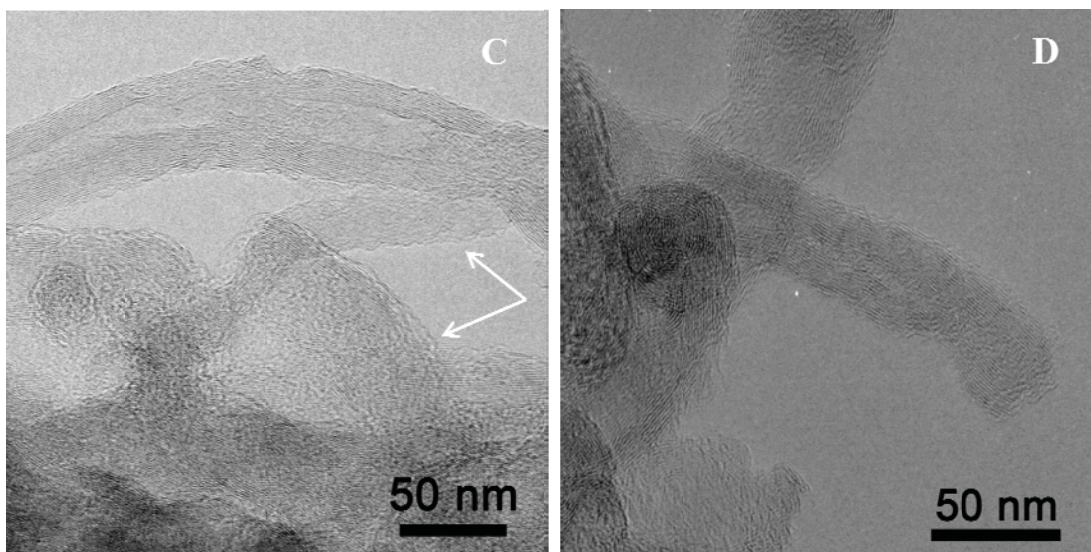
Figure 5.12. TEM images of C1-CNTs after the ODEB.

In Table 5.5, the coke deposition (Δm) of as-received CNTs is about 2%, whereas on p-, C1- and C2-CNTs about 18, 21 and 20%, respectively. It is suggested that on the surface of purified and ozonated MWCNTs may exist a lot of strong adsorptive sites of aromatics, i.e., carboxylic acids that might convert such adsorbates to coke deposit.

It should be noted that it could not be found any direct relationship between the surface areas and the catalytic performance on p-, C1- and C2-CNTs, as previous reports [41, 42].

The IR spectra of p-, C1-, and C2-CNTs after the ODEB under conventional heating are presented in Figure 5.13. Compared with FTIR spectra of these samples before the ODEB tests (Figure 5.6), it can be found that the frequencies of all specific peaks as C=C, C-O-C and C=O shifted towards lower wave numbers after the reaction, suggesting that some changes in the surface and structure of MWCNTs have been taken place [43].
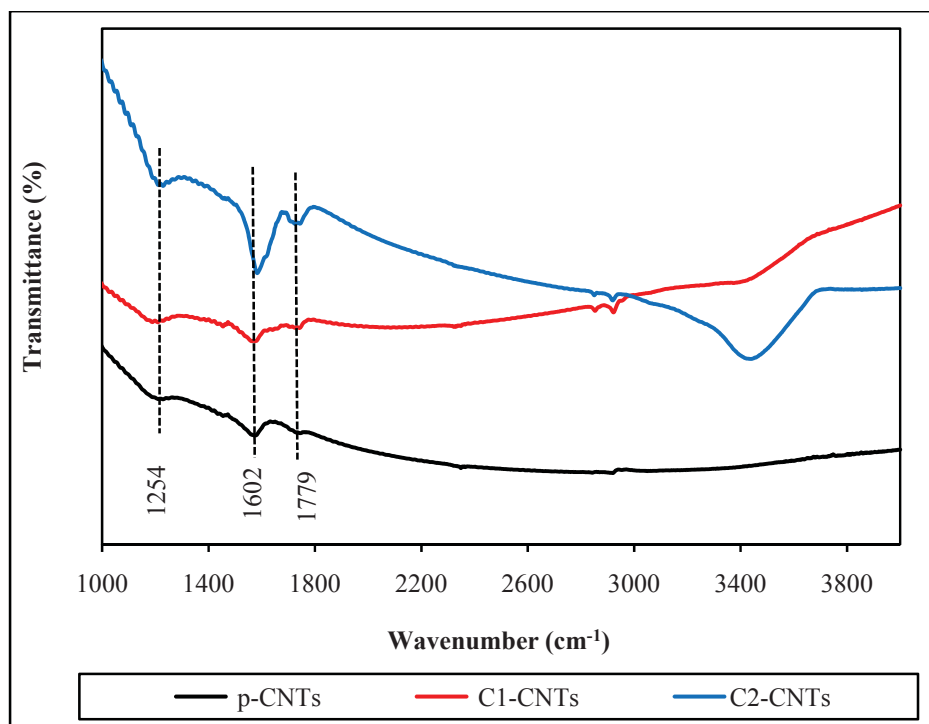
Figure 5.13. FTIR spectra of different MWCNTs after the ODEB.

The Raman spectra of C1- and C2-CNTs after the ODEB are shown in Figure 5.14.
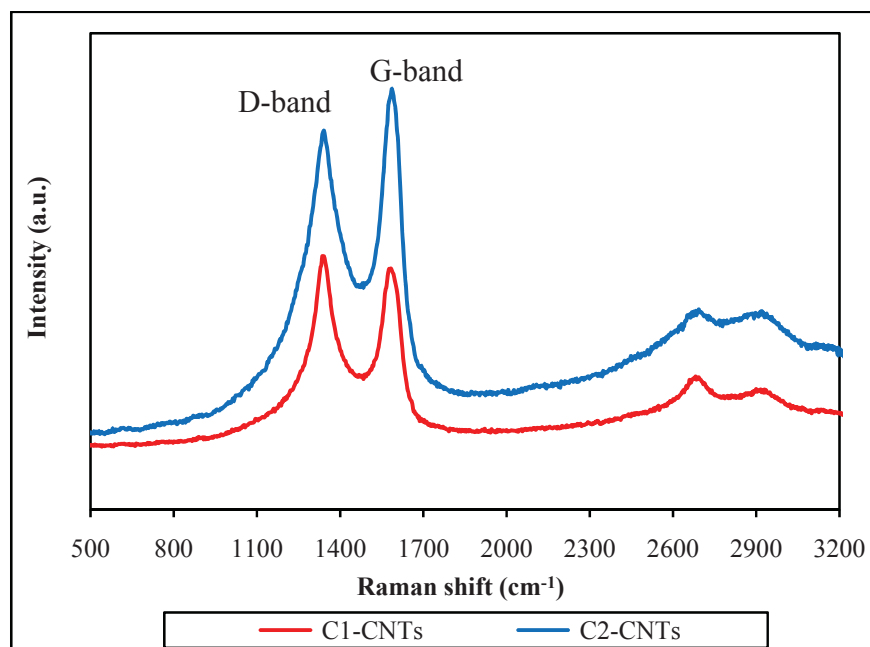
Figure 5.14. Raman spectra of C1- and C2-CNTs after the ODEB under conventional heating.

The relative intensity ratio I_D/I_G of C1- and C2-CNTs before the ODEB are 1.89 and 2.02, respectively (Table 5.2). After several hours time on stream, the I_D/I_G of C1- and C2-CNTs (Table 5.6) increased to 2.00 and 2.13, respectively, implying more defects generated on the surface of these samples. Such defects can supplies the sites for the attachment of oxygenated functional groups. This can be confirmed by the XPS results of samples.

Table 5.6. Frequencies of D- and G-band, relative intensity ratio I_D/I_G of C1- and C2-CNTs after the ODEB under conventional heating.

Sample	vD(cm^{-1})	vG (cm^{-1})	I_D/I_G
Tested C1-CNTs	1342.9	1585.5	2.00
Tested C2-CNTs	1343.7	1589.8	2.13

Table 5.7 provides the fraction of C1s functional groups and surface oxygen content (at.%) of different MWCNTs after the ODEB under conventional heating. A significant increase of oxygen surface on the tested CNTs has been observed. As shown in Table 5.7, on tested p-CNTs, the oxygen surface oxygen increased from 1.4 to 5.1 at.%, for tested C1- CNTs from 5.3 to 7.7 at.% and for tested C2-CNTs from 9.4 to 10.4 at.%. Simultaneously, the fractions of hydroxyl and carbonyl groups of the tested catalysts are higher than those of the fresh catalysts. The carboxylic groups of the tested catalysts were reduced after the reaction.

Table 5.7. Fraction of XPS C1s functional groups and surface oxygen content on different MWCNTs after the ODEB under conventional heating.

Sample	C=C	C-OH	C=O	COOH	O (at%)
Tested p-CNTs	54.2	22.8	8.7	5.0	5.1
Tested C1-CNTs	55.6	24.8	6.5	3.5	7.7
Tested C2-CNTs	56.9	19.0	9.5	4.3	10.4

It is noteworthy that the significant increase in weight of p-, C1- and C2-CNTs occurred in parallel with the raises of surface oxygen contents on these samples, suggesting that

there more oxygenated functional groups have been introduced to the tested catalysts during the activation period at the beginning of reaction. The study of Pereira et al. [4] showed that pretreated CNTs with oxygen at elevated temperature obtained higher styrene yield than that on CNTs treated with HNO_3. Moreover, more coke deposit on the oxygen-oxidized sample than that on acid-oxidized one has been found. In this study, it is observed that the drastic changes of coke deposit only occurred on the oxidized samples. The oxidative treatments have altered the morphology of the samples, and increased the amount of oxygenated functional groups, leading to enhance of coke deposit after the ODEB tests. Coke deposit itself is active toward the ODEB reaction [4, 8].

5.3.3. Catalytic reactivity under microwave heating

Figure 5.15A and B compare the EB conversion and ST selectivity of C2-CNTs with reaction time on stream at $450^{o}C$, EB/O_2 molar ratio of 1:2 under conventional heating (CH) and microwave heating (MW). On both heating methods, C2-CNTs catalyst exhibits an activation period, about half an hour. Afterwards, the conventional heating induces a high long-term stability of EB conversion and reached about 82% conversion, while the EB conversion on microwave heating has a tendency towards decreasing. At steady-state, EB conversion of the catalyst obtained 80% under microwave heating (Figure 5.15A)
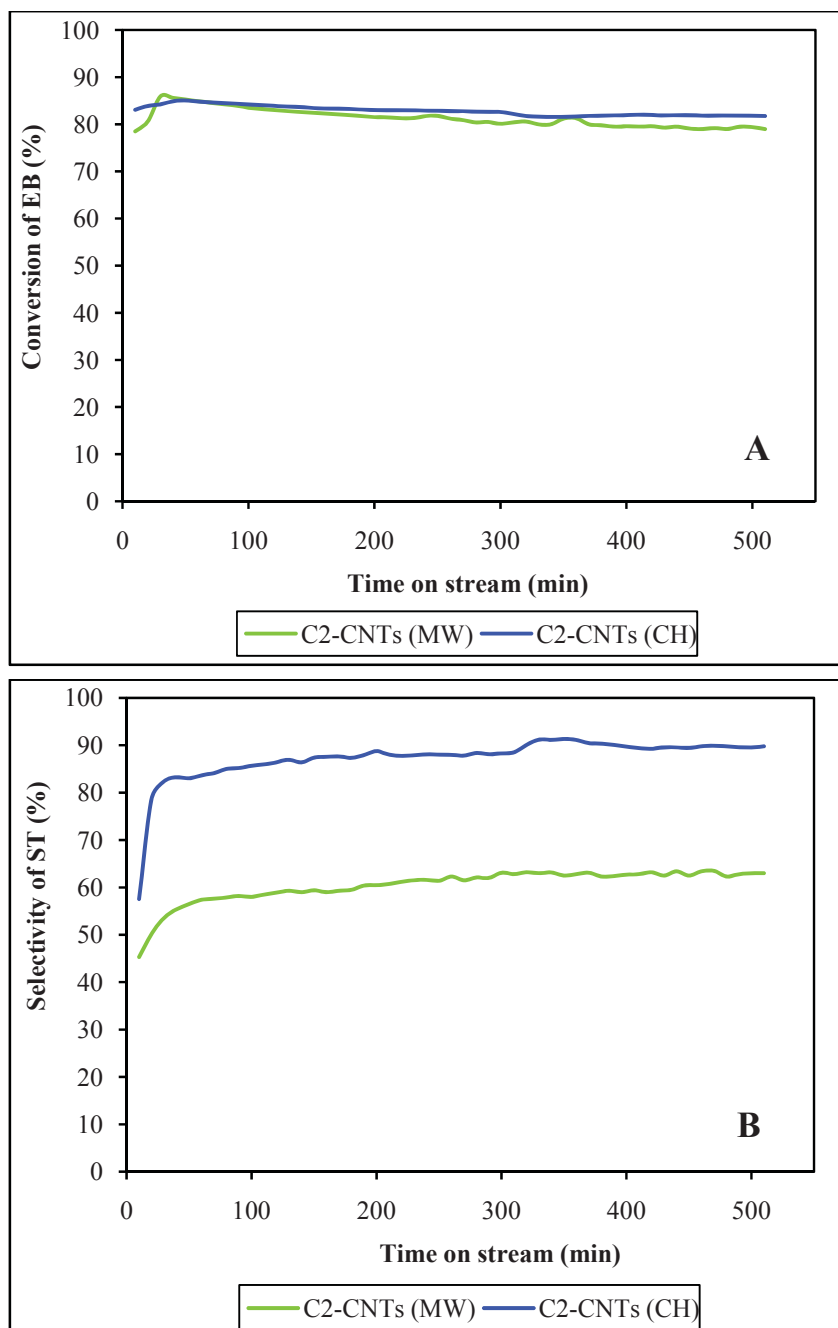
Figure 5.15. Influence of conventional and microwave heating on EB conversion (A) and ST selectivity (B) of C2-CNTs catalyst with time on stream. Test conditions: 1 g catalyst; $EB/O_2/N_2=2.3:4.6:93.1$ (vol.%); total flow of 55 ml min^{-1}; 450 ^{o}C.

The influence of different heating methods to the selectivity is significant. In Figure 5.15B, the ST selectivity under conventional heating is much higher than that under

microwave heating. In particular, under conventional heating ST selectivity reached 90% after 8 h time on stream, whereas the selectivity gained only 63% under microwave heating. This result is in contradiction with the previous report [9] in which the selectivity on acid-treated MWCNTs was higher for the microwave-assisted reaction.

In order to understand the change of catalyst structure after the reaction, the sample was examined by Raman and XPS spectroscopy. The Raman spectra of C2-CNTs after the reaction under conventional heating and microwave heating are presented in Figure 5.16. It is indicated that under conventional heating the D band is partially depleted, and the G band is strongly attenuated. In contrast, under microwave heating the D band is higher, and the G band is lower. The relative intensities I_D/I_G of the samples after the reaction (Table 5.8) are 2.13 and 2.34 for the process under conventional and microwave heating, respectively. This indicates that microwave irradiation induces more defects on the surface of nanotubes than under conventional heating.
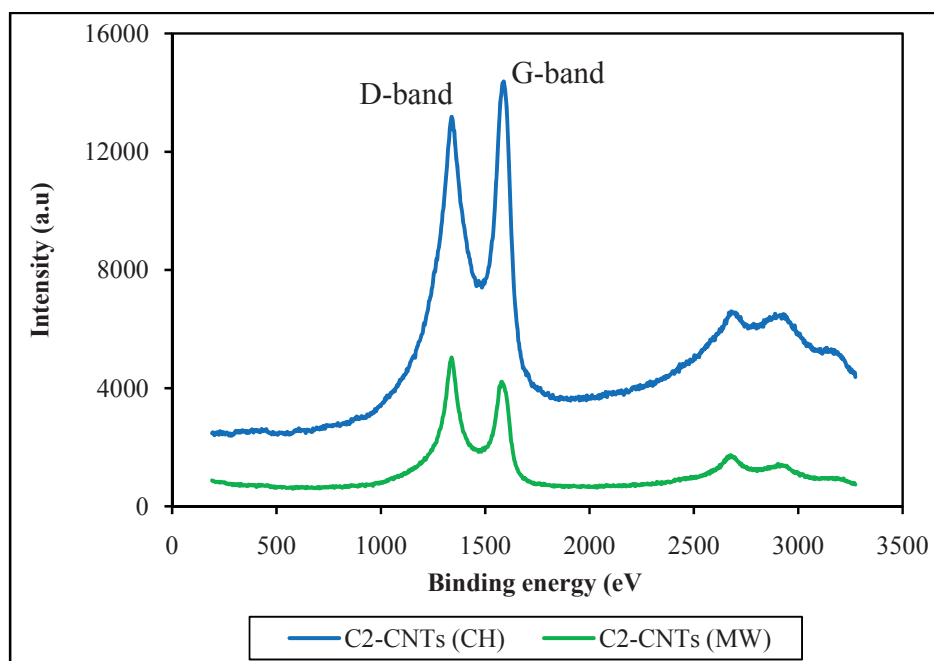
Figure 5.16. Raman spectra of C2-CNTs after the ODEB under conventional and microwave heating.

Table 5.8. Frequencies of D- and G-band, relative intensity I_D/I_G of C2-CNTs after the ODEB under conventional (CH) and microwave heating (MW).

Sample	νD (cm^{-1})	νG (cm^{-1})	I_D/I_G
Tested C2-CNTs (CH)	1343.7	1589.8	2.13
Tested C2-CNTs (MW)	1339.3	1588.7	2.34

The survey XPS spectra of C2-CNTs after the ODEB under conventional and microwave heating are illustrated in Figure 5.17.
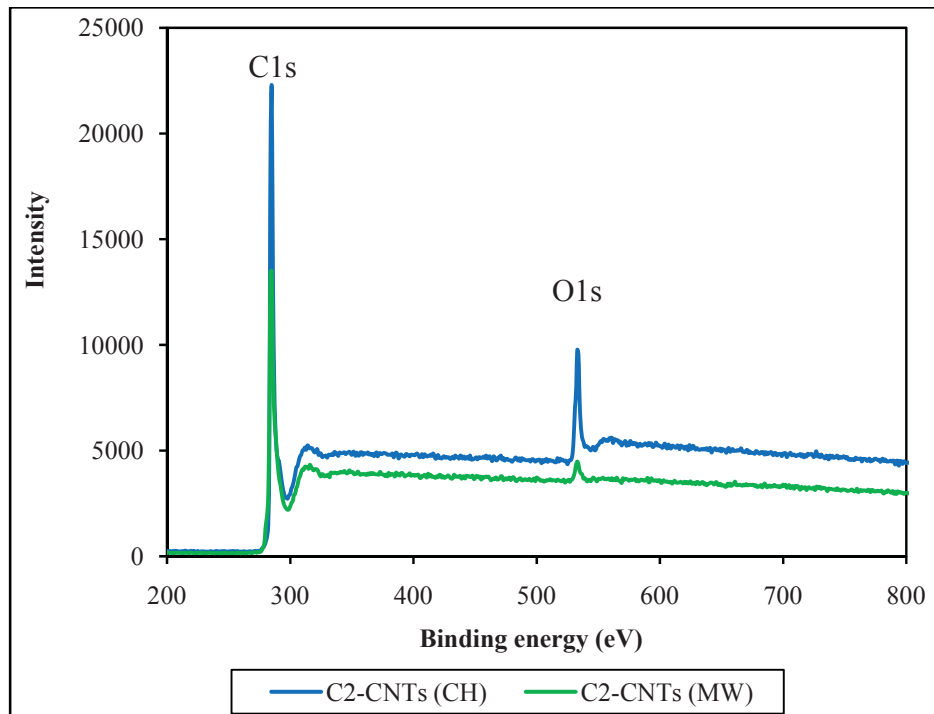
Figure 5.17. XPS survey of C2-CNTs after the ODEB under conventional heating (CH) and microwave heating (MW).

It is indicated that the intensity of O1s of the conventional-heated C2-CNTs is higher than that of the microwave-heated C2-CNTs. The surface oxygen and the fraction of specific oxygenated groups are summarized in Table 5.9.

Table 5.9. Influence of conventional (CH) and microwave heating (MW) on the chemical surface of C2-CNTs after the ODEB

Sample	C=C	C-OH	C=O	COOH	O (at%)	Δm (%)
C2-CNTs (CH)	56.9	19.0	9.5	4.3	10.4	20.0
C2-CNTs (MW)	60.1	18.4	6.7	4.2	3.1	20.7

Compared the surface oxygen content on C2-CNTs before and after the reaction (Table 5.3 and Table 5.9) under conventional heating are 9.4 and 10.4 at.%, respectively. The values on C2-CNTs before and after the reaction under microwave heating are 9.4 and 3.1 at.%. It is clearly that conventional heating induced the accumulation of oxygenated groups on the catalyst after the ODEB reaction. In contrast the microwave heating declined drastically these groups, which is evidenced by the fraction of sp^2-carbon of the sample after the reaction. Moreover, the fraction of C=O, corresponding to carbonyl/quinone groups, on conventional-heated C2-CNTS is much higher than that on microwave-heated ones, suggesting that carbonyl/quinoid groups may be the active sites for the reaction.

In Table 5.9, the increased mass of coke deposit on C2-CNTs under conventional heating and microwave heating are similar, suggesting that the formation of coke on C2-CNTs seems to be independent of how the heat is supplied to the reaction.

5.4. Conclusions

As-received MWCNTs have been purified prior the functionalization using ozone in gas phase at room temperature. The purification process removed effectively amorphous carbon and residual catalysts confirmed by TGA analysis result. MWCNTs could be totally oxidized in ozone flow of 1.3% for 24 h. Ozonation of MWCNTs in lower ozone concentrations produced a variety of oxygen-containing groups, such as ether, epoxy, carbonyl, carboxylic groups, attached on the defect sites of surface CNTs. The BET surface area increased linearly with increasing ozone concentration, while the average pore size and total pore volume decreased slightly with increasing ozone concentration

in flow. The surface oxygen content identified by XPS increased significantly with the ozone concentration.

The catalytic performance in the ODEB on different MWCNTs has been performed under conventional heating and microwave heating. The EB conversion and ST selectivity depend distinctly on the reaction temperatures and the EB/O_2 molar ratio. In this study, the optimal conditions were established at 450 ^oC and molar ratio EB/O_2 of 1:2. The ozonated MWCNT reached 80% conversion and 92% selectivity to ST at steady-state under conventional heating, whereas under microwave heating the conversion and ST selectivity were 79% and 63%, respectively. The increased mass of coke deposit on the catalysts after the ODEB reaction seems to be independent of heating modes. A significant increase in surface oxygen content as a result of activation period of the reaction has been identified on the catalyst after the reaction under conventional heating, but this phenomenon has been taken place under microwave heating. Instead of this, microwave heating induced a declination of the oxygenated surface groups on the catalyst. It is indicated that the activation period induces the introduction of oxygenated groups that may be the crucial parameter to catalytic activity.

5.5. References

[1] D.S. Su, N. Maksimova, J.J. Delgado, N. Keller, G. Mestl, M.J. Ledoux, R. Schlögl, Catal. Today 102-103 (2005) 110.

[2] T.J. Zhao, W.Z. Sun, X.Y. Sun, M. Ronning, D. Chen, Y.C. Dai, W.K. Yuan, A. Holmen, Appl. Catal. A 323 (2007) 135.

[3] D.S. Su, N.I. Maksimova, G. Mestl, V.L. Kuznetsov, V. Keller, R. Schlögl, N. Keller, Carbon 45 (2007) 2145.

[4] M.F.R. Pereira, J.J.M. Orfao, J.L. Figueiredo, Appl. Catal. A 184 (1999) 153.

[5] G. Mestl, N.I. Maksimova, N. Keller, V.V. Roddatis, R. Schlögl, Angew. Chem. Int. Ed. 40 (2001) 2066.

[6] Y. Iwasawa, H. Nobe, S. Ogasawara, J. Catal. 31(1973) 444.

[7] G. Emig, H. Hofmann, J. Catal. 84 (1983) 15.

[8] M.F.R. Pereira, J.L. Figueiredo, J.J.M. Orfao, P. Serp, P. Kalck, Y. Kihn, Carbon 42 (2004) 2807.

[9] B. Nigrovski, P. Scholz, T. Krech, N.V. Qui, P. Pollok, T. Keller, B. Ondruschka, Catal. Commun. 10 (2009) 1473.

[10] S. Kundu, PhD Dissertation, Bochum, Germany, 2009.

[11] http://www.air-purifier-power.com/ozone-air-purification-danger.html   (06. 2011)

[12] D. Heymann, S.M. Bachilo, R.B. Weisman, F. Cataldo, R.F. Fokkens, N.M.M. Nibbering, R.D. Vis, L.P.J.F. Chibante, J. Am. Chem. Soc. 122 (2000) 11473.

[13] R.B. Weisman, D. Heymann, S.M. Bachilo, J.Am. Chem. Soc. 123 (2001) 9720.

[14] J.P. Deng, C.Y. Mou, C.C. Han, Fullerene Sci. Technol. 5 (1997) 1033.

[15]   J.P. Deng, C.Y. Mou, C.C. Han, Fullerene Sci. Technol. 5 (1997) 1325.

[16]   R. Criegee, Angew. Chem. Int. Ed. Engl. 14 (1975) 745.

[17]   D.B. Mawhinney, V. Naumenko, A. Kuznetsova, J.T. Yates, J. Liu, R.E. Smalley, J. Am. Chem. Soc. 122 (2000) 2383.

[18]   D.B. Mawhinney, V. Naumenko, A. Kuznetsova, J.T. Yates, J. Liu, R.E. Smalley, Chem. Phys. Lett. 324 (2000) 213.

[19]   E. Najafi, J.Y. Kim, S.H. Han, K. Shin, Colloids Surf. A 284-285 (2006) 373.

[20]   A.B. Sulong, C.H. Azhari, R. Zulkifli, M.S. Othman, J. Park, Eur. J. Sci. Res. 33 (2009) 295.

[21]   K.G. Kostov, R.Y. Honda, L.M.S. Alves, M.E. Kayama, Braz. J. Phys. 39 (2009) 322.

[22]   B. Parekh, T. Debies, P. Knight, K.S.V. Santhanam, G.A. Takacs, J. Adh. Sci. Tech. 20 (2006) 1833.

[23]   K.E. Haque, Int. J. Miner. Process. 57 (1999) 1.

[24]   R. Gedye, F. Smith, K. Westaway, H. Ali, L. Baldisera, L. Laberge, J. Rousell, Tetrahedron Lett. 27 (1986) 279.

[25]   H. Tai, C.J.G. Jou, Chemosphere 38 (1999) 2667.

[26]   J.M. Oespchuck, IEEE Transactions on Microwave Theory and Techniques 32 (1984) 1200.

[27]   J.A. Menendez, A. Arenillas, B. Fidalgo, Y. Fernandez, L. Zubizarreta, E.G. Calvo, J.M. Bermudez, Fuel Process. Technol. 91 (2010) 1.

[28]   U.O. Mendez, O.V. Kharissova, M. Rodriguez, Rev. Adv. Mater. Sci. 5 (2003) 398.

[29]   C.C. Chen, C.F. Chen, C.M. Chen, F.T. Chuang, Electrochem. Commun. 9 (2007) 159.

[30]   J. Liu, M.R. Zubiri, B.Vigolo, M. Dossot, Y. Fort. J.J. Ehrhardt, E. McRae, Carbon 45 (2007) 885.

[31]   C.J. Ko, C.C. Lee, F.H. Ko, H.S. Chen, T.C. Chu, Microelectronic Engineering 73-74 (2004) 570.

[32]   B. Nigrovski, U. Zavyalova, P. Scholz, K. Pollok, M. Muller, B. Ondruschka, Carbon 46 (2008) 1678.

[33]   H. Will, P. Scholz, B. Ondruschka, Top. Catal. 29 (2004) 175.

[34]   M.S.P. Shaffer, X. Fan, A.H. Windle, Carbon 36 (1998) 1603.

[35]   H.M. Heise, R. Kuckuk, A.K. Ojha, A. Srivastava, V. Srivastava, B.P. Asthana, J. Raman Spectrosc. 40 (2009) 343.

[36]   T.H. Benny, T.J. Bandosz, S.S. Wong, J. Colloid Interface. Sci. 317 (2008) 375.

[37]   H.M. Heise, R. Kuckuk, A.K. Ojha, A. Srivastava, V. Srivastava, B.P. Asthana, J. Raman Spectrosc. 40 (2009) 343.

[38]   Z. Xu, C. Min, L. Chen, L. Liu, G. Chen, N. Wu, J. Appl. Phys. 109 (2011) 054303.

[39]   M.F.R. Pereira, J.J.M. Orfao, J.L. Figueiredo. Appl. Catal. A 218 (2001) 307.

[40]   J. Zhang, H.L. Zou, Q. Qing, Y.L. Yang, Q.W. Li, Z.F. Liu, X.Y. Guo, Z.L. Du, J. Phys. Chem. B 107 (2003) 3713.

[41]   M.F.R. Pereira, J.J.M. Orfao, J.L. Figueiredo. Appl. Catal. A 196 (2000) 43.

Chapter 6

Effects of surface carboxylic groups on the catalytic performance of MWCNTs in ODEB

6.1. Introduction

In the previous chapter, we observed that there has been a significant increase in mass of the treated MWCNTs, including purified and ozonated MWCNTs, after the ODEB. Examining survey XPS identified a remarkable increase in oxygen surface on the samples after the reaction. Coke deposit on the surface of the sample has been observed after the ODEB reaction also. Compared with as-received, the catalytic performance in the ODEB on purified and ozonated MWCNTs improved remarkably due to the enhancement of oxygenated coke. This result is similar to the previous observation [1].

 Although oxygenated coke may be the active material for the reaction, until now it is not known exactly how it is contributed to the catalytic activity.

Since the oxygenated coke phenomenon occurs on acidic sites of the metal catalysts during the ODEB reaction [2], presumably, the formation of coke on carbonaceous catalysts could also occur on acidic groups. The acidic surface properties are caused by the presence of carboxyl groups, lactones, and hydroxyl groups of phenol. These groups differ in their acidities and can be differentiated by Boehm's titration [3]. Therefore, it is possible to exploit this method for examining the influence of carboxylic groups on the reactivity and coke deposit on catalysts after the ODEB. The catalytic testing in the ODEB on MWCNTs with and without carboxylic groups can evaluate the contribution of this type of functional groups and coke to the catalytic activity.

6.2. Experimental

6.2.1. Materials

In this research the 'blank' sample was purified MWCNTs (p-CNTs) which were prepared as described in chapter 5.

6.2.2. Neutralization of surface carboxylic groups

Carboxylic groups on p-CNTs were neutralized with a solution of 0.05 N $NaHCO_3$. 2 g p-CNTs were equilibrated with 200 ml solution of 0.05 N $NaHCO_3$ for 24 h at room temperature. The resulting mixture was then filtered and the black solid was washed with deionized water to fully remove the excess of sodium salt. This material was dried overnight in an oven at 120 °C.

6.3. Results and discussion

6.3.1. Characterization of MWCNTs after neutralization

Figure 6.1 presents the IR spectra of purified MWCNTs (p-CNTs) and neutralized MWCNTs (n-p-CNTs).
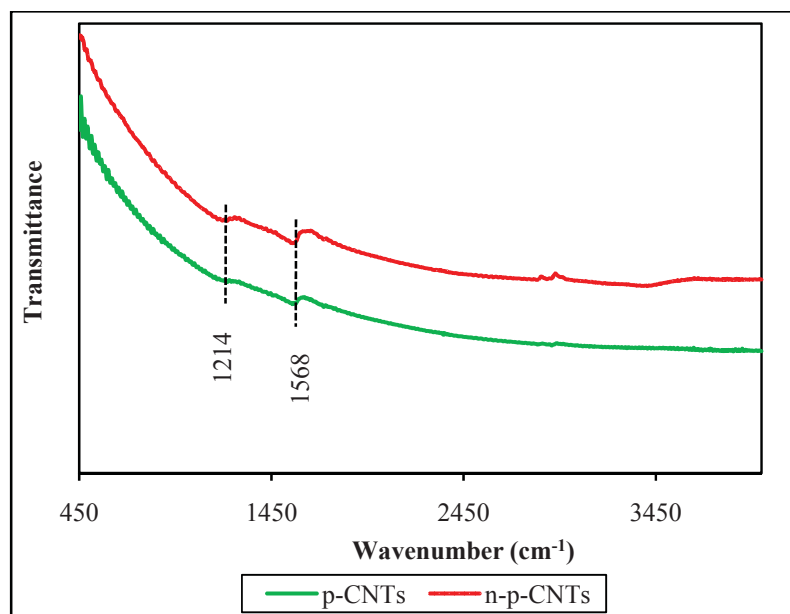
Figure 6.1. FTIR spectra of p-CNTs and n-p-CNTs.

IR spectra of both samples were nearly similar. The peak at around 1568 cm^{-1} could be ascribed to C=C graphite stretching mode of MWCNTs. The peak at around 1214 cm^{-1} was assigned to C-O-C stretching vibration of the ether and epoxy groups [4].

The thermogravimetric analysis (TGA) experiments in oxygen flow at a heating rate 20 K min^{-1} were conducted for p- and n-p-CNTs. The TGA results are presented in Figure 6.2. It was demonstrated that CNTs having more physical defect sites associated to oxygenated surface functional groups would be expected to show weight loss at a lower temperature [5, 6]. As shown in Figure 6.2, the thermal stability in oxidative environment of the neutralized MWCNTs was slightly lower than that of the purified ones. At 450 ^{o}C, the mass n-p-CNTs has been lost around 2 wt%, while p-CNTs remained their initial weight. This indicates that the neutralization of carboxylic groups has not altered significantly the surface morphology of MWCNTs.
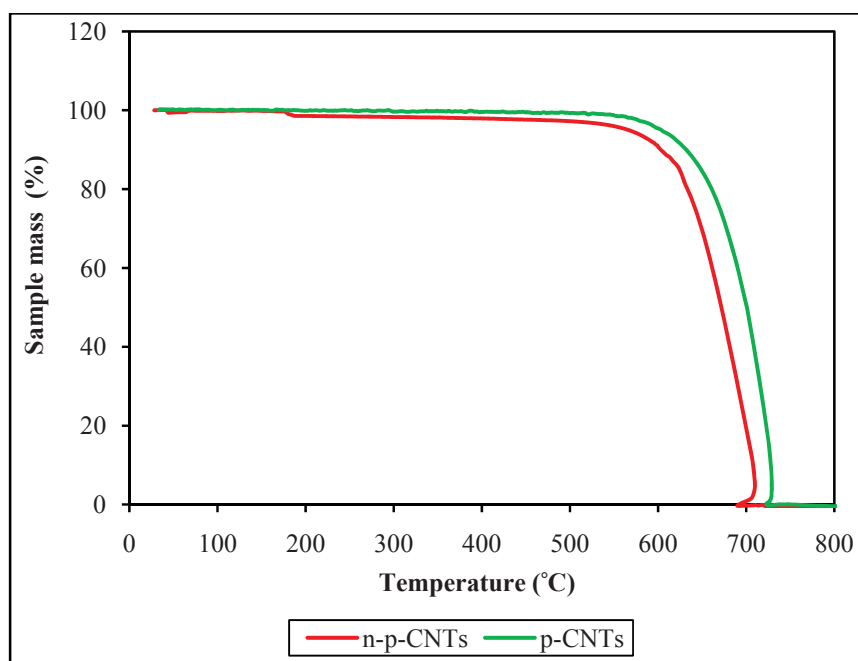
Figure 6.2. TGA curves of p- and n-p-CNTs under oxygen flow of 30 ml min^{-1}and heating rate of 20 K min^{-1}.

The XPS survey spectra of p- and n-p-CNTs are presented in Figure 6.3.
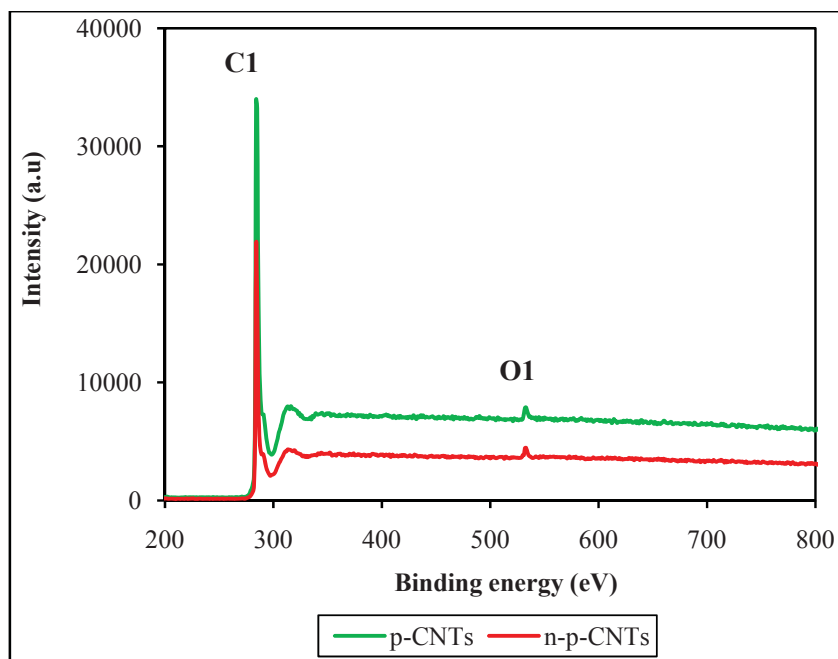
Figure 6.3. XPS survey spectra of p- and n-p-CNTs before the ODEB.

The XPS C1s of samples could be deconvoluted into five peaks C=C (284.6), C-OH (285.8), C=O (287.2), COOH (290.8) and π-π^{*} stacking (290.9 eV). The fractions of functional groups of p- and n-p-CNTs before and after the ODEB are presented in Table 6.1. The surface oxygen content (O at.%) identified by XPS of different samples are added in Table 6.1 also.

Table 6.1. Fractions of XPS C1s functional groups and oxygen surface content of p- and n-p-MWCNTs before and after the ODEB.

Sample	C=C	C-OH	C=O	COOH	O (at.%)	Δm (%)
p-CNTs	59.9	16.3	7.5	6.1	1.4	-
n-p-CNTs	59.2	17.2	7.7	5.1	1.5	-
tested p-CNTs	54.2	22.8	8.7	5.0	5.1	18
tested n-p-CNTs	59.6	16.0	7.1	6.7	1.4	- 3

The XPS survey spectra (Figure 6.3) indicate that the surface oxygen contents of p-CNTs and n-p-CNTs seem to be similar. This could be confirmed by the deconvoluted

102

data listed in Table 6.1. The fractions of functional groups on p- and n-p-CNTs changed insignificantly during the carboxylic neutralization process.

6.3.2. ODEB catalytic performance on purified and neutralized MWCNTs

Figure 6.4 shows the EB conversion and ST selectivity as the function of time on stream over p- and n-p- CNTs.
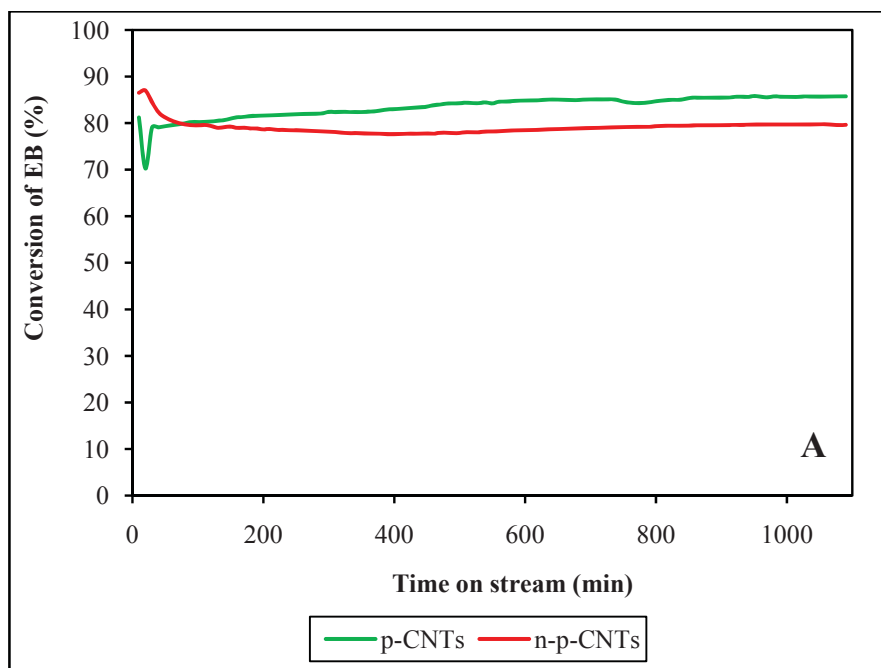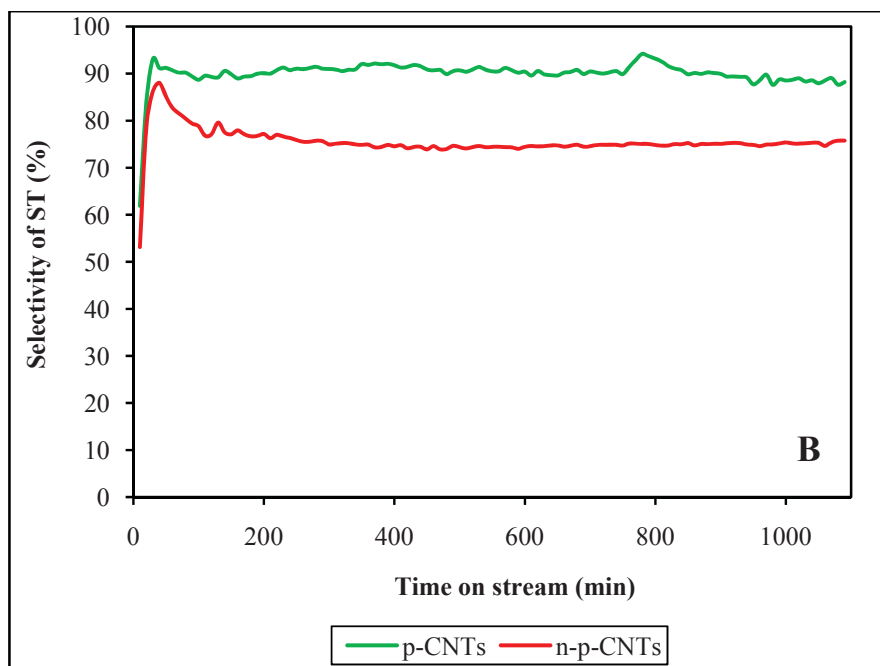
Figure 6.4. EB conversion (A) and ST selectivity (B) of p- and n-p-CNTs as a function of time on stream. Test conditions: 1 g catalyst; $EB/O_2/N_2=2.3:4.6:93.1$ (vol.%); total flow of 55 ml min^{-1}; 450 ^{o}C.

At the steady-state p- and n-p-CNTs reached 86 and 80% EB conversion, respectively. ST selectivity is 88% for p-CNTs and 75% for n-p-CNTs. We can calculate the ST yield of n-p-CNTs is lower 16% than that of purified CNTs. This reduction could be caused by the lack of carboxylic groups on the neutralized MWCNTs.

Figure 6.5 compares the Raman spectra of the n-p-CNTs before and after the ODEB. The Raman spectra of the samples display two distinct D- and G-band located at around 1352 and 1582 cm^{-1}, respectively. D- and G-band are contributed to the defects and ordered graphene structure, respectively. It is shown that the positions of these bands have not removed after the reaction test. The intensity ratios I_D/I_G of fresh and tested n-p-CNTs are 1.78 and 1.80, respectively. This result indicates that the texture of n-p-CNTs is almost unchanged after the ODEB.
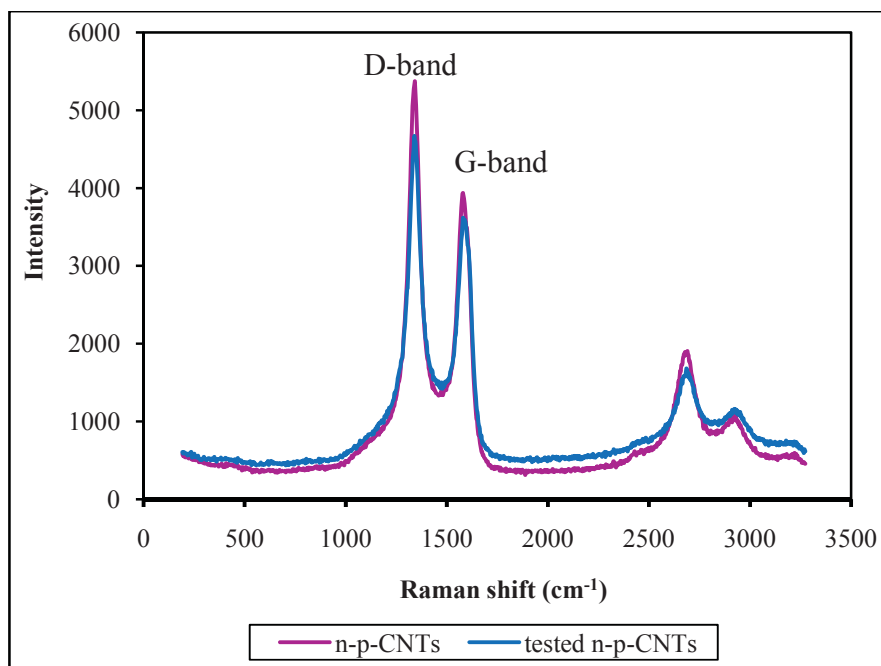
Figure 6.5. Raman spectra of n-p-CNTs before and after the ODEB.

A change in mass of the catalyst has been observed after the reaction. The mass of p-CNTs increased in 18 wt.% , in contrast n-p-CNTs have been reduced 3 wt.% (Table 6.1).

The XPS survey spectra of p- and n-p-CNTs after the ODEB are shown in Figure 6.6. It is revealed that the intensity of XPS O1s peak of tested p-CNTs is higher than that of tested n-p-CNTs. Indeed, the surface oxygen contents of the tested p- and n-p-CNTs are 5.1 and 1.4 at.%, respectively (Table 6.1).

An increase in surface oxygen content and catalyst mass have been found only for tested p-CNTs, whereas the concentration of oxygen surface on n-p-CNTs are almost unchanged and coke deposit could not be occurred after the reaction (Table 6.1). Consequently, the catalytic performance of n-p-CNTs is lower than that of p-CNTs.

The carboxylic groups on the p-CNTs may act as the active sites for the conversion ST and/or EB to oxygenated coke that has been known as active phase of the ODEB reaction. This agrees with the results of chapter 5 that the better catalyst has been found over the tested catalyst with accumulation of oxygenated coke. In the case carboxylic

free-CNTs (n-p-CNTs), the reaction may be catalyzed by –OH and –C=O groups existed previously.
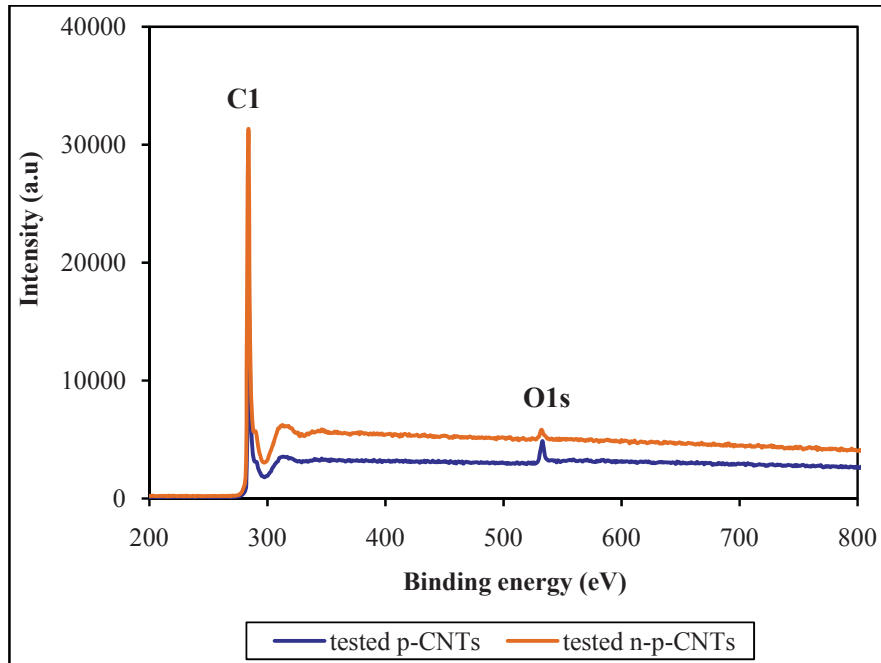
Figure 6.6. XPS survey spectra of p- and n-p-CNTs after the ODEB.

On the other hand, the C1s fraction of hydroxyl and carbonyl carbon of p-CNTs increased after the ODEB (Figure 6.7 and Table 6.1).
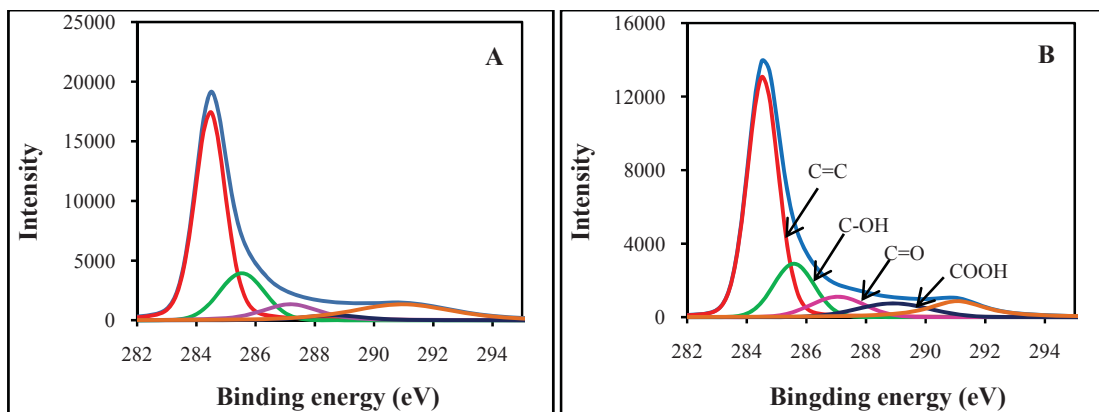
Figure 6.7. XPS C1s deconvolution of n-p-CNTs before (A) and after the ODEB (B).

Probably, the reaction seems to take place on the couple carbonyl/hydroxyl group linked to styrene/ethylbenzene redox couple, suggesting that these oxygenated groups are the active sites in the ODEB.

Therefore, it is concluded that carboxylic groups on the p-CNTs contributed indirectly 16% styrene yield to the total yield of the catalyst.

6.4. Conclusions

Carboxylic groups on the surface of MWCNTs have been neutralized by aqueous $NaHCO_3$ solution, and the received materials were catalytically tested in the ODEB reaction. The results indicated that the structure of neutralized MWCNTs was almost unchanged after the catalytic reaction. Coke deposition has not been found as in terms of the increase in the catalyst mass after the reaction. An increase of surface oxygen content on the treated MWCNTs has also not been observable after the reaction. This result is in contrast to the untreated MWCNTs in which the accumulation of oxygenated coke has been found.

As a result of the treatment, the yield of styrene for the reaction with neutralized MWCNTs is 16% lower than for that employing the untreated samples. This demonstrates that the presence of carboxylic groups on the nanotubes promotes the formation of oxygenated coke that enhances the activity.

6.5. References

[1]   M.F.R. Pereira, J.L. Figueiredo, J.J.M. Orfao, P. Serp, P. Kalck, Y. Kihn, Carbon 42 (2004) 2807.

[2]   E.G. Shcheglova, T.G. Alkhazov, Kinet. Katal. 23 (1982) 1272.

[3]   H.P. Boehm, Carbon 40 (2002) 145.

[4]   T.H. Benny, T.J. Bandosz, S.S. Wong, J. Colloid Interface. Sci. 317 (2008) 375.

[5]   E. Najafi, J.Y. Kim, S.H. Han, K. Shin, Colloids Surf. A 284-285 (2006) 373.

[6]   J. Miyawaki, M. Yudasaka, S. Iijima, J. Phys. Chem. B 108 (2004) 10732.

Summary

Since the coke deposition on the inorganic oxide in the course of ODEB to styrene has been considered as the true catalytically active substance, various carbonaceous materials have shown to be active and selective catalysts for this reaction. It has been confirmed that oxygenated surface functional groups of catalyst, especially carbonyl/quinoid and hydroxyl groups, are responsible for the catalytic performance. Therefore, the focus in this study is in the creation of oxygen-containing functional groups on the surface of carbon nanotubes by partial oxidation using high potential oxidizing agents, including hydroxyl radicals, and ozone in gas phase followed by investigating the influences of these groups on the ODEB catalytic behavior.

The effects of the oxidative treatment methods on the textural, structural and chemistry surface of MWCNTs, as well as comparative investigations on the catalysts before and after the ODEB have been conducted by using a series of analytical techniques including TGA, BET surface area, Raman spectroscopy, TEM, FTIR and XPS.

It is found that as-received MWCNTs possessed a number of oxygenated surface groups, as a result of CVD method. Further oxidation treatment with highly active hydroxyl radicals generated via UV/H_2O_2 process increased substantially the formation of oxygenated surface functional groups compared to as-received MWCNTs, particularly hydroxyl and carbonyl groups. Using hydrogen peroxide solutions with concentrations higher than 35 wt.% for the radical oxidation of MWCNTs did not enhance the surface oxygen content as expected. The effectiveness of the oxidation could be declined by the scavenging of radicals instead. As a result, the catalytic performance of UV/H35 catalyst is better than that of UV/H50 or UV/H60. At 400 $^{\circ}$C and molar ratio EB/O_2 of 1:1, ethylbenzene conversion and styrene selectivity of UV/H35 catalyst achieved 47% and 91%, respectively, for several hours time on stream. The styrene yield of UV/H35 is two times higher than that of as-received MWCNTs.

Purification of as-received MWCNTs followed by ozone corona discharge oxidation of samples generated various oxygenated functional groups on the MWCNTs as identified by FT-IR. The surface oxygen content of the ozonated MWCNT increased significantly with increasing ozone concentration in gas flow, leading to highly stable ethylbenzene conversion and styrene selectivity reaching up to 80 and 92%, respectively, at 450 $^\circ$C, and EB/O$_2$ molar ratio of 1:2 in long-term experiments under conventional heating. That is the best result for the ODEB community to the best of our knowledge. The catalyst performance does not depend on the porosity of the MWCNTs.

At the same reaction conditions (EB/O$_2$ molar ratio of 1:1, 400 °C), the catalytic activity/ selectivity of the MWCNTs treated with ozone is better than that of the MWCNTs oxidized with hydroxyl radicals.

The catalytic performance is substantially affected by the supplied heating mode for the reaction. A comparative investigation on catalyst performance under conventional and microwave heating indicated that the conversion difference between both heating methods is negligible, but conventional heating results in higher styrene selectivity than the microwave-assisted process.

Generally, coke deposit has been observed for all the tested catalysts after the ODEB. However, the extent of coke formation depends strongly the oxidative treatment of nanotubes. For conventional heating, an increase in coke weight incorporated with oxygenated groups has been occurred, while for microwave heating coke deposit has been observed but the oxygenated groups are reduced after the ODEB. This fact could be the reason for the lower selectivity under microwave heating.

In order to investigate the contribution of carboxylic groups on the nanotubes to the catalytic behavior, Boehm's titration has been employed. By selective neutralization of carboxylic groups on the MWCNTs with NaHCO$_3$ solution, and by comparison of the catalytic activity/selectivity with that of untreated samples, it has been shown that the styrene yield of neutralized MWCNTs is 16% lower than that of non-neutralized catalysts. Examining both catalysts after the reaction indicated that oxygenated coke is

not deposited on carboxylic neutralized MWCNTs after the reaction test. This result demonstrates that carboxylic surface groups improve the catalytic performance indirectly.

After the ODEB reaction, it is found that an enhancement of oxygen-containing groups on the surface of MWCNTs, particularly hydroxyl and carbonyl groups, have been observed, suggesting that these oxygenated groups could be able to be the main active phases in the reaction.

Danksagung

Allen, die mich bei der Anfertigung dieser Arbeit unterstützten, möchte ich an dieser Stelle sehr herzlich danken

Insbesondere gilt mein Dank

- Herrn Prof. Dr. habil. Bernd Ondruschka (Friedrich-Schiller-Universität Jena, Institut für Technische Chemie und Umweltchemie) für seine wissenschaftliche Anleitung und Unterstützung und besonders dafür, mir die Gelegenheit zu geben, diese Doktorarbeit anfertigen zu können,
- dem Zweitgutachter, Herrn Prof. Dr. habil. Rainer Beckert, für die Begutachtung der Arbeit,
- Herrn Dr. rer. nat. Peter Scholz für die intensive und produktive Betreuung, viele Diskussionen während meiner Arbeit und für die Korrektur meiner Artikel und der Dissertation, besonders für die Hilfe während meines gesamten Aufenthaltes in Jena.
- Herrn Dr. rer. nat. Achim Stolle für die Korrektur meiner Dissertation.
- Frau Dipl.-Ing. (FH). Beate Fähndrich für die Einweisung in die TGA, die IR-Analyse und für die freundliche Unterstützung bei Experimenten.
- Herrn Dr. rer. nat. Thomas Keller und Herrn Ralf Wagner (Institut für Materialwissenschaft, FSU Jena) für die Durchführung von und die Diskussion über XPS Spektren.
- Herrn Dr. rer. nat. Killian Pollok (Bayerisches Geoinstitut-Universität Bayreuth) für die Durchführung von und die Diskussion über die TEM-Aufnahmen.
- Herrn Dr. rer. nat. Nicolae Tarcea (Institut für Physikalische Chemie-FSU Jena) für die Durchführung von und die Diskussion über Raman-Spektren.
- Frau Anna Schmidt (Institut für Physikalische Chemie-FSU Jena) für die Durchführung der BET-Messungen.
- der Katalysemannschaft: Thomas Krech, Boriss Nigrovski, Benjamin Jäger, Thomas Mollenhauer, Marcus Präger für die gute Zusammenarbeit.

Appendix A: Abbreviations

CNTs – Carbon nanotubes

MWCNTs – Multiwalled carbon nanotubes

SWCNTs – Single-walled carbon nanotubes

AC – Activated carbon

CNFs – Carbon nanofibers

ADC – Arc discharge

CVD – Chemical vapor deposition

ODEB – Oxidative dehydrogenation of ethylbenzene

DHEB – Dehydrogenation of ethylbenzene

FTS – Fischer-Tropsch synthesis

EB – Ethylbenzene

ST – Styrene

X_{EB} – Conversion of ethylbenzene

S_{ST} – Selectivity of styrene

Y_{ST} – Yield of styrene

BET – Brunauer-Emmet-Teller

TEM – Transmission electron microscopy

FT-IR – Fourier transform infrared

XPS – X-ray photoelectron spectroscopy

TGA – Thermogravimetric analysis

GC – Gas Chromatography

FID – Flame ionization detector

TCD – Thermal conductivity thermal

AOP – Advanced oxidation processes

UV – Ultraviolet

CH – Conventional heating

MW – Microwave heating

Appendix B: Figures and tables

Figures

Tables

Appendix C: Setup gas chromatography and calibration factors of components EB and ST

C.1.Detector setup

	FID-Front	TCD-Back
Heater	300 °C	250 °C
H_2 flow	30 mL min^{-1}	-
Air flow	400 mL min^{-1}	-
Reference flow (He)	-	10 mL min^{-1}
Makeup flow (N_2)	10 mL min^{-1}	5.822 mL min^{-1}

C.2. Column setup

- HP-5: 50 m x 320 μm x 1.05 μm

  Flow: 3.1601 mL min^{-1}; Post run: 1.5 mL min^{-1}

- Molsieve 5A: 60 m x 320 μm x 32 μm

  Flow: 1.1783 mL min^{-1}; Post run: 0.5593 mL min^{-1}

C.3. Oven temperature programme

Rate (°C/min)	Value (°C)	Hold time (min)	Run time (min)
-	120	8	8

- Auxiliary heater: 80 °C
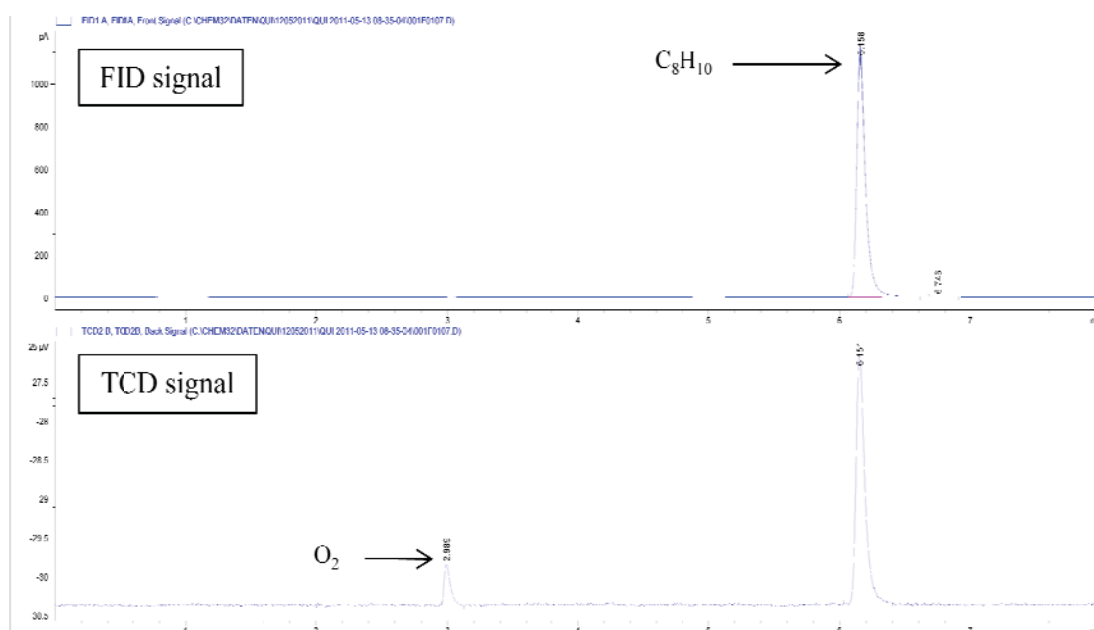- Equilibration time: 1 min

C.4. Split/splitless-injector

- Split inlet ratio: 50:1

- Septum purge flow: 3 mL min^{-1}

C.5. Peak retention time

| Retention time (min)	FID signal	TCD signal
1.796	Methane	-
3.017	-	Oxygen
3.098	-	Water
3.987	Benzene	-
4.825	Toluene	-
6.163	Ethylbenzene	Ethylbenzen
6.762	Styrene	Styrene

C.5.1. Chromatograph of educts separated on HP-5 column

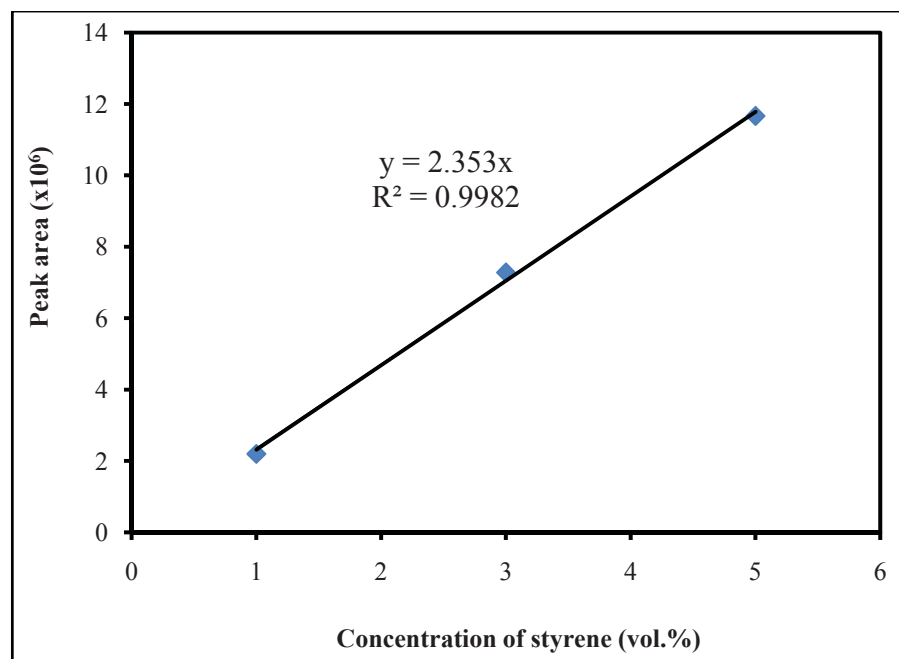*C.5.2. Chromatograph of products separated on HP-5 column*
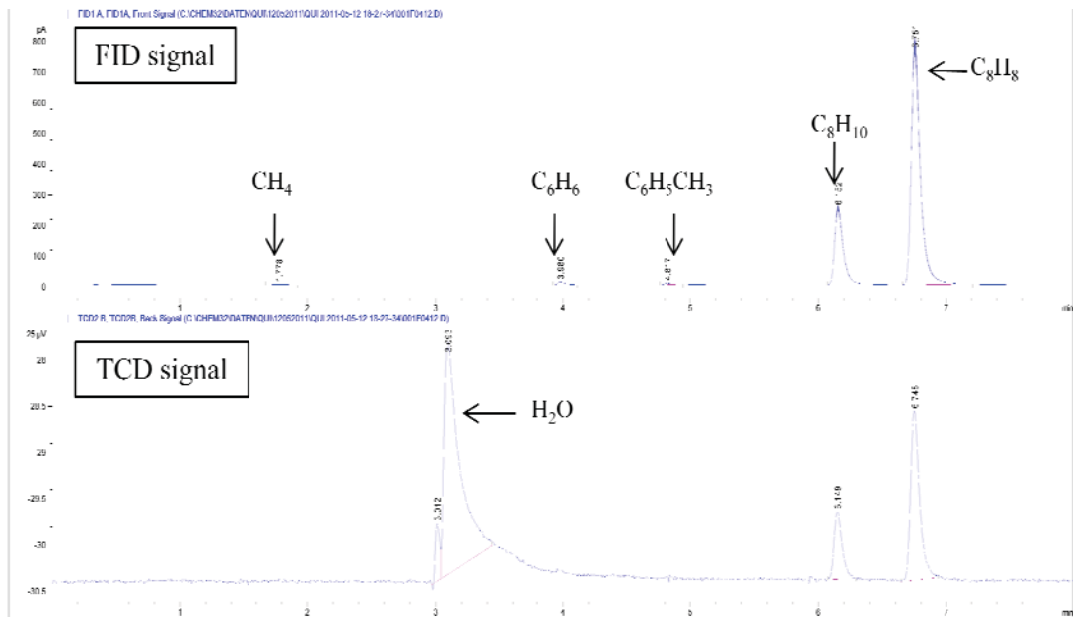
C.6. Calibration factors of the components ethylbenzene and styrene

$y = 2.353x$
$R^2 = 0.9982$

Peak area (x10^6)

Concentration of styrene (vol.%)
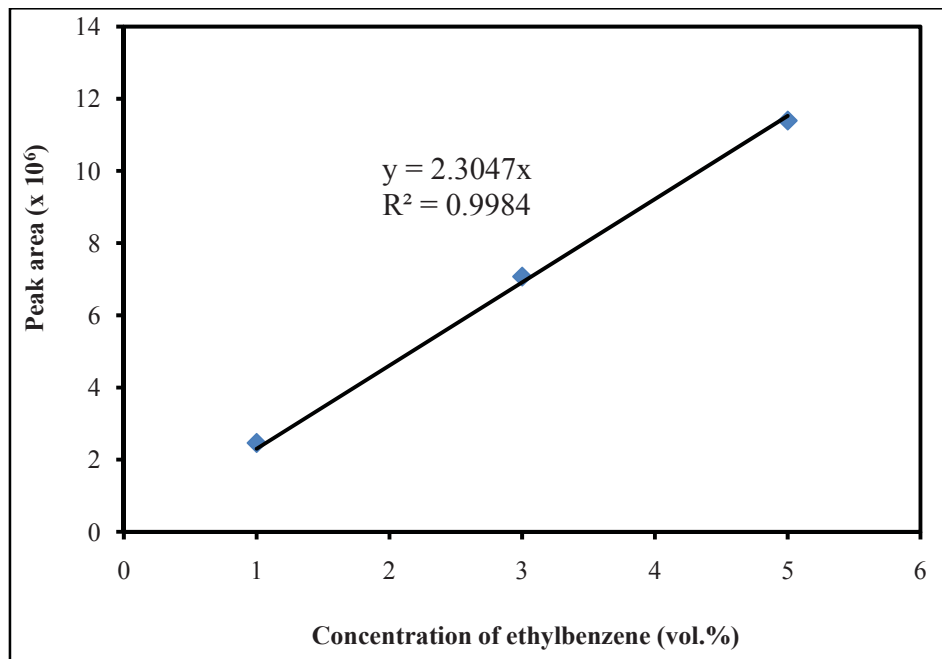
List of publications

1. Tran Thi Minh Nguyet, Nguyen Quang Huan, Tran Que Chi, Do Que Chi, Nguyen Doan Thai, Nguyen Cong Trang, Luu Tien Hung, Le Van Tiep, <u>N.V. Qui</u>, The role of Zn doping on the catalytic activity of the nanoparticle perovskite $La_{0.7}Sr_{0.3}MnO_3$, J. Korean Phys. Soc. 52 (2008) 1341.

2. B. Nigrovski, P. Scholz, T. Krech, <u>N.V. Qui</u>, K. Pollok, T. Keller, B. Ondruschka, The influence of microwave heating on the texture and catalytic properties of oxidized multi-walled carbon nanotubes, Catal. Commun. 10 (2009) 1473.

3. <u>N.V. Qui</u>, P. Scholz, T. Krech, T.F. Keller, K. Pollok, B. Ondruschka, Multiwalled carbon nanotubes oxidized by UV/H_2O_2 as catalyst for oxidative dehydrogenation of ethylbenzene, Catal. Commun. 12 (2011) 464.

4. <u>N.V. Qui</u>, P. Scholz, T. Krech, T. Keller, B. Ondruschka, Oxidative dehydrogenation of ethylbenzen over multi-walled carbon nanotubes oxidized by hydroxyl radicals, 43. Jahrestreffen Deutscher Katalytiker, Weimar, Poster (März 2010)

5. <u>N.V. Qui</u>, P. Scholz, T. Krech, Z. Wu, B. Ondruschka, Ozone-functionalised multi-walled carbon nanotubes as catalysts in the oxidative dehydrogenation of ethylbenzene, 44. Jahrestreffen Deutscher Katalytiker und Jahrestreffen Reaktionstechnik, Weimar, Poster (März 2011).

6. <u>N.V. Qui</u>, P. Scholz, T. Krech, T.F. Keller, K. Pollok, B. Ondruschka, Hydroxyl radical-assisted oxidation of multiwalled carbon nanotubes for oxidative dehydrogenation of ethylbenzene, 21st European conference on diamond-like material, carbon nanotubes and nitriles, Budapest, Poster (September 2010).

Lebenslauf

Angaben zur Person

Name / Vorname	**Nguyen Van Qui**
Adresse	Hügelstr. 1, Haus 2, Zi. 229, D-07749 Jena
Telefon	(+49) 151 2406 2151
E-Mail	nvquy@vast-hcm.ac.vn
Staatsangehörigkeit	Vietnamesisch
Geburtsdatum	01.04.1974
Geburtsort	Saigon Stadt, Vietnam
Geschlecht	männlich
Familienstand	verheiratet

Schulbildung

Datum	09.1988 – 06.1991
Schulabschluss	Abitur
Name, Ort und Art der Schule	Gia Dinh Gymnasium, HoChiMinh Stadt, Vietnam
Datum	09.1993 – 04.1999
Studienabschluss	Diplom-Ingenieur
Name und Art der Ausbildungseinrichtung	Lebensmittelchemietechnologie, HoChiMinh Stadt Tecchnische Universität, Vietnam
Datum	09.2002 – 01.2005
Studienabschluss	Master of Engineering
Name und Art der Ausbildungseinrichtung	Technische Chemie und Petroleum Fakultät HoChiMinh Stadt Technische Universität, Vietnam
Datum	Seit 07.2008
Position	Doktorand

Thema der Promotionsarbeit	„Carbon nanotubes: Innovative heterogeneous gas phase catalysts"
Name und Art des Bildungs-oder	Institut für Technische Chemie und Umweltchemie
Ausbildungseinrichtung	Friedrich-Schiller-Universität Jena, Deutschland

Berufsbildung

Datum	06.1999 – 12.2000
Firma	Vifon-Acecook Food processing company
Bereich	Quality Control
Datum	Seit 01.2001
Firma	Institute of Applied Materials Science (IAMS)
Bereich	Heterogeneous Catalysis for Environment

Jena, 26. September 2011

Erklärung

Ich erkläre, daß ich die vorliegende Arbeit selbständig und nur unter Verwendung der angegebenen Hilfmittel, persönlichen Mitteilungen und Quellen angefertigt habe.

Jena, 26. 09. 2011